Finanziato dall'Unione europea NextGenerationEU | Ministero dell'Università e della Ricerca | Italiadomani PIANO NAZIONALE DI RIPRESA E RESILIENZA

multi-Risk sciEnce for resilienT commUnities undeR a changiNg climate

Codice progetto MUR: **PE00000005** – CUP LEAD PARTNER: I33C22006910006

Deliverable title: Reports on climate-related service interruption threats over critical infrastructures – Methodology Report

Deliverable ID: 6.3.3

Due date: February 2025

Submission date: February 2025

AUTHORS

Elisabetta Colucci, Luca Bruno, Lorenzo Raffaele, Fulvio Rinaudo, Fabio Giulio Tonolo (POLITO), Pierluigi Claps, Paola Mazzoglio (POLITO), Francesco Napolitano, Elena Ridolfi, Benedetta Moccia (UNIROMA1), Bruno Colavitto, Tatiana Ghizzoni, Eva Trasforini (CIMA), Laura Longoni, Matteo Antelmi, Monica Corti, Lorenzo Panzeri (POLIMI), Elena Toth, Mattia Neri (UNIBO), Gabriele Freni, Mariacrocetta Sambito (UNIKORE).

Approved by Paola Mazzoglio (WP leader)

1. Technical references

Project Acronym	RETURN
Project Title	multi-Risk sciEnce for resilienT commUnities undeR a changiNg climate
Project Coordinator	Domenico Calcaterra UNIVERSITA DEGLI STUDI DI NAPOLI FEDERICO II domcalca@unina.it
Project Duration	December 2022 – November 2025 (36 months)

Deliverable No.	DV3.3
Dissemination level*	PU
Work Package	WP3 - Dynamic mapping of natural and climatic hazards over the infrastructure systems
Task	T3.3 - Climate specific hazard maps: e.g. drought, fire, wind, heatwaves, pluvial flooding (link with Spokes 4 and 8)
Lead beneficiary	POLITO, CIMA
Contributing beneficiary/ies	POLITO, UNIROMA1, CIMA, POLIMI, UNIBO, UNIKORE

* PU = Public

PP = Restricted to other programme participants (including the Commission Services)

RE = Restricted to a group specified by the consortium (including the Commission Services)

CO = Confidential, only for members of the consortium (including the Commission Services)

Document history

Version	Date	Lead contributor	Description
0.1	05.02.2025	POLITO and CIMA	First draft
0.2	15.02.2025		Critical review and proofreading
0.3	20.02.2025		Edits for approval
1.0	28.02.2025		Final version

2. ABSTRACT

Activities in this task are mostly connected to the goals and outcomes of the Spokes 4 and 8, where most of the climate change effects are envisaged. New instances of hazard mapping are proposed for the increasing climate risks, as those related to windstorms and wildfires.
This deliverable describes the products that were developed within the RETURN project to address these goals, which can be summarized in:

- remote sensing-based datasets of the wind hazard along critical infrastructures (Section 3.3.a);
- a national-scale evaluation of the impact of extreme rainfall events on the residual risk assessment for hydraulic infrastructures, complemented with some general guidelines (Section 3.3.b);
- dynamic maps of the pluvial flooding under current and future climatic conditions (Section 3.3.b);
- a methodology for improving rainfall monitoring in urban areas by integrating crowdsourced personal weather stations into official networks (Section 3.3.b);
- national-scale evaluation of temporal trends in short-duration rainfall extremes (Section 3.3.b);
- probabilistic risk assessment for isolated areas in connection to forest fires (Section 3.3.c);
- new method for wildfire hazard mapping and consequent hydrological risk management (Section 3.3.c);
- reservoir and water supply management under drought conditions, including analysis of future scenarios of water availability and user demand (Sections 3.3.d.1 and 3.3.d.2);
- assessment of water shortage hazard on urban water distribution users (Section 3.3.d.3).

The second part of the deliverable will instead focus on the application performed and the main results achieved.

3. Table of contents

1. Technical references 2

Document history 3

2. ABSTRACT 4

3. Table of contents 5

3.3 Reports on climate-related service interruption threats over critical infrastructures 9

3.3.a Enhanced methodology for wind hazard mapping over network CI - Remote sensing-based mapping of the wind hazard along CI 9

3.3.a.1 Introduction 9
3.3.a.1.1 Literature review and gap analysis of wind hazard along Critical Infrastructures 9
3.a.1.2 Aims and goals of the present study 11
3.3.a.2 Wind modelling and reanalysis approach 11
3.3.a.2.1 Forecast-reanalysis-downscaling models 13
3.3.a.2.2 Critical analysis of the selected in situ measurements 15
3.3.a.2.3 A novel reanalysis-based approach 16

3.3.b Enhanced methodology for defining pluvial flood hazard and risk over network CI, under CC ... 18

3.3.b.1 Updating Residual Risk Assessment for Hydraulic Infrastructures: Evaluating the Impact of Extreme Rainfall Events in Italy 18
3.3.b.1.1 Introduction 18
3.3.b.1.2 Methodology 19
3.3.b.1.2.1 Fitting Procedure 19
3.3.b.1.2.2 Monitoring procedure of the probability of failure 19
3.3.b.2 Dynamic maps of pluvial flooding under current and future climatic conditions 20
3.3.b.2.1 Introduction 20
3.3.b.2.1.1 Optimal operating policies 21
3.3.b.2.1.2 Dynamic vulnerability maps 21
3.3.b.2.1.3 Dynamic exposure maps 22
3.3.b.2.1.4 Infrastructure assessment 22
3.3.b.2.2 Methodology 22
3.3.b.3 Enhancing rainfall monitoring in urban areas by integrating crowdsourced personal weather stations into official networks 25
3.3.b.3.1 Introduction 25
3.3.b.3.2 Methodology 25
3.3.b.4 Evaluation of temporal trends in short-duration rainfall extremes 26
3.3.b.4.1 Introduction 26
3.3.b.4.2 Dataset 26
3.3.b.4.3 Methodology 28

3.3.c Enhanced methodology for analyzing forest fires impacts on network CI and on slope instability 29

3.3.c.1 Probabilistic risk assessment for isolated areas in connection to forest fires 29
3.3.c.1.1 Introduction 29
3.3.c.1.2 The Forest Fires Probabilistic Risk Assessment (PRA) framework 29
3.3.c.1.3 Sub-problems at network level and formalization of the approach 31
3.3.c.1.4 Conclusions 34
3.3.c.2 New method for wildfire hazard mapping and consequent hydrological risk management 34
3.3.c.2.1 Introduction 34

3.3.c.2.2 Literature and remote sensing analysis of area recently affected by wildfires 35
3.3.c.2.3 Field case description..... 36
3.3.c.2.4 Remote sensing analysis 37
3.3.c.2.5 Experimental analysis: field test execution..... 38
3.3.c.2.6 Experimental analysis: laboratory test execution 39

3.3.d Enhanced methodology for deriving drought effects on the water supply system 41

3.3.d.1 Drought water service interruptions - Water supply management (reservoir management and integration of different sources) under drought conditions, including analysis of future scenarios of water availability and user demand 41
3.3.d.1.1 Introduction 41
3.3.d.1.2 Methodology..... 42
3.3.d.1.3 Required data..... 43
3.3.d.1.4 Companion studies to enhance the replicability of the approach and connections with other Spokes 44
3.3.d.2 Water supply service interruptions: reservoir management under drought conditions 45
3.3.d.2.1 Introduction 45
3.3.d.2.2 Inflow prediction and management optimization 46
3.3.d.2.2.1 Streamflow forecasting..... 46
3.3.d.2.2.2 Experimental Framework 47
3.3.d.2.2.3 Model Architecture..... 47
3.3.d.2.2.4 Optimal operating policies..... 47
3.3.d.2.3 Assessing the Impact of Climate Change on Hydropower Production 48
3.3.d.3 Water shortage hazard on urban water distribution users, under current and future climate scenarios 49
3.3.d.3.1 Introduction 49
3.3.d.3.2 Estimating the impact of water shortage on urban population 51

6. References 54

Figures

Figure 1. Location of the 69 stations (Ballio et al., 1999), their areas of competence, and the resulting Italian wind map (DM 17-01-2018, 2018; CNR-DT 207 R1/2018, 2018) (a), schema of the current coded 'map-and-return' approach (b). 9
Figure 2. Average horizontal resolution of anemometric stations (a) and average duration of time series (b) used to define national maps of design wind speed for Canada (Hong and Ye, 2014), China (Mo et al., 2015), Australia (Spassiani and Mason, 2021), France (Sacrè, 1993). 10
Figure 3. Space and time scales of the atmospheric processes, synopsis of the time series duration T, horizontal resolution L and sampling period Δts of the reanalysis models [REA, specifically ERA-15, ERA-40, ERA-Interim (ERA-I), ERA5, ERA5-Land (ERA5L), VHR-REA_IT (VHR)], and of the Italian land anemometric stations used in Ballio et al. (1999) to draw the Italian wind map (DM 17-01-2018). 13
Figure 4.Voronoi cell of the anemometric station in Torino Caselle airport, sampled by the horizontal grids of ERA5 (a, 22 cells), ERA5L (b, 169 cells) and VHR (c, 2425 cells). 14
Figure 5. Mapping of z_0 according to ERA5 (a) and VHR (b, courteously provided by CMCC Foundation). Detailed view around the whole Rome region (c), and further closeup views around the anemometric stations at Roma Fiumicino (d), Genova (e), and Trieste (f). 15
Figure 6. Resulting compliance indices for yearly maxima $c(v)$ and averages $c(v)$. 16
Figure 7. Probability of failure updating procedure. 20
Figure 8. Location of the rain gauges used in this work. 27
Figure 9. Number of rain gauges active in each year. 27
Figure 10. Contingency matrix for defining the wildfire hazard levels 30
Figure 11. Example of wildfire hazard map (Fiorucci et al., 2024). 31
Figure 12. Location of the study area and of the three sub-areas identified for monitoring (B is burnt woods, G is burnt grassland, Ub is unburned woods). Fire severity is also displayed as the difference of NDVI before and after the wildfire, according to Chafer et al. (Chafer et al., 2004). 37
Figure 13. Single (a) and double (b) ring infiltrometers used to perform falling head infiltration tests in Sorico. 39
Figure 14. Landslide simulator setup. 40
Figure 15. Methodological framework for the sustainable management of a water resource system, through the optimisation of the withdrawal rule curves from the reservoir(s). 43
Figure 16. Distribution node numerical scheme. 53

Tables

Table 1. Cumulative distribution functions of the four tested probability distributions. 19
Table 2. Fuel type of classification and empirical association with the potential intensity. 30
Table 3. Example of vulnerability table for physical infrastructure. 31
Table 4. Remote sensing indices taken into account for the burnt recovery analysis, referred to Sentinel-2 spectral bands (B3 is Green, B4 is Red, B8 is Near InfraRed, B8A is Narrow NIR, B11 and B12 are Short-Wave InfraRed) 38

3.3 Reports on climate-related service interruption threats over critical infrastructures

3.3.a Enhanced methodology for wind hazard mapping over network CI - Remote sensing-based mapping of the wind hazard along CI

3.3.a.1 Introduction

Determining the design wind speeds is the first and key constituent ring of the 'Alan G. Davenport Wind Loading Chain' (Davenport, 1961). The wind speed design at a given site is traditional and still obtained using a two-stage, forth-and-back approach. The first stage is transparent to the designer. It consists of zoning the synoptic extreme winds at the lower bound of countrywide macroscale resolution (hundreds of km) based on suitable extreme statistics of time series records measured at land anemometric stations. The stage includes the acquisition, correction, transformation and probabilistic analysis of the measurements (see e.g. Ballio et al., 1999; Safaei Pirooz et al., 2021, for applications to Italy and New Zealand, respectively). Resulting wind maps are available to designers in standards (e.g., DM 17-01-2018, CNR-DT 207 R1/2018, AS/NZS 1170.2:2021 (2021), for the Italian and New Zealand in force standards, respectively). The second step is conversely directly entrusted to the designer using the so-called 'return criterion' (Ballio et al., 1999) to recover from the reference mapped speed (also called $vb0$ in e.g. EN 1991-1-4:2005) the design value (also referenced to vm in e.g. EN 1991-1-4:2005) accounting for the site and construction local characteristics, i.e. altitude above the sea level, aerodynamic roughness, orography and distance from the shoreline, reference height of the construction. The basic principles of the approach above were laid out in the early Sixties by Davenport (1960), further developed during the 20th century and applied in different Countries by other funding fathers of Wind Engineering (e.g. Solari et al., 1991a, 1991b and Ballio et al., 1999, in Italy). It should be considered as the accomplishment of a pioneering and brilliant modelling effort to provide a practical design tool based on relatively scarce, uneven, point-wise anemometric measurements available at that time. Despite such an effort, both stages of the 'map-and-return' approach are affected by some weaknesses early pointed out by Davenport himself (Davenport, 1960) and later faced by scholars in a panoply of informing studies.

3.3.a.1.1 Literature review and gap analysis of wind hazard along Critical Infrastructures

The two-phase 'map-and-return' approach, definitively established by Ballio, et al. (1999), is schematized in Figure 1b.

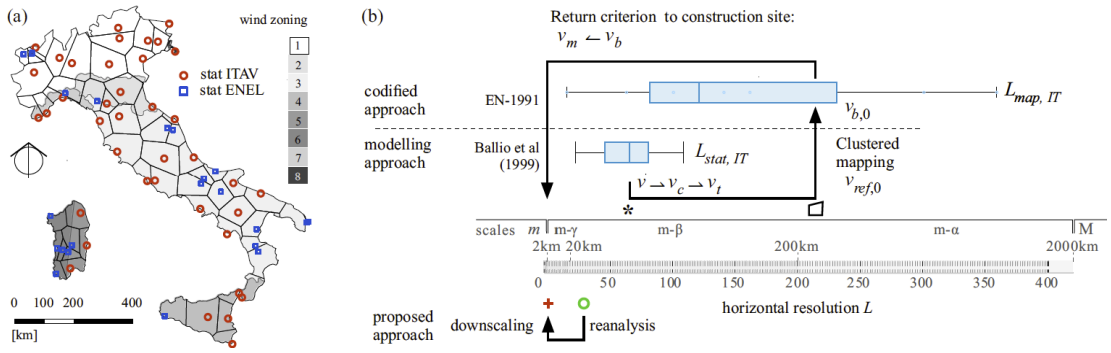

Figure 1. Location of the 69 stations (Ballio et al., 1999), their areas of competence, and the resulting Italian wind map (DM 17-01-2018, 2018; CNR-DT 207 R1/2018, 2018) (a), schema of the current coded 'map-and-return' approach (b).

The mapping stage, 'map', involves the acquisition of the 10-minute average wind speed v measured at local anemometric stations spaced at various intervals (denoted as its statistics and average value). This speed is then corrected v_c, transformed v_t, and subjected to a probabilistic analysis of extreme values $v_{ref,0}$. This process is not necessarily disclosed to the designer except for its final codified outcome (DM 17-01-2018, 2018; CNR-DT 207 R1/2018, 2018), which is the national wind map. This map groups climate zones—9 for Italy—spanning areas ranging from a few dozen to hundreds of kilometres (and its statistics in Fig. 1a). The second phase, on the other hand, is directly entrusted to the designer through the so-called "return criterion" (Ballio et al., 1999). This criterion derives the design wind speed ($v_{b,0}$; EN 1991-1-4:2005) from the mapped reference speed (v_m; EN 1991-1-4:2005). The derivation considers the local characteristics of the construction site: elevation above sea level, aerodynamic roughness, topography, distance from the coastline, and reference height of the structure. On the one hand, this innovative study represented the culmination of a brilliant and pioneering modelling effort to provide a practical design tool based on ground-based anemometric station measurements, which were relatively scarce at the time - approximately 10 million data points from 69 stations (Ballio et al., 1999). On the other hand, the dissemination of the method (Ballio et al., 1991a, 1991b) and its subsequent incorporation into standards (DM 17-01-2018, 2018; CNR-DT 207 R1/2018, 2018; EN 1991-1-4:2005) had an extraordinary impact on the design of wind-exposed structures, becoming a shared cultural asset among Italian and European engineers and architects. Despite such successes, both phases of the "map-and-return" approach present certain critical issues, previously highlighted by Davenport (1960) and Ballio et al. (1991a, 1991b). These issues are briefly revisited below, with separate references to the mapping and return stages.

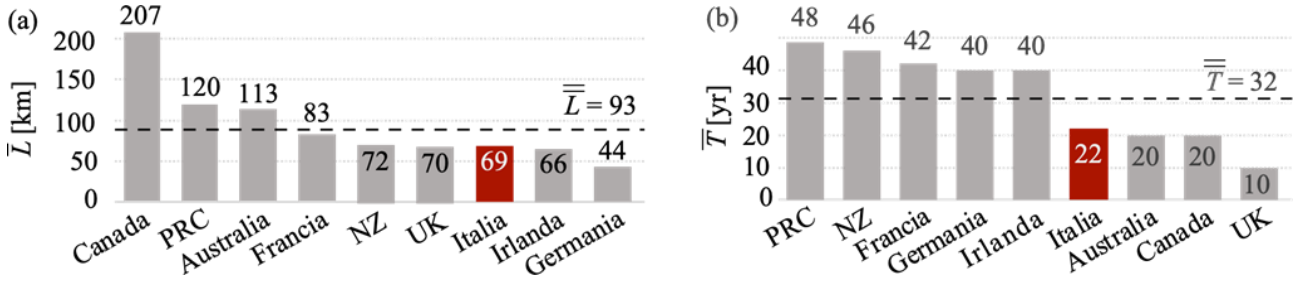

Figure 2. Average horizontal resolution of anemometric stations (a) and average duration of time series (b) used to define national maps of design wind speed for Canada (Hong and Ye, 2014), China (Mo et al., 2015), Australia (Spassiani and Mason, 2021), France (Sacrè, 1993).

The critical issues in the map stage stem directly from the quantity and quality of available anemometric measurements, i.e., the spacing of the ground measurement stations, the duration of the time series, the local characteristics of each station's installation site, and the specifications of the measuring instruments. The station spacing, hereafter referred to as the 'horizontal resolution' L, over the portion of Earth's surface of interest, such as a single country, is often low. Figure 2a diagrams the value of $\bar{L}$ averaged over the stations that define the national maps of extreme wind speed in 9 countries. The value averaged further over all nations, $\bar{\bar{L}}$, is on the order of magnitude of 100 km, while the average value for Europe is about 66 km. Furthermore, L is usually non-uniform within a single country. For example, Figure 1a maps the Voronoi tessellation of Italian territory concerning the 69 stations used to define the extreme winds of Italy, and Figure 1b shows the statistic of where the area of the i-th tessellation. The measurement time series T length is usually shorter than the return period of the reference wind speed for the design wind of interest and varies between stations. Despite the guidelines of the World Meteorological Organization (World Meteorogical Organization, 2021), the actual configuration of anemometric stations is not necessarily homogeneous in space or constant over time. Although anemometers should be positioned at a height of 10 meters above the ground and situated in open, flat terrain within a 2 km radius to avoid local effects on the measured wind, their actual position, height above the ground, and the aerodynamic roughness of their surroundings are not necessarily standardized, uniform in space, or constant over time. Regarding the anemometer itself, numerous characteristics can affect the measurement (Picozzi et al., 2022): type, model and related specifications, acquisition threshold value, resolution, degradation of accuracy during its service life, and data acquisition chain.

The critical issues in the return stage indirectly reflect those in the mapping stage, making it necessary for the designer to model the specific characteristics of the project site and their effects on the wind. These include the subjective and challenging evaluation of aerodynamic roughness (Yu et al., 2023), variations between different terrain categories and their corresponding z_0 values in the design codes, and estimating the effects of local terrain orography. It is indeed difficult for the designer to unambiguously link the construction site to the terrain categories, which are often qualitatively described in the design codes (Ballio et al., 1991a; Ballio et al., 1991b), adopt a value of z_0 in the face of different provisions for the same nominal terrain category (e.g., z_0 = 0.003 m and z_0 = 0.01 m for coastal areas in Eurocode 1 and DM 2018, respectively), and refer to simplified two-dimensional scenarios to evaluate the local effects of the site's real, three-dimensional orographic features. Each of the critical issues highlighted can translate into a source of measurement error or modelling uncertainty that affects the accuracy of the evaluation of the design wind speed. More than thirty years later, vast computational and satellite-based databases and innovative analysis methods offer the possibility of a paradigm shift in the definition of current and extreme wind maps for Italy. These methods and data have been developed over the last 25 years by the atmospheric physics scientific community. The author's contribution to this study lies in adapting a small portion of this knowledge to the needs of Structural Engineering to refine the modelling from synoptic winds, which were previously considered with spatial scales of hundreds of kilometres, to those at the mesoscale, down to its lower limit of about 2 km.

3.a.1.2 Aims and goals of the present study

The present study aims to shed light on three main issues:

i. Is reanalysis, eventually coupled with down-scaling by deterministic interpolation or by a higher resolution climate model, suitable to map current and extreme winds accurately?

ii. Are reanalysis datasets suitable for all wind spatial and time scales and for all orographical and exposure types? If not, what is their smallest threshold scale for application?

iii. Can reanalysis offer the opportunity to conceive an approach to design wind mapping that is an alternative to the in-force codified two-stage ‘map-and-return’ approach based on land anemometric stations? If yes, what are the advantages and limitations?

To answer the above questions, we consider three reanalysis datasets. Their performances in predicting current and extreme wind speeds with different return periods are assessed concerning the measurements at multiple land anemometric stations critically analysed and selected. The Italian land is adopted as a well-adapted, particularly challenging benchmark because of its geomorphological features, where roughness and orographical high variability ubiquitously occur along extensive coastal and mountainous zones. An alternative reanalysis-based approach is finally proposed, qualitatively and quantitatively compared with the traditional codified one currently in force in Italy (DM 17-01-2018, CNR-DT 207 R1/2018).

3.3.a.2 Wind modelling and reanalysis approach

The reanalysis approach, generally called ‘REA’ in the following, blends observations with past short-range weather forecasts rerun with cutting-edge weather forecasting models. Modern climate reanalysis has at least four main recognized potentials:

i. it “delivers a complete and consistent picture of the past weather” (Thépaut et al., 2018), “relying on a numerical weather prediction model to assimilate historical observations (e.g., from satellite, in situ, multiple variables) that are not homogeneously distributed around the globe” (Raffa et al., 2021);

ii. over time, it secures long term time series, eventually continuously updated to account for climate or exposure changes;

iii. over space, it offers ‘maps without gaps’ having horizontal resolution higher than the codified extreme wind maps in Wind Engineering, with global worldwide covering to avoid conflicts of the national wind maps at boundaries (Miller, 2003);

iv. datasets are easily accessible in open access via institutional web-based repositories to guarantee analysis repeatability.

Apart from the potentialities above, the accuracy of reanalysis models versus anemometric field measurements is not univocal and currently debated, namely concerning current wind speed in the fields of climatology (e.g. Molina et al., 2021; Doddy Clarke et al., 2021; Gumuscu et al., 2023) and renewable energy (e.g. Gualtieri, 2021, 2022). Reanalysis predictions are found to significantly depend on the quantity of interest (e.g. 1, 6, or 24-hour current wind speed), height above the ground (the conventional 10 m level, or e.g. the height of tall wind turbine towers), exposure type (e.g. offshore, flat onshore, coastal or mountainous sites), beyond the adopted reanalysis model. To provide a general key to understanding such variable performances, in Fig. 4, we explicitly refer to the average horizontal and time resolutions of the ECMWF REA models to the space and time scales of the atmospheric processes initially set in meteorology (Orlanski, 1975; Fujita, 1986) and well-known in Wind Engineering as well (Dyrbye and Hansen, 1996). Since the release of the first global reanalysis in 1997 (ERA-15, Gibson et al., 1997) to the very last one in 2023 (ERA5, Hersbach et al., 2020), the ECMWF models progressively refined their horizontal resolution from $L \sim 187$ km to $L \sim 31$ km, i.e. crossing the whole range of meso-β scales. Correspondingly, the time resolution increased from 6 hours wind speed (meso-β time scale in ERA-15, -40, -Interim) to 1-hourly (meso-γ time scale in ERA5), and the duration of the historical time series increased from T = 14 years in ERA-15 to T = 83 years in ERA5. In parallel, reanalysis evolved in physical models and observation assimilation systems. Thanks to such a reading key, it is clear that ERA5 reanalysis is expected to be sufficiently reliable at locations with orography and land cover homogeneous fetch over about dozens of km (lower bound of the m-β scale), such as offshore or nominally flat onshore locations (Gualtieri, 2022). However, further spatial downscaling is required to cover, both in figurative and strict use, the 'last mile', i.e. to reach the lower bound of the meso-γ scale (2 km) and potentially describe corresponding winds (e.g. thunderstorms, sea or mountain breezes) over mountainous and coastal sites, where current wind speed is under- and over-estimated, respectively, even by the best-performing global reanalysis models such as ERA5 (Gualtieri, 2022). Different approaches to regional downscaling of the reanalysis are proposed in the literature. Among these, two approaches move from ERA5 as input: the ERA5-Land reanalysis (ERA5L in the following) and the Very High-Resolution REA over Italy (VHR-REA_IT, VHR in the following) convection-permitting RCM. It is clear from Fig. 3 that both datasets can resolve the meso-γ scale, even if to a different extent, i.e. to account for winds over sites with discontinuous roughness and orographical changes at the mesoscale. Fig. 3 also shows, for the sake of comparison, the statistics of the horizontal resolution $L_{stat,T}$ and the time series duration $L_{stat,IT}$ of the anemometric stations used to set the map of the Italian extreme wind speeds. ERA5, ERA5L, and VHR models equal anemometric stations sampling period. At the same time, they are competitive with stations in terms of time series duration and spatial resolution, i.e. able to fully cover the meso-γ scale by equal or longer observations.

The wind speed datasets considered in the present study result from the three REA models above. All the models are quite large and complex, encompassing decades of development. The detailed description of each model is largely beyond the range and scope of this paper. In the following, reference is made to the parent papers/documentation. The specific features of the three REA models are recalled first. Then, a comparative analysis of common issues is carried out. For a comprehensive review of the features and relative performances of REA models besides the ones discussed here, interested readers can refer to the comprehensive survey by Gualtieri (2022), where the performances of multiple global reanalysis models (MERRA, CFSR, NCEP/NCAR R2, ERA5, among others) and several regional downscaling models (NARR, COSMO-REA2, MÉRA, HARMONIE, among others) are compared in predicting the averaged wind speed for wind energy applications.

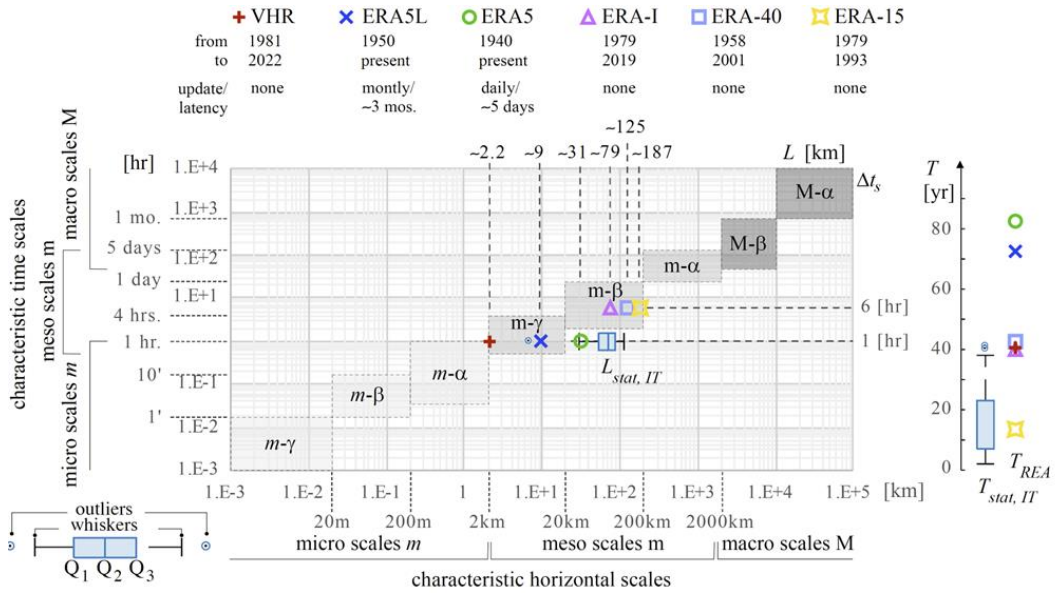

Figure 3. Space and time scales of the atmospheric processes, synopsis of the time series duration T, horizontal resolution L and sampling period Δts of the reanalysis models [REA, specifically ERA-15, ERA-40, ERA-Interim (ERA-I), ERA5, ERA5-Land (ERA5L), VHR-REA_IT (VHR)], and of the Italian land anemometric stations used in Ballio et al. (1999) to draw the Italian wind map (DM 17-01-2018).

3.3.a.2.1 Forecast-reanalysis-downscaling models

ERA5 is the fifth-generation reanalysis developed by ECMWF (Hersbach et al., 2020). It covers the whole Earth globally with a horizontal resolution equal to θ = 0.28°, i.e. about $L \approx 31$ km. ERA5 combines a numerical weather prediction model of the atmosphere's dynamical and moist thermodynamical state with empirical observation data properly assimilated. About 95 billion observations were assimilated within 40 years from 1979 to 2019, i.e. 65 million per day on average (Hersbach et al., 2020). Wind observables at high altitudes come from radiosondes, weather meteorological balloons, wind profilers, and aircraft-based instruments. With regard to wind velocity components at 10 m height, measurements made near the sea surface on ships and drifting/moored buoys are retained only, while assimilated observations at land airport weather stations are limited to surface pressure. The land characteristics are described in ERA5 using several time-invariant fields, the land-sea mask, the lake cover and depth, the soil and vegetation type, and the vegetation cover, among others.

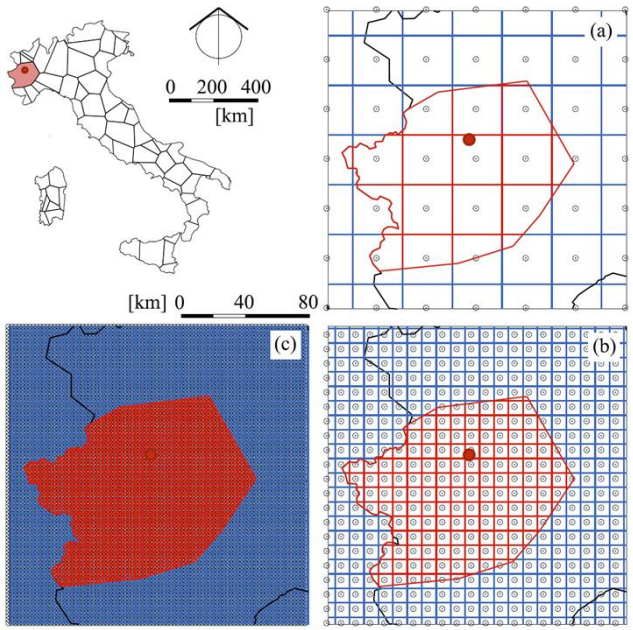

Figure 4.Voronoi cell of the anemometric station in Torino Caselle airport, sampled by the horizontal grids of ERA5 (a, 22 cells), ERA5L (b, 169 cells) and VHR (c, 2425 cells).

ERA5L is a reiteration of the land component of the ERA5 reanalysis at a horizontal resolution equal to θ = 0.1◦, i.e. about $L \approx 9$ km (Muñoz Sabater et al., 2021). ERA5L model is driven by the atmospheric forcing resulting from ERA5 near-surface meteorology state and flux fields, including air temperature, specific humidity, surface pressure, wind speed, downward shortwave and longwave radiation and liquid and solid total precipitation. These ERA5 fields are interpolated to the 9 km resolution via a linear interpolation method based on a triangular mesh (Muñoz Sabater et al., 2021). VHR results from the dynamical downscaling of ERA5 reanalysis to the so-called convection-permitting scale, allowing for explicit resolution of convection on the model grid (Raffa et al., 2021). Initial conditions and lateral boundary conditions (updated every 3 h) are set by interpolating ERA5 data from the ERA5 coarse grid to the finer VHR grid. The regional downscaling covers a domain around Italy (lon = 5°:20° E, lat = 36°:48° N) with a horizontal resolution equal to θ = 0.02°, i.e. about $L \approx 2.2$ km. The dynamical downscaling is carried out with the regional climate model COSMO-CLM, i.e. a non-hydrostatic and limited-area model designed for dynamically downscaling simulations at different horizontal resolutions varying from the meso-β to the meso-γ scales (Adinolfi et al., 2023). Land use, surface elevation and soil type are determined through the GLC2000 (Bartholomé and Belward, 2005), GLOBE, and FAO Digital Soil Map datasets, respectively.

For visual comparison purposes, Fig. 4 exemplifies the grid by ERA5, ERA5L and VHR over the Voronoi cell of a single station in Italy. All the REA models above require the setting of z_0, assuming it as homogeneous over each cell face adjacent to the ground. We stress that setting the exposure is one of the most crucial tasks in determining the design wind speed (Yu et al., 2023), in charge of the designer in the map-and-return approach (e.g. EN 1991-1-4:2005). Conversely, REA models directly consider explicitly mapping z_0 over land and sea surfaces. ERA5 and ERA5L set z_0 as a function of the vegetation type over land, while the wind-wave interaction effect is considered to estimate z_0 over sea. Conversely, VHR defines z_0 as the sum of two contributions, namely, the roughness associated with the subgrid-scale variance of orography according to the GLOBE Digital Elevation Model (Hastings et al., 1999) and the roughness associated with the land-use category according to GLC2000 (Bartholomé and Belward, 2005). It follows that z_0 differs between ERA5 and VHR models in terms of both definition and value. To highlight such differences, z_0 is mapped according to ERA5 and VHR models in Fig. 5a and 5b. Despite the striking difference in resolution, the horizontal distribution of z_0 qualitatively follows an analogous pattern, i.e. z_0 is higher in correspondence with the Alpine region and along the Apennines. Some closeup views pairing z_0 contours with the VHR cell centres of the region around Rome and more closely around the stations of Roma Fiumicino, Genova Sestri and Trieste Lanterna are shown in Fig. 5c, 5d, 5e, 5f, respectively. VHR enriches the resolution of z_0 and can catch changes in z_0 induced by vegetation and urban fabric (Doms et al., 2013).

Fig. 5c shows how the resolution of VHR allows to clearly distinguish zones with very low z_0, such as lakes (i.e. Bracciano lake) and sea, and zones with high z_0, such as Rome conurbation and forests (i.e. Castelli Romani and Castelporziano). The close-up view of Roma Fiumicino station (Fig. 5d) shows homogeneous z_0. In contrast, the closeup views of the Genova and Trieste stations (Fig. 5e,f) reflect its rapid transition from the sea, low z_0 values to urban and forest terrain, large z_0 values. All the REA models above are inevitably affected by assumptions and multiple potential sources of errors, as usual in Computational Wind Engineering (CWE, e.g. Bruno et al., 2023). On the one hand, physical and mathematical models inevitably take with them hypotheses and approximations. On the other hand, further approximations and related errors result from discretization methods, computational grids and numerical schemes.

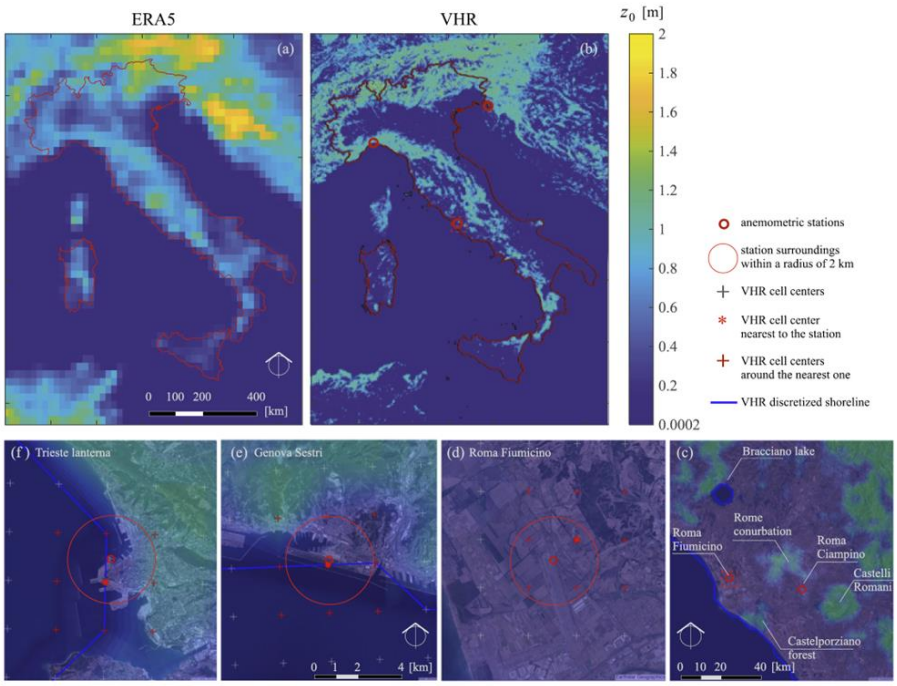

Figure 5. Mapping of z_0 according to ERA5 (a) and VHR (b, courteously provided by CMCC Foundation). Detailed view around the whole Rome region (c), and further closeup views around the anemometric stations at Roma Fiumicino (d), Genova (e), and Trieste (f).

3.3.a.2.2 Critical analysis of the selected in situ measurements

Historical time series of in situ measurements at land anemometric stations ('stat' in the following) are adopted as a term of reference to assess the relative performances of REA models in terms of

i. representativeness, i.e. REA performances under different mesoscale types of climatic zones, site orography and exposure, and

ii. relative accuracy, i.e. the scatter between REA results and stat measurements.

21 Italian anemometric stations are selected among the 129 available in the Met Office Hadley Centre's Integrated Surface Database (HadISD, Dunn et al., 2016; Dunn, 2019), an open-access global sub-daily dataset based on the ISD dataset from NOAA's NCDC. The a priori selection of the stations and the subsequent critical analysis of the measurements are intended to pursue both the above goals.

I. *Representativeness.* Station locations are primarily selected to attain the first goal based on two criteria:

(I.a) they are as evenly distributed as possible over the Italian land to catch the largest number of climatic zones concerning the current wind zoning defined in DM 17-01-2018, CNR-DT 207 R1/2018;

(I.b) they are potentially representative of qualitatively different orography and exposure conditions at mesoscale: Torino, Milano Malpensa, Bologna and Firenze Peretola are located in nearly flat onshore sites; Bolzano and Monte Paganella in mountainous sites; Genova Sestri, Messina Torre Faro and Reggio Calabria along mountainous coastlines, the remaining stations along coastal zones with almost flat surrounds.

II. *Relative accuracy*. The setup and dataset of each station are further analysed to judge the comparability between them and the REA approach as a required precondition to achieve the second goal. Comparability is discussed regarding data quality and climatological representativeness at the mesoscale of the stations.

(II.a) Data quality. The observations in the ERA5 reanalysis were thoroughly quality-checked. Analogously, all the stat time series from the HadISD database guarantee a fully automated QC by running 15 tests to flag the poorest records as invalid data Vi (Dunn et al., 2012).

(II.b) Station WMO-compliance. REA models do not inherently change in time, do not systematically account for microscales because of their maximum resolution in time and space, and the resulting datasets are standardized and without gaps. The stat WMO-compliance is clearly not trivially guaranteed in the light of the previous studies on the weaknesses of the mapping stage. We critically discuss and quantify any discrepancies between the setup/measurements of the selected stations and the WMO provisions. In such a way, we also indirectly point out the possible systematic differences between REA and stat datasets. To do so, we propose a synthetic compliance index $C \in [0, 1]$ in its very general form as:

$$C = 1 - \frac{\sum_{j=1}^{n} \mu_j I_j}{n} \tag{3.3.1}$$

where $I_j \in [0, 1]$ are n partial, maximum-normalized inconsistency indices related to time series completeness ($I_1 = I_v$), steadiness of station setup within T ($I_2 = I_s$), uniformity of flat orography over the 2 km radius fetch ($I_3 = I_t$), uniformity of roughness over the same fetch as above ($I_4 = I_r$), anemometer height ($I_5 = I_h$), and $\mu_j \in [0, 1]$ are the corresponding weighting factors. It follows that $C = 1$ denotes a station fully compliant with WMO provisions and fully comparable REA and stat datasets, while other values are generally intended to relatively rank the stations among the selected ones. For the sake of simplicity, all weights are set $\mu_j = 1$ in the present study, i.e. all inconsistencies are considered equally important.

Given the above, the compliance index in Eq. 3.3.1 is systematically evaluated for each station with $j = 2{:}5$ and $n = 4$. The synthetic compliance is plotted in Fig. 6.

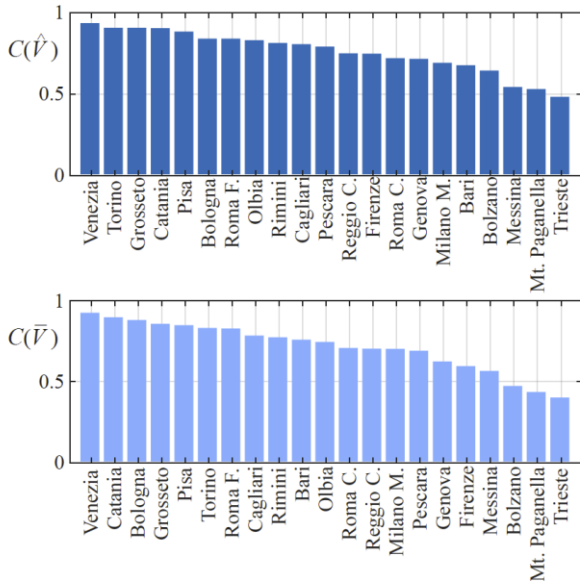

Figure 6. Resulting compliance indices for yearly maxima $c(\hat{v})$ and averages $c(\bar{v})$.

3.3.a.2.3 A novel reanalysis-based approach

The REA modelling approach's specific features and promising performances allow us to imagine a novel 'reanalysis-and-height adjust' (REA-HA) approach as an alternative to the in-force codified 'map-and-return' one. The first 'reanalysis' stage, including Numerical Weather Prediction, Reanalysis, Downscaling, and EVA, is entrusted to the specialist in charge of drawing the map, while the 'height adjust' stage is entrusted to the designer, in analogy with the two-step 'map-and-return' codified approach. The proposed

approach involves some conceptual and technical advantages concerning the in-force codified approach. At the reanalysis stage:

i. forth-and-back across scales, and transformation of non-homogeneous, scattered data are no longer needed;

ii. every effect, including the orographic one, are consistently and explicitly accounted for up to the meso-γ scale, while microscale effects are knowingly excluded;

iii. the high horizontal resolution offers the designer detailed 'maps without gaps' of the wind speed and aerodynamic roughness, including values evaluated quite close to the design site.

At the height adjust stage:

i. the designer is relieved of some tasks that require specialized know-how in wind engineering, namely the obligation to evaluate the aerodynamic roughness at the design site subjectively, and to ascribe the actual, 3D, sometimes complex site orography to simplified schemes and related orographic coefficients;

ii. the designer is made conscious of what the approach accounts for and what it does not, i.e. microscale effects of local site features inside a 2 km radius fetch.

Given the above advantages, the REA-based extreme wind speed modelling generally underestimates measurements. As such, REA-based extreme wind speed estimates shall be adjusted employing a suitably tuned model correction factor. As a result, the design wind speed $v_m(h_d)$ is expressed in REA-HA as:

$$\gamma_m = \frac{V_{REA}}{V_{stat}} = \frac{1}{1 + Q_2(\varepsilon_{REA-stat})} \tag{3.3.2}$$

where γ_m is the model correction factor, $VREA(x_d, y_d)$ and $z_0(x_d, y_d)$ are the wind speed and aerodynamic roughness at the design site position (x_d, y_d) as mapped in the REA stage, h_d is the reference design height relevant to the structure under consideration, h_{ref} = 10 m is the reference height at which $VREA$ is mapped. In other words, the designer is only called upon to select the return period relevant to the design, apply the related model correction factor γ_m and adjust the height. In the following, a first exploratory step towards the estimate of γ_m is proposed.

3.3.b Enhanced methodology for defining pluvial flood hazard and risk over network CI, under CC

3.3.b.1 Updating Residual Risk Assessment for Hydraulic Infrastructures: Evaluating the Impact of Extreme Rainfall Events in Italy

3.3.b.1.1 Introduction

Water-related disasters, especially floods and storms, are the most frequent and impactful natural hazards globally (CRED, 2023). Their impacts are projected to intensify due to population growth, urbanization, unsustainable land management, and climate change (Singh et al., 2023, Treppiedi et al., 2023, Kreibich et al., 2023).

Understanding and modeling extreme rainfall is crucial for mitigating these effects, prompting countries to invest in resilience strategies. Various methods have been developed for modeling and analyzing extreme rainfall, both as a scientific approach to understanding the impacts of severe weather events and as a practical tool for civil and environmental engineering design (Forestieri et al., 2018). Extreme event analysis is typically carried out using probabilistic techniques based on historical data, where the main objective is to link the magnitude of an event to its probability of occurrence. Assuming independence and identical distribution conditions (i.i.d.), it is possible to estimate the frequency of rare events, including those exceeding the observed data. In Earth sciences, the frequency of an event with a specified magnitude is often described using the concept of the return period (T). This is defined as the reciprocal of the exceedance probability or the average time interval over which an event of that magnitude is expected to occur (Volpi, 2019). The upper portion of a probability distribution, commonly referred to as the right tail, determines both the magnitude and frequency of extreme events. As a result, it significantly influences the estimation of design rainfall values. Consequently, evaluating precipitation tails at regional and global scales is of critical importance. Numerous researchers have explored various approaches to identify the most effective methods for modeling extremes, including examining sample selection techniques, choosing probability distribution functions, estimating parameters, and conducting Goodness-of-Fit tests (for a comprehensive review, see Nerantzaki and Papalexiou, 2022). Recently, there has been a growing consensus among researchers advocating for the use of heavy-tailed distributions to characterize rainfall extremes (Villarini, 2012; Papalexiou et al., 2013; Cavanaugh et al., 2015; Gupta and Chavan, 2021; Moccia et al., 2021a, 2021b). Relying on light-tailed distributions can significantly underestimate the extreme rainfall amounts with a consequent possible miscalculation of the risks posed to structures and infrastructure. Risk is formally defined as the convolution of three factors: i) the hazard, which refers to the likelihood of a dangerous event occurring, ii) the exposure, encompassing the assets at risk, including economic values and human lives, and iii) the vulnerability of the land exposed to the hazard (Koutsoyiannis, 2022).

Risk reduction measures are typically categorized into two types: *structural interventions*, which aim to mitigate the hazard, and *non-structural interventions*, designed to simultaneously reduce both exposure and vulnerability. Structural protection measures are engineered to withstand extreme events with a predetermined annual exceedance probability, often expressed as a return period (Volpi and Fiori, 2014). Events whose intensities exceed the design values of these structures are referred to as cases of overload. Such occurrences are associated with the probability of failure, also known as residual risk, which is mathematically formulated as:

$$R = 1 - (1 - 1/T_d)^l \tag{3.3.3}$$

where T_d represents the design return period and l is the design (or expected) lifespan of the structure (Chow et al., 1988). The probability of failure is defined as the likelihood that at least one overload event occurs during the structure's design life (Hartmann et al., 2021). From Equation 3.3.3, when the design return period equals the design life ($T_d = l$) and approaches infinity, the probability of failure converges to 0.63 (Read and Vogel, 2015). This indicates that, in hydraulic structure design for water control, it is implicitly accepted that a structure may fail to perform its intended function due to an overload event.

In this work we emphasize the importance of updating design variables over the lifespan of structures and infrastructure to manage the probability of failure effectively and adopt a risk-based approach for management and intervention planning (Moccia et al., 2024).

3.3.b.1.2 Methodology

3.3.b.1.2.1 Fitting Procedure

In this study, we first identify the most suitable probability distribution to model extreme daily rainfall across Italy. Specifically, we extract the Annual Maxima (AM) samples from rainfall time series and evaluate the performance of four commonly used bi-parametric probability distributions for rainfall extremes: Lognormal (LN), Weibull (W), Gumbel (G), and Fréchet (F). The cumulative distribution functions (CDFs) for these distributions are provided in Table 1.

Table 1. Cumulative distribution functions of the four tested probability distributions.

Probability distribution	Cumulative distribution function
Lognormal ($\mathcal{LN}$)	$F_{\mathcal{LN}}(x) = 1 - \left(\frac{1}{2}\text{erfc}\left(\ln\left(\frac{x}{\beta}\right)^{1/\gamma}\right)\right)$
Weibull ($\mathcal{W}$)	$F_{\mathcal{W}}(x) = 1 - \exp\left(-\left(\frac{x}{\beta}\right)^{\gamma}\right)$
Gumbel ($\mathcal{G}$)	$F_{\mathcal{G}}(x) = \exp(-\exp(-\beta(x-\alpha)))$
Fréchet ($\mathcal{F}$)	$F_{\mathcal{F}}(x) = \exp\left(-\frac{x}{\beta}\right)^{-\gamma}$

erfc is the complementary error function; α, β and γ are location, scale, and shape parameters, respectively

.

The four distributions exhibit different tail heaviness. Fréchet, Lognormal, and Weibull (with $\gamma < 1$) are considered heavy-tailed, whereas Gumbel and Weibull (with $\gamma \geq 1$) are classified as light-tailed (El Adlouni et al., 2008). To assess and compare the performance of these distributions, we employ a robust and widely used metric: the minimization of a modified norm of the mean square error (MSEN; Papalexiou et al., 2013; Moccia et al., 2021a). The MSEN metric (Equation 3.3.4) provides a reliable method for evaluating the fit of the tested distributions, enabling an objective comparison of their effectiveness in capturing the statistical properties of extreme rainfall events:

$$MSEN = \frac{1}{N}\sum_{i=1}^{N}\left(\frac{F_N(x_i) - F(x_i)}{1 - F_N(x_i)}\right)^2 \quad (3.3.4)$$

3.3.b.1.2.2 Monitoring procedure of the probability of failure

The quantile function of the best-fitting probability distribution enables the estimation of rainfall values corresponding to specific return periods (or probabilities of exceedance). These values, referred to as design values for hydraulic works ($h_{d,Td}$ where d stands for design), are used in the planning and construction of hydraulic structures. At the design time, only historical rainfall data are available for determining these quantiles. However, after construction and throughout the design life of the structure, new observations can be incorporated into the analysis.

In this study, we use daily precipitation as a design variable, though the outlined methodology is equally applicable to other hydrological variables (e.g., peak flows) and different time scales (e.g., sub-daily data). To illustrate, consider a 30-year observation period used to estimate rainfall quantiles for designing a hydraulic structure. This 30-year period is chosen based on best practices in time series statistical analysis (World Meteorological Organization, 1988; Li et al., 2018). In practice, however, these best practices are not always satisfied due to challenges in acquiring reliable, long-term rainfall records. During the design phase, the design variable is determined for a fixed return period, and the design life of the structure is

established, which allows for the calculation of the probability of failure. Over the design life, the probability of failure decreases yearly as the term l in Equation 3.3.3 diminishes. Nevertheless, as new observations of the design variable become available, they can be added to the original dataset, enhancing the statistical robustness of the analysis. The yearly updating process for evaluating the probability of failure, with $y = 1, \ldots, N - 30$ can be summarized in the following steps:

1. Add the y^{th} recorded annual maximum (AM) rainfall value to each subsample;
2. Refit the probability distribution function to estimate the updated rainfall quantile associated with the design return period ($h_{u,y}$ where u stands for updated);
3. Quantify the updated return period (T_y) corresponding to $h_{u,y}$ using the original 30-year probability distribution parameters;
4. Evaluate both the design probability of failure $R_{d,y} = 1 - (1 - 1/T_d)^{l-y}$ and the updated probability of failure $R_{u,y} = 1 - (1 - 1/T_y)^{l-y}$;
5. Calculate the differences in probability of failure $\Delta R_y = R_{u,y} - R_{d,y}$ and design rainfall $\Delta h_y = h_{u,y} - h_d$.

This procedure is illustrated in Figure 7, providing a clear visual representation of the steps involved. The iterative updating process ensures that the design remains robust and reflective of evolving climatic and hydrological conditions, enhancing resilience against extreme rainfall events.

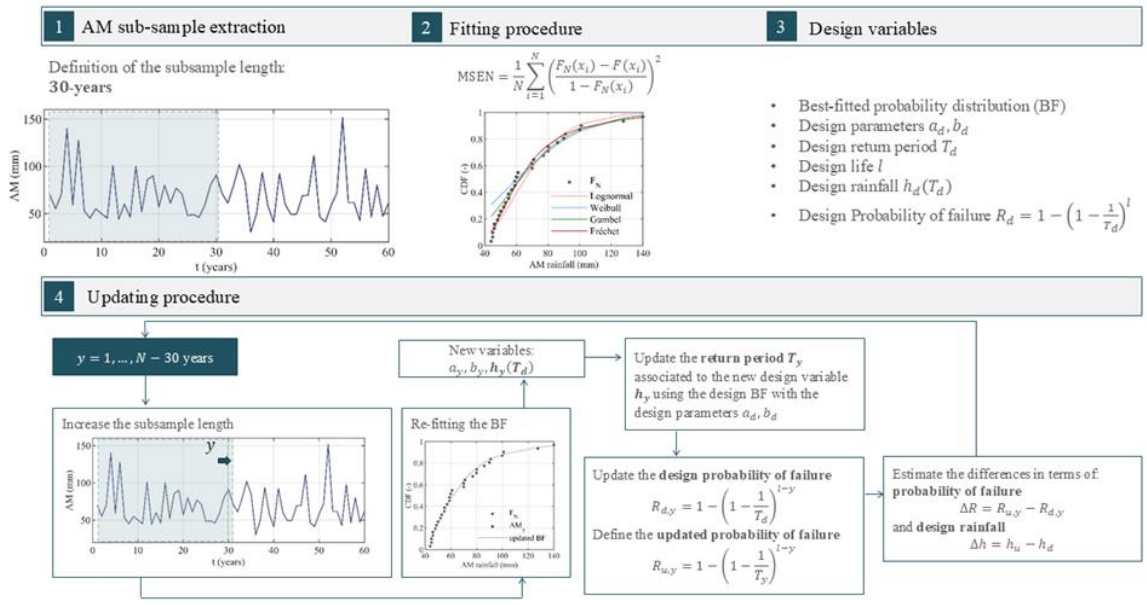

Figure 7. Probability of failure updating procedure.

3.3.b.2 Dynamic maps of pluvial flooding under current and future climatic conditions

3.3.b.2.1 Introduction

Over the past decades, urbanization has led to the expansion of impervious surfaces, which reduces the soil's natural ability to absorb rainfall. This increase in impervious areas raises the volume of urban runoff, thereby overwhelming drainage systems and leading to more frequent flooding events (Hammond et al., 2013).

In addition to urbanization, climate change also contributes to the increased occurrence of urban pluvial flooding. Rising global temperatures have led to more intense and frequent rainfall events, stressing the

capacity of urban drainage systems and causing surface water to accumulate in low-lying areas (Zimmermann et al., 2016). The impacts of urban flooding are multifaceted, encompassing both direct and indirect consequences. It significantly affects societies, infrastructure, economies, the environment, and public health. One of the most critical public health concerns is the contamination of water supplies, which facilitates the spread of waterborne diseases. In many urban areas, intense rainfall has led to severe flooding, resulting in extensive damage to critical infrastructure such as transportation networks, energy systems, and healthcare facilities. Among the others, we can list the issued caused to the railway in Swarzędz, Poland, where the drainage system was unable to handle the extreme rainfall events (Kundzewicz & Pińskwar, 2022). Similarly, Denmark presented several pluvial flooding events due to extreme rainfall, causing significant disruption to critical infrastructure (Rosenzweig et al., 2019). Urbanization determines dramatic increases in human exposure and vulnerability. Furthermore, urban flooding may be exacerbated by the social context, as it may disproportionately impact vulnerable communities. Consequently, effective urban flood disaster management demands integrated approaches that combine both structural and non-structural mitigation measures to enhance urban resilience against flooding (Tingsanchali, 2012).

In this context, understanding the population exposure to floods is essential for effectively mitigating pluvial flood risk. A valuable tool in this regard is the use of dynamic maps, which assess flood impacts as spatiotemporally variable. These maps are particularly critical in urban areas, where the convective nature of rainfall events and the fluctuating presence of populations in space and time necessitate a dynamic approach. Dynamic mapping involves the representation of flood hazard, vulnerability, and exposure over varying time periods in a specific area. It integrates temporal changes in environmental conditions (e.g. rainfall intensity, water levels, and storm surges), human activities (e.g. population movements and daily routines), infrastructure status (e.g., drainage capacity and road networks), and other socio-economic variables (e.g. adaptive capacity and community resilience) to capture the evolution of flood risk over space and time (Cian et al., 2021; Deville et al., 2014; Islam & Meng, 2024; Simões et al., 2015).

3.3.b.2.1.1 Optimal operating policies

Dynamic hazard mapping methods typically use advanced modeling techniques to capture the time-varying nature of flood events. For example, hydrodynamic models, either 1D or 2D, simulate changes in rainfall intensity, storm surge and water levels progression over time (Simões et al., 2015; Thrysøe et al., 2021). Some approaches, such as stochastic rainfall generators combined with hydrodynamic models, enable the creation of probabilistic flood hazard maps that account for uncertainty and variability in rainfall patterns (Simões et al., 2015). These maps are continuously updated through the integration of real-time data, advanced weather forecasts, and sophisticated hydrological models, providing information for both immediate emergency response and long-term planning (Balistrocchi et al., 2020; Deville et al., 2014). However, these methods face several challenges, including the need for high-quality data and significant computational resources, which can limit their applicability, especially for real-time assessments.

3.3.b.2.1.2 Dynamic vulnerability maps

Dynamic flood vulnerability assessment involves the integration of spatial and temporal data, capturing changes in vulnerability over time. For instance, GIS and spatial clustering techniques are used to analyze socio-economic factors and their distribution across different areas, as demonstrated in studies examining minority communities in urban flood-prone areas (Islam & Meng, 2024). Other methods include using simplified dynamic models to simulate different flood and climate change scenarios, allowing stakeholders to explore various adaptation strategies (Giupponi et al., 2013). Additionally, multi-temporal Flood Vulnerability Indices (FVIs) are developed by integrating Earth Observation data with census information, capturing how urban growth and socio-economic changes impact vulnerability over time (Cian et al., 2021). Despite their utility, these methods often require extensive data and may be constrained by data quality and availability, particularly in developing countries. Moreover, the use of simplified indicators and aggregation methods may overlook complex socio-ecological factors, reducing the comprehensiveness of vulnerability assessments (Giupponi et al., 2013).

3.3.b.2.1.3 Dynamic exposure maps

Dynamic exposure mapping assesses the temporal variation in exposure of population or assets to flood hazards. This approach often relies on real-time data, such as mobile phone records, to create spatiotemporal maps that reflect human movements and changing exposure levels (Balistrocchi et al., 2020; Giupponi et al., 2013). For example, dynamic population models combined with flood hazard maps can show how exposure varies between day and night, identifying periods characterized by higher risk to inform emergency planning (Smith et al., 2016). Similarly, analysing mobile phone data over daily and seasonal cycles may lead to capturing more precise dynamic exposure patterns (Deville et al., 2014). However, these methods can be limited by data availability and quality, particularly when relying on a single source or provider, which might not fully represent the population. Additionally, integrating dynamic human behavior with static flood hazard maps can create discrepancies in the overall exposure assessments (Balistrocchi et al., 2020).

3.3.b.2.1.4 Infrastructure assessment

Evaluating the vulnerability and exposure of infrastructure systems is one of the most challenging aspects of pluvial flood assessment. Assessing infrastructure vulnerability is inherently complex and multidisciplinary, necessitating the use of diverse methodologies to address the interconnected dimensions effectively (Papilloud et al., 2020; Pescaroli & Kelman, 2017).

3.3.b.2.2 Methodology

Flood modelling of urban areas can be particularly challenging due to the intricate and irregular topography, which is more complex than that of fluvial or coastal flood modeling. This complexity is heightened by the presence of buildings, drainage networks, and other critical infrastructure. The dynamics and non-linear interactions of hydrological, hydrodynamic, and hydro-morphological processes in such terrain present considerable modeling difficulties. Additionally, the heterogeneous nature of urban surfaces complicates the parameterization of urban flood models. A widely used approach for urban pluvial flood modelling is the coupling of 1D-2D hydrodynamic models, which enables the integration of urban drainage networks. This method allows for a two-way interaction between surface water and the drainage system: runoff enters the network through inlets, while excess water surcharges back onto the surface when system capacity is exceeded, contributing to urban flooding (Li et al., 2020).

For this study, pluvial flood maps are developed by using the rain-on-grid model from HEC-RAS (USACE, 2024), i.e. a 2D physically based hydrodynamic model designed to simulate surface water flow across a high-resolution grid-based terrain (Brunner, 2016).

This direct rainfall application approach assigns precipitation to each cell of the Digital Surface Model (DSM), allowing runoff to be generated and propagated across the urban landscape. By modelling hydrological and hydraulic processes entirely within a 2D hydrodynamic framework, this method captures detailed interactions between rainfall intensity, topography, and surface flow dynamics, making it particularly well-suitable for urban environments.

To ensure an accurate representation of urban topography, a 1x1 meter resolution DSM is required. Special attention should be paid to the architectural characteristics of the study area's buildings, which may feature internal courtyards (or “kiosks”), that create artificial depressions in the model, leading to incorrect flood depth estimates. These courtyards can be erroneously interpreted as low-lying areas (30-50 meters deep), resulting in significant distortions in flood simulations. To correct these issues, internal courtyards are filled, aligning their elevation with the surrounding building heights. Additionally, rooftops were smoothed to prevent unrealistic water accumulation, and a 0.5-meter buffer was applied around building edges to reduce cupping effects that could artificially trap water. These preprocessing adjustments improved the realism of urban flow obstructions, enhancing the accuracy of rain-on-grid flood simulations.

After defining the terrain, a land cover layer was generated using data from the Copernicus Urban Atlas Land Cover dataset (2018), which provides raster-based information at a 10x10 meter resolution. This dataset allowed the study area to be categorized into distinct land use types. To incorporate infiltration processes,

a curve number (CN) layer was integrated into RAS Mapper (USACE, 2024) to estimate the infiltration capacity based on of different land cover types and soil conditions. Thus, the land cover and infiltration layers provided the parameters required for simulating surface water flow and infiltration within the hydrodynamic model.

Boundary conditions were classified into inflow and outflow components. The outflow boundary condition was defined using the normal depth method, based on the average slope of the study area (Brandimarte and Di Baldassarre, 2012). This approach ensures that excess surface runoff exits the model domain in a hydraulically consistent manner, allowing for realistic floodwater propagation across the urban landscape.

Although reports of past pluvial flooding events exist, rainfall data from nearby monitoring stations showed low return periods (often <2 years), making them unsuitable for modelling critical hydraulic conditions. Therefore, synthetic rainfall inputs were preferred to ensure temporal coherence, consistent spatial distribution, and replicability across simulation scenarios. Synthetic design hyetographs, based on Intensity-Duration-Frequency (IDF) curves representative of the study area, were used to simulate the rainfall event that triggered the flooding and serve as the boundary conditions for the model. In urban areas, convective events, i.e. short and heavy rainfall, may significantly impact the society and the infrastructures. Therefore, two different scenarios are simulated, corresponding to rainfall events with 10 minutes and 1 hour duration, respectively. Since the area is characterised by critical linear transportation infrastructures, i.e. high-capacity roads, we focused on events with 50 years return period. This value should be preferred in areas whereby flooding results in unacceptable levels of damage to human settlements and to the mobility (Becciu and Paoletti, 2010).

IDF curves are estimated from raingauges data deployed in the case study area. Then, punctual information was spatially interpolated to create a gridded dataset over the study domain. The decision to use different rain gauges is driven by the need to optimize spatial representativeness and data reliability over the area under analysis, ensuring that the observed precipitation patterns accurately captured the hydrological response of the study area. The final study area selection adhered to the following criteria.

1. *Susceptibility to pluvial flooding.* The selected area had to exhibit a documented history of pluvial flooding events. This was verified through the analysis of historical records, including photographic evidence and reports from local agencies and climate observatories. A key resource in this process was the Osservatorio Nazionale di Città Clima (Legambiente, 2025) which provides a climate risk map for Italian cities, allowing users to filter historical events by region, year, and flood type (e.g., intense rainfall-induced flooding vs. riverine flooding), as well as previous studies that specifically analyzed pluvial flood events in Rome (Di Salvo et al. 2017).
2. *Availability of rainfall data.* Once a flood-prone area was identified, the next step involved verifying whether the extreme event had been recorded by one or more rain gauges within the proximity. This ensured that the observed precipitation data could be directly linked to the flooding event under analysis.
3. *Consistency with DSM coverage.* The final selection of the study area had to ensure complete overlap between the flood-prone region and the available high-resolution DSM dataset. This requirement was essential to maintain the geospatial integrity of the model and allow for precise rain-on-grid flood simulations.

By meeting these criteria, the study area was effectively delineated, ensuring that the hydrodynamic model was supported by reliable rainfall inputs, high-resolution topographic data, and validated historical flood evidence.

It is worth noting that the model does not incorporate the drainage system, as this information is not available. Consequently, the presented results may be overestimated, particularly in areas where stormwater infrastructure could mitigate surface water accumulation. Additionally, while the Tiber River is present within the study area, it has not been explicitly modelled as part of the hydrodynamic simulations. This means that the river does not influence the hydraulic behaviour of the model, as the focus remains solely on pluvial flood dynamics.

To enhance the robustness of the analysis, multiple simulation scenarios will be incorporated to assess the model's sensitivity to key parameters. To address uncertainties related to land surface characteristics, a

sensitivity analysis was performed on the Manning's roughness coefficients assigned to the three main land use categories in the study area: Green areas (GA); Buildings (B); Roads (R).

The Manning's roughness coefficients (n-values) for each land use type can be derived from literature (Chow et al., 1988; US Army Corps of Engineers, 1989) ensuring that the hydraulic resistance properties of different surfaces (e.g., roads, vegetation, and impervious areas) are accurately represented in the model.

To account for uncertainty in land surface characteristics, several simulations were performed by varying Manning's roughness coefficients across different land use categories. For each category (green areas, buildings, and roads), minimum, average, and maximum values were considered based on literature benchmarks. This sensitivity analysis supported the identification of roughness configurations that most significantly affect flood extent and water depth values.

Each scenario was simulated using the HEC-RAS 2D rain-on-grid framework, producing a flood depth (hazard) raster. The resulting outputs were compared by computing differential flood depth maps (Δ-depth), which quantify changes in water accumulation across scenarios. By analyzing the Δ-depth distributions across the domain, the worst-case configuration was identified, defined as the scenario that consistently generated the greatest flood depth across the urban area. This configuration was then selected for downstream analysis, serving as a conservative input for the mapping of exposure, vulnerability, and potential flood-induced damage.

Once the worst-case flood hazard scenario was identified, based on maximum flood depth corresponding to a 50-year return period rainfall event, it was used to guide the spatial and temporal flood exposure and vulnerability assessment (Nasiri et al. 2016). The aim of this phase was to estimate the number of people potentially exposed to pluvial flooding throughout the day and to characterize the structural vulnerability of affected buildings, enabling a spatiotemporal understanding of risk.

The analysis follows a widely accepted risk framework where damage (D) is conceptualized as the product of exposure (E) and vulnerability (V) (Dewan, 2013). Although no monetary estimation was performed, this formulation guided the integration of flood hazard, population exposure, and building vulnerability within a unified spatial workflow.

Population exposure was assessed by applying hourly occupancy coefficients to each building, reflecting typical fluctuations in use (residential, commercial, recreational, etc.) (Wang et al. 2023). These values were then overlaid onto the flood depth raster to produce dynamic exposure maps, highlighting how the number and spatial distribution of exposed people change over time. The dynamic exposure model allows for the identification of critical time windows when population presence in flood-prone areas is highest, particularly in residential and recreational buildings located near potential water accumulation zones.

Buildings vulnerability assessment was conducted based on building characteristics, including construction period, material, number of floors, and typology. This classification, derived from Taramelli et al. (2022), allowed the identification of structures more susceptible to flood damage due to age or fragility. Notably, the study area features numerous buildings dating back to the late 19th and early 20th centuries, which were assigned high vulnerability levels.

This integrated approach enables:

- the identification of critical hours of elevated population exposure;
- the mapping of high-risk building types based on structural fragility;
- the creation of dynamic population exposure maps to support urban resilience strategies.

While no monetary loss estimation or infrastructure prioritization was performed at this stage, the framework provides a basis for future integration of such components and supports risk-informed decision making in urban flood management and climate adaptation planning.

3.3.b.3 Enhancing rainfall monitoring in urban areas by integrating crowdsourced personal weather stations into official networks

3.3.b.3.1 Introduction

Reliable rainfall predictions traditionally rely on long-term data from rain gauges, which have provided essential records for centuries. Italy, for example, hosts one of the oldest rainfall monitoring networks in the world. However, these networks face growing challenges, including decentralization, inconsistent data sharing, maintenance costs, and administrative limitations, which have contributed to a decline in the number of active stations (Moccia et al. 2024, Mazzoglio et al. 2020). Consequently, data gaps and outdated records hinder effective rainfall monitoring, particularly in urban areas where rainfall variability can be high.

Emerging technologies, such as Personal Weather Stations (PWSs), offer a promising opportunity to address these challenges. PWSs are low-cost tipping bucket rain gauges installed by citizens for home automation, which use Internet-of-Things (IoT) technologies to share real-time rainfall data on online platforms (McCabe et al., 2017). These stations are increasingly popular due to their affordability, ease of installation, and ability to provide data in near real-time. They aggregate vast amounts of crowdsourced weather observations, forming an extensive and accessible data repository. However, PWSs were not initially designed for hydrological or hydroclimatic monitoring, and their accuracy is influenced by installation practices and other user-dependent factors. Despite these possible limitations, recent studies demonstrate the potential of PWSs to enhance traditional rainfall monitoring networks. Indeed, several researchers have explored various methodologies to validate, correct, and integrate PWS data with official rain gauge networks, yielding promising results (de Vos et al., 2017, 2019; Bardossy et al., 2021; Chen et al., 2021). These methods include real-time correction algorithms, geostatistical techniques, machine learning frameworks, and quality control systems (El Hachem et al., 2024). PWS data has also been used to refine radar precipitation estimates, highlighting its potential for improving spatial rainfall resolution (Overeem et al., 2024; Nielsen et al., 2024).

In this study, we aim to improve precipitation monitoring in small catchments and urban areas, where traditional rain gauge networks might often fail to capture rainfall's spatio-temporal variability. By leveraging the widespread use of PWSs, which outnumber official rain gauges but suffer from data quality issues due to inconsistent deployment and maintenance, we aim at integrating PWS data with official datasets using robust and tailored quality control (QC) algorithms. Drawing on and refining existing QC methods from the literature, our framework will address errors arising from suboptimal installation and non-expert maintenance, adapting to Italy's diverse geographical and climatic conditions. Through validation across regions and timescales, the framework will standardize QC procedures, enhancing the reliability of PWS data for hydrological modeling, flood forecasting, urban planning, agriculture, and other sectors dependent on accurate rainfall information.

3.3.b.3.2 Methodology

Netatmo is one of the leading platforms for PWSs (https://www.netatmo.com/it-it/smart-weather-station), offering rain gauges that transmit data via wireless technology to an internal module. These measurements are sent to a cloud service every five minutes, allowing users to access them through an API. Despite their potential for enhancing rainfall monitoring, PWS networks face challenges. High spatial and temporal resolution is offset by systematic errors and a lack of standardized installation and maintenance, often compromising data reliability. QC procedures are therefore essential to ensure the suitability of PWS data for hydrological applications.

In this study we aim at developing a framework to integrate PWS data with official monitoring networks to enhance spatial rainfall resolution. Our framework identifies eligible Netatmo PWSs in Italy and applies a two-step QC process. In a first step, measurements from the Netatmo and the official meteorological networks are compared to capture the correlation and deviations in recorded precipitation. Each PWS station is here compared to the closest official station. In a second step, by synthesizing and refining existing

QC methods from scientific literature and adapting them to the diverse geographical and climatic conditions of Italy, we aim to provide, assess and improve the reliability of PWS rainfall observations.

3.3.b.4 Evaluation of temporal trends in short-duration rainfall extremes

3.3.b.4.1 Introduction

Over the past few decades, the frequency and intensity of extreme rainfall events have garnered significant attention on a global scale (Alexander et al., 2006; Westra et al., 2014; Guerreiro et al., 2018; Papalexiou and Montanari, 2019; Fowler et al., 2021; Poschlod and Ludwig, 2021).

In the Mediterranean region, Italy represents a particularly intriguing case study due to its diverse and complex topography. In Italy, elevations range from areas below sea level in the Po River floodplain to peaks exceeding 4,800 meters in the Alps. Additionally, the geographic distribution of the country, with large portions shielded by the Alps while two-thirds of the territory is exposed to the Mediterranean Sea, introduces further complexity in understanding rainfall patterns. These factors make it challenging to achieve homogeneous results in analyses conducted at the national scale.

Historically, comprehensive nationwide studies were constrained by the fragmentation of datasets, managed independently by various regional hydrological services. Despite these challenges, recent reconciliations of datasets have allowed for broader and more integrated investigations (Libertino et al., 2018; Mazzoglio et al., 2020).

Regional-scale studies conducted over the past two decades have often found that trends in rainfall extremes (1 up to 24 h duration) lack statistical significance over large portions of Italy. These findings were consistent across numerous investigations, regardless of the dataset or method used (Crisci et al., 2002; Bonaccorso et al., 2005; Arnone et al., 2013; Persiano et al., 2020; Avino et al., 2021; Treppiedi et al., 2021; Roseto et al., 2023; Avino et al., 2024). A closer examination of data reveals significant spatial heterogeneity: trends differ markedly even within small geographic areas, with distinct tendencies emerging for the same rainfall duration in neighboring locations (Crisci et al., 2002; Libertino et al., 2019; Mazzoglio et al., 2022; Roseto et al., 2023; Avino et al., 2024). Furthermore, rainfall durations such as 1, 3, 6, 12, and 24 hours often exhibit opposing trends within the same region, highlighting the variability and localized nature of rainfall extremes.

The timeframe of analysis also plays a critical role in the observed trends. For example, Crisci et al. (2002) identified a change in rainfall extremes in Tuscany during the 1970s. Using data from the 1970s up to 1994, they observed a pronounced increase in extreme events. However, when extending the analysis to include earlier records (1951–1994), negative trends dominated for shorter durations, illustrating the temporal sensitivity of trend analyses. Such variability underscores the importance of carefully defining the temporal window for any investigation into rainfall extremes.

Italy's fragmented datasets and the diversity of methodologies used in previous studies have posed challenges for synthesizing findings and making robust comparisons (Caporali et al., 2021). Despite these limitations, each investigation has provided valuable insights into the dynamics of rainfall extremes. The need for more comprehensive and unified research efforts remains critical to advance understanding of the temporal and spatial variability of extreme rainfall across the country.

3.3.b.4.2 Dataset

In this work, trends in short-duration rainfall extremes (1 to 24 hours) are evaluated across Italy using the most up-to-date version of the Improved Italian Rainfall Extreme Dataset (I^2-RED) (Mazzoglio et al., 2020). The dataset's coverage of both convective events (represented by 1-hour maxima) and stratiform events (captured by 12- and 24-hour maxima) provides valuable insights into different rainfall phenomena.

This dataset comprises annual maximum rainfall depths from 5,563 time series (Figure 8), covering the period from 1916 to 2022 (Figure 9). Rain gauges included in this dataset are distributed across elevations ranging from -3 meters to over 3,000 meters above sea level. Compared to a previous dataset used in Libertino et al. (2019), this version includes over 28,000 additional records for each rainfall duration, significantly

enhancing the scope of the analysis. However, the dataset still contains discontinuities caused by station relocations, sensor upgrades, and malfunctions, which are inherent challenges in long-term hydrological datasets.

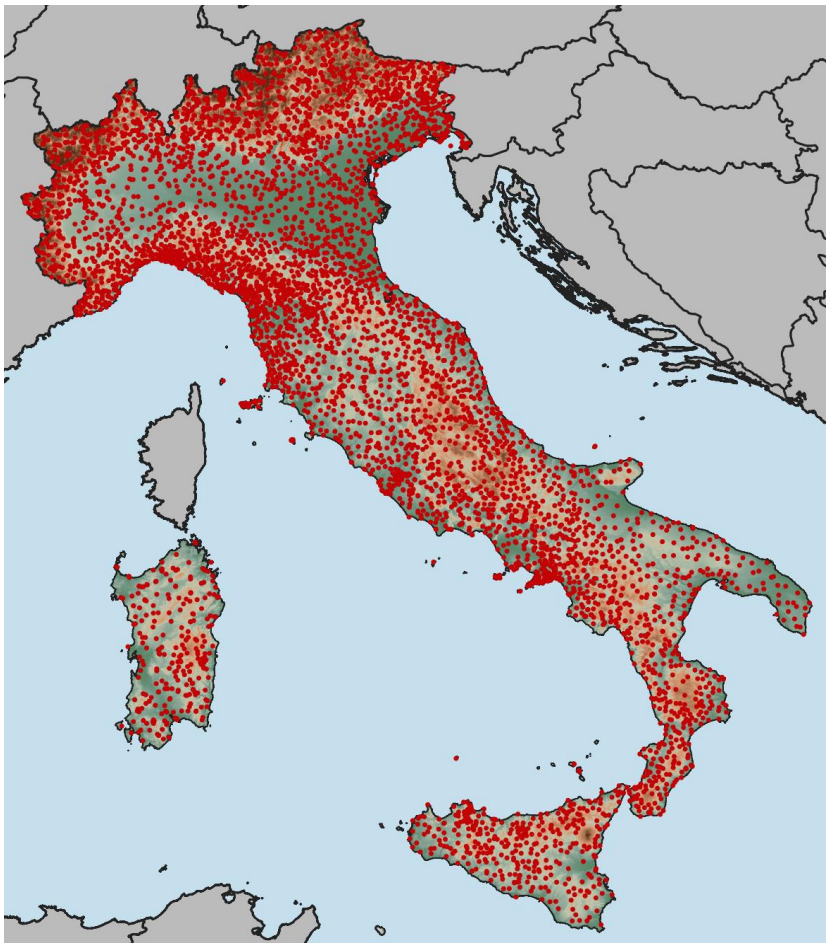

Figure 8. Location of the rain gauges used in this work.

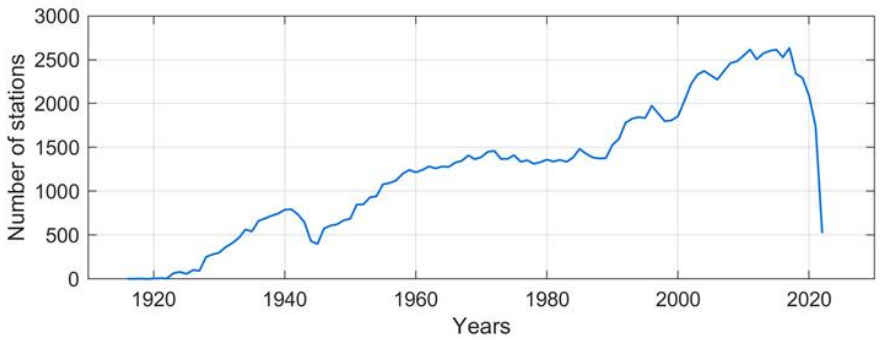

Figure 9. Number of rain gauges active in each year.

This rainfall observation dataset was selected because, within the framework of EXTRAFLOOD (Spoke VS1), an analysis was conducted comparing annual maximum precipitation values from a high-resolution convection-permitting model (CPM) named VHR-PRO_IT with observational data. The comparison revealed significant underestimations of the rainfall depths derived from the CPM, particularly in coastal areas. Additionally, the dataset starts in 1980. As a result, we deemed I^2-RED the most suitable choice for our study.

3.3.b.4.3 Methodology

To address these data fragmentation challenges, the study employs two complementary methodologies:

i. the Mann-Kendall test for detecting trends, combined with Sen's slope for estimating their magnitude;

ii. a distributed quantile regression.

The Mann-Kendall test is a widely used non-parametric method that evaluates the statistical significance of trends, while Sen's slope provides a measure of their magnitude. The MK is based on the ranking of observations, and not on their absolute values; being nonparametric it does not require assumptions on the distribution of observations. To obtain meaningful results, the analysis requires time series with at least 30 years of data. No constraints on the possible presence of missing data or different periods covered is put in place. However, to maximize the number of usable time series, data from rain gauges located less than 1 km apart were merged, selecting the maximum recorded value in cases of discrepancies. This preprocessing step increased the number of usable time series from 1,562 to 1,614, enabling a more comprehensive analysis. Quantile regression, a robust method for analyzing trends across different quantiles rather than focusing solely on the mean, was employed to address issues of data fragmentation and variability. This approach allows for the examination of trends in the median (0.5 quantile), as well as in higher quantiles such as the 95th (0.95) and 99th (0.99) percentiles. By pooling data within specific spatial areas, quantile regression overcomes limitations caused by fragmented time series and allows for consistent analysis across the country. The analysis uses grid resolutions of 10, 20, and 25 km, with data pooled from circular areas with radii of 1.5 to 3 times the grid size. This method ensures that trends are assessed using a consistent time window (1960–2022) across all regions, enabling direct comparison of results. The chosen timeframe aligns with other European and national-scale studies, facilitating broader comparisons (Blöschl et al., 2019; Persiano et al., 2020; Bertola et al., 2021).

3.3.c Enhanced methodology for analyzing forest fires impacts on network CI and on slope instability

3.3.c.1 Probabilistic risk assessment for isolated areas in connection to forest fires

Critical infrastructure – especially electricity networks and roads – are highly vulnerable to climatological threats and especially forest fires (Sfetsos et al., 2021). In this context, we analyse direct and indirect effects of forest fires on critical infrastructures according to two main processes:

i. the effects of the fire on road networks in terms of disruptions or temporary lack of functionality, with the aim of analyzing the indirect effects in terms of risk of isolation for rural/remote areas;

ii. the modifications induced by forest fires on the mountain environment, and the consequent modifications in hydrological risk conditions that could affect critical infrastructures.

3.3.c.1.1 Introduction

In this activity, we aim to identify, with a probabilistic approach, those areas (e.g. small towns) that can remain potentially isolated because of forest fire events.

From the methodological point of view, the problem is analogous to the one analysed and described in D.3.1.1 for flood events; therefore, many similarities are present in the two formalizations. The problem of identifying the potential isolation of (small) areas in connection to natural events is already well recognized; usually, it is studied in the context of the potential impacts of single events using classical approaches of network analysis (Taylor and Susilawati, 2012; Alasia et al., 2017). However, up to date we are not aware of studies that address the problem of isolation (that involves road functionality analysis) from a probabilistic point of view. The true value of probabilistic risk assessment (PRA) is often misunderstood, primarily because it is perceived as a complex and challenging method to implement and interpret. This complexity can create communication barriers when presenting results. However, a probabilistic risk profile should be viewed as a diagnostic tool, providing critical insights into potential hazards and their consequences. These profiles encompass all possible risk scenarios within a given geographical area, accounting for both low-frequency, high-impact events and high-frequency, lower-impact events. They quantify the probability of occurrence while incorporating all components of the risk equation—risk = hazard × exposure × vulnerability—along with their variability and associated uncertainties. Crucially, PRA also considers events that have never been recorded but could arise under future climate projections. This capability is particularly significant as climate change increases uncertainty about hazard patterns. By calculating worst-case scenarios, societies can better prepare for potential impacts. In this context, probabilistic analysis emerges as the only viable method to address such uncertainty in a practical, quantitative manner. For these reasons, this methodological paper presents the formalization of an approach for introducing the evaluation of isolation of remote areas in connection to forest fire events in the framework of probabilistic risk assessment. The methodological approach presented here is in line with the one described in activity D.3.1.1 for flood events. Differences arise in the approach for scenario generation, in the identification of areas that can be considered as homogeneous from the potential impact point of view, and in the integration of the vulnerability component. This work will start from summarizing the main characteristics of PRA; then, a possible decomposition of the isolation problem will be introduced, designed for its integration on the PRA framework.

3.3.c.1.2 The Forest Fires Probabilistic Risk Assessment (PRA) framework

In this activity we want to assess risk for isolated areas in a probabilistic way: to perform a scientifically sound probabilistic study it is necessary to produce a set of scenarios that result in a collectively exhaustive and mutually exclusive sample. Aim of the forest fires scenarios generation is the simulation of all the possible events that can affect different areas of the region/country with different intensities. The methodology for scenarios generation that is used in this project is based on a consolidated approach already applied and tested in several countries in Africa (e.g., Rudari et al., 2019; CIMA Research Foundation and Internal Displacement Monitoring Centre, 2024; Trasforini et al., 2024) in this case adopted and modified to assess

forest fires. The scenario generation process consists of two components: the first one is the event definition and selection and the second one is the probabilistic events generation. Events are selected where meteorological conditions could lead to the development of a wildfire. The meteorological variables considered are wind speed and relative humidity, as provided at the scale of the climate model. To simplify and optimize risk calculation, the spatial domain is divided in homogenous areas from a hazard point of view (HHAs). The event selection is based on a consolidated approach that balances the need of capturing small scale events and the limited computational resources during the generations process. The event selection process is able to identify localized events affecting only one or few HHAs and more distributed ones affecting several HHAs contemporary. These events are the basis for the probabilistic scenarios' generation. The methodology that CIMA Foundation uses for the events generation relies on a multivariate statistical approach that takes in input the selected independent events and, by preserving their spatial correlation, it is able to simulate events not yet observed both in terms of intensities as well as geographical distribution. The approach used for the events generation covers all the possible range of intensities and spatial dependencies and assures that:

- the spatial correlation of small- and large-scale events is preserved in the simulated event set;
- the statistical properties of the observed events at each location is preserved in the simulated event set.

The probabilistic approach applied for the scenarios' generation is based on a probability domain perturbation of the selected events via a multivariate gaussian distribution and uses a gaussian transformation in the probability domain to improve the representation of the tail dependencies and overcome boundary issues: this approach allows to capture and describe very well the correlation between the different HHAs but, at the same time, the scenario generation allows to simulate events that never occurred but may occur in the future. The strength of this approach is linked with the capability of the scenarios modelling of preserving the statistical properties of what has been observed, on one side, but going beyond that, on the other side. The output of the scenario generation process is an event catalogue covering thousands of years providing information on climate conditions able to lead to the development of a wildfire. This event catalogue is then merged with the forest fire hazard map. This map is obtained as a combination of two elements: the wildfire susceptibility map, defined as the static probability of experiencing wildfires in a certain area, and fuel information. Fuel type maps can be defined starting from common land cover/land use maps; further details on the elements described in the following can be retrieved in (Fiorucci et al., 2024) Four fuel types (Table 2) are retrieved with the purpose of discriminating the potential fire behavior given the land cover characteristics.

Table 2. Fuel type of classification and empirical association with the potential intensity.

Fuel Type	Description of fire behavior
Grassland and Cropland	LOW maximum potential intensity
Low flammable forest	MEDIUM maximum potential intensity, forests composed mainly by broadleaves
Shrubland	HIGH maximum potential intensity
High flammable forest	VERY HIGH maximum potential intensity likely characterized by crown fires, forest composed mainly by coniferous

The wildfire hazard map is obtained combining susceptibility and fuel information using a contingency matrix. The drafted contingency matrix reported below allow (Figure 10) to define six levels of hazard from very low to extreme.

S / Fuel	Grassland	Low Flammable Forest	Shrub land	High Flammable Forest
Low Susc.	Very low	Low	Medium	Medium-High
Med. Susc.	Low	Medium	Medium-High	High
High Susc.	Medium	Medium-High	High	Extreme

Figure 10. Contingency matrix for defining the wildfire hazard levels.

An example of wildfire hazard map is shown below (Figure 11) for Western Balkans and Turkey.

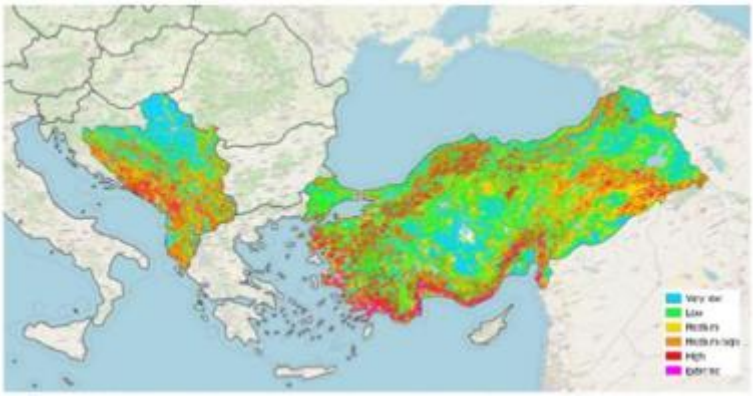

Figure 11. Example of wildfire hazard map (Fiorucci et al., 2024).

When climate conditions, provided by the event set catalogue, are capable in one or multiple HHAs to lead to a forest fire, it is possible to assess the impact that such fire can have on the exposed elements using vulnerability curves. Each exposure category has its own characteristics (physical, structural, etc.) thus they can be affected in a different way from a wildfire characterized by the same severity level. This implies using different vulnerability function depending on the asset and hazard level. An example of vulnerability table for physical infrastructure is shown in Table 3.

Table 3. Example of vulnerability table for physical infrastructure.

Hazard level	Potential damage [%]
1 (Very Low)	0
2 (Low)	0
3 (Medium)	10
4 (Medium-High)	20
5 (High)	30
6 (Extreme)	50

For each event included in the event catalogue it is possible to estimate direct losses that can be used to assess classical risk metrics (e.g., AAL and PML). In this activity the goal is to move from direct impacts to the road network to impacts to road network functionality. A description of the methodological approach to go from direct to indirect impacts is provided in the next session.

3.3.c.1.3 Sub-problems at network level and formalization of the approach

Road networks are a critical component of Critical Infrastructure (CI), essential for the transport of goods, people, and services. Recognizing their importance, international frameworks such as the Sendai Framework for Disaster Risk Reduction, the EU Commission's infrastructure initiatives, and the COP26 agreements emphasize minimizing damage to CI and ensuring service continuity.

Key elements for analyzing road networks as CI include:

1. *Structural Element*: Examines physical damage to components like bridges and tunnels.
2. *Functional Element*: Focuses on operational performance and disruptions to travel.
3. *Topological Element*: Assesses network connectivity and resilience during failures.
4. *Logical Element*: Investigates dependencies and how disruptions propagate.
5. *Dynamic Element*: Considers temporal changes due to construction, urban development, or disasters.

For isolated locations, it is crucial to evaluate the network's ability to maintain connectivity and functionality under specific hazardous events. The process involves addressing the following sub-problems:

- Identification of potentially isolated locations, based on the road network analysis.
- Identification of centroids representative of service providing locations
- Identification of optimal paths between pairs of origin and destination nodes
- Assessing the Impact of Road Segment Loss on Network Connectivity and Functionality
- Inclusion in the probabilistic risk assessment process

The first three steps are not tied to any specific hazardous event, as they concentrate on defining and characterizing the road network. These steps are consistent with those outlined in Deliverable 3.1.1, which focuses on the impact of river floods. For a more detailed explanation of these preliminary steps, refer to the methodological report in D.3.1.1. In this context, we provide only a brief summary to avoid redundancy and ensure clarity.

Identification of Potentially Isolated Locations (*o*):

The identification of isolated locations using road network analysis involves assessing areas that exhibit limited connectivity and accessibility. Literature presents various approaches to defining and measuring isolation (Taylor et al., 2012, Alasia et al., 2017). Our analysis aims to pinpoint localities that are intrinsically poorly connected within the road network while hosting a resident population.

These are nodes ($o = 1, \ldots, O, O \subseteq N$) in the road network graph $G = (N, A)$, where N represents nodes and A represents arcs. The focus is on population centers with limited connectivity, identified using metrics like the remoteness index or network-based measures.

Identification of Service-Providing Locations (*d*):

Service centers ($d = 1, \ldots, D, D \subseteq N$) are defined as nodes in the network that attract or serve local populations. Metrics like the Population Weighted Index and Opportunity Weighted Index are used to quantify accessibility to these service centers (Wachs and Kumagai, 1973; Chen et al., 2015; Papilloud et al., 2021).

Determination of Optimal Paths:

Connections between origin (*o*) and destination (*d*) nodes are analyzed using the *k*-shortest paths ($P_{o,d}^{k}$, $k=1,\ldots,K$), which represent the *K* most efficient routes between pairs of nodes. The analysis employs a generalization of Dijkstra's algorithm (Dijkstra, 1959) to compute these paths, enabling the identification of alternative routes and redundancy in the network. The analysis focuses on the subset of the network composed of the K-shortest paths for each origin-destination pair. Disruptions to these paths because of forest fire events are evaluated to measure their direct and indirect effects on network performance. In the context of probabilistic risk assessment (PRA), direct impacts are typically evaluated using fragility or vulnerability curves/functions. These models are essential components of disaster risk assessments, as they link hazard intensity to the potential extent of damage or loss. A review of existing functions is behind the scope of this paper; nevertheless, we can assume that proper models for the area under analysis can be identified for forest fires, like the one introduced in Section 3.3.c.1.2. We evaluate direct impacts at the level of homogeneous hazard area (HHA), identifying with $y = 1, \ldots, Y$ the generic homogeneous hazard area, we can indicate as

$$P_{o,d}^{k,y} \tag{3.3.5}$$

the set of road links belonging to the *k*-shortest path between origin *o* and destination *d*, localized within homogeneous hazard area *y*. When considering a specific scenario event, characterized in terms of hazard level for each location, we can apply the proper vulnerability function and obtain a further sub-set of links, namely:

$$\left(\bar{P}_{o,d}^{k,y}\right)_e \tag{3.3.6}$$

the set of road links belonging to the *k*-shortest path between origin *o* and destination *d*, localized within homogeneous hazard area *y* and that are non-negligibly damaged by the event *e*. In addition, let's define:

$$\delta_{(i,j)}^{y,e} = \begin{cases} 1 \; if \; (i,j) \in \bigcup_k \bigcup_{o,d} \left(\bar{P}_{o,d}^{k,j}\right)_e \\ 0 \; otherwise \end{cases} \tag{3.3.7}$$

a Boolean variable assuming value equal to 1 if the arc (*i*,*j*) belonging to set *A* is part of any of the *K* shortest paths between origin *o* and destination *d*, it is localized homogeneous hazard area *y* and it's non-negligibly damaged by the event *e*.

A synthetic indicator of direct impacts at homogeneous hazard area *y* for the generic event *e* can be defined as:

$$DI_e^{xy} = \sum_{(i,j)\in A} \delta_{(i,j)}^{y,e} \tag{3.3.8}$$

In road network analysis, the impacts of an event are not confined to the footprint of physical damage but extend to broader connectivity disruptions. Therefore, it is crucial to explicitly account for these connectivity impacts using appropriate methodologies and metrics derived from network analysis.

The concept of centrality, initially developed in social sciences, is particular useful in this context; conceptually, centrality measures how central an individual is positioned in a social network (Peng et al., 2018). Several metrics for measuring centrality have been proposed in literature, as for instance betweenness and closeness. Betweenness centrality quantifies the frequency with which a node or edge falls on the shortest paths connecting other pairs of nodes in the network. Such a metric highlights critical points in the network whose disruption could significantly impact overall connectivity (Freeman, 1977). Closeness centrality, on the other hand, measures the average distance (in terms of the number of edges or their length) from one node to all other nodes in the network. It provides insights into how efficiently a node can access other parts of the network, emphasizing its role in maintaining overall connectivity. An overview on betweenness and closeness can be found in Bozzo and Franceschet (2013) and Newman (2010). For each vertex in the network, both betweenness and closeness centrality can be calculated to identify vulnerabilities and critical nodes. This approach helps to assess the cascading effects of disruptions beyond the physical damage area, offering a more comprehensive understanding of the event's impact on the road network. Let's define:

$$c_i \;\; \forall i \in N \tag{3.3.9}$$

a value representing betweenness or closeness centrality of node *i*. A synthetic index representing the loss of connectivity for a generic event *e* for a homogeneous hazard area *y* can be defined as in the following:

$$CL_e^y = \sum_{(i,j)\in A} \delta_{(i,j)}^{y,e} \cdot c_i \cdot c_j \tag{3.3.10}$$

Assuming that the *k* paths between each pair of potential origins and destinations are sufficiently representative of the actual connection between the corresponding locations, the non-functionality of one or more of these paths indicates possible isolation. Under the assumption that:

$$\mu_{o,d}^{k,y,e} = \begin{cases} 1 \; if \; P_{o,d}^{k,y} \neq 0 \\ 0 \; otherwise \end{cases} \tag{3.3.11}$$

That is, it takes the value of one only when, within the homogeneous hazard area *y*, there are links belonging to the *k*-shortest path that connects the pair (*o*, *d*).

$$\gamma_{o,d}^{k,y,e} = \begin{cases} 1 \; if \; P_{o,d}^{k,y} \neq 0 \; and \; \left(\overline{P}_{o,d}^{k,y}\right)_e \neq 0 \\ 0 \; otherwise \end{cases} \tag{3.3.12}$$

That is, it takes the value of one only when, within the homogeneous hazard area *y*, there are links belonging to the *k*-shortest path that connects the pair (*o*, *d*), and at least one of these links is damaged by the effects of event *e* within the same area.

The isolation index associated with a generic origin *O*, as a function of the effects of an event *e* within the homogeneous hazard area *y*, can be defined as:

$$II_o^{y,e} = \begin{cases} \frac{\sum_{k=1}^{K} \sum_{d\in D} \gamma_{o,d}^{k,y,e}}{\sum_{k=1}^{K} \sum_{d\in D} \mu_{o,d}^{k,y,e}} \; if \; \sum_{k=1}^{K} \sum_{d\in D} \mu_{o,d}^{k,y,e} > 0 \\ 0 \; otherwise \end{cases} \tag{3.3.13}$$

If the set of impacted links has a non-empty intersection with $P_{o,d}^{k}$, we can assume that such a path is no longer usable; consequently, the connection between *o* and *d* will be reduced, up to the extreme case where none of the *k*-shortest paths connecting *o* and *d* are functional.

The fraction of functional paths serves as an index of potential reachability (indirect impacts).

Integrating this type of network analysis, which captures both the direct and indirect impacts of forest fire events, into a Probabilistic Risk Assessment (PRA) framework allows to assess traditional risk assessment metrics, such as the Annual Average Loss (AAL) and the Probable Maximum Loss (PML).

Specifically, this approach enables the calculation of the annual average loss of connectivity and functionality at various geographic scales, including provincial, regional, and national levels. Furthermore, it offers a detailed assessment of losses associated with specific return periods, such as 5, 10, or 25 years. By quantifying these metrics, stakeholders gain a comprehensive understanding of the systemic effects of forest fires on infrastructure networks and can identify critical locations where disruptions could significantly increase isolation risk.

3.3.c.1.4 Conclusions

The present study focuses on identifying areas, particularly small towns, that may become isolated due to forest fires, using a probabilistic risk assessment (PRA) approach. It builds on methodologies previously developed for flood events (Deliverable 3.1.1) while introducing refinements specific to forest fires. PRA is emphasized as a diagnostic tool for understanding hazards, integrating the probabilities of occurrence with exposure, vulnerability, and climate-change-related uncertainties. The objective is to incorporate isolation risks within the PRA framework by developing a formalized methodology, enabling a quantitative analysis to enhance societal preparedness.

The methodological coherence in the event generation for PRA, and in the inclusion of network analysis elements, both for floods and forest fires open the floor to the possibility to develop a multi-hazard framework. A first step in this direction is the possibility to use coherent metrics, like AAL and PML, for both tha hazards, even if they are treated as indipendent. In addition, the scenario generator that is at the basis of the PRA allows for a wider integration of the two hazards, starting from the scenario generator: a) by considering the same climate model as direct input for the scenario generator for forest fires and as input for the hydrological modelling for floods b) by using the scenario generator for defining a set of multi-hazard event, as in CIMA Research Foundation et al. (2023).

3.3.c.2 New method for wildfire hazard mapping and consequent hydrological risk management

3.3.c.2.1 Introduction

The activity of the subtask is aimed at studying landslides hazard in relation to forest fires, by taking into account the modifications induced by forest fires on the mountain environment (e.g., loss of vegetation inducing erosion phenomena, modification of the soil infiltration rate). To this end, it is essential to define the timeframe for the restoration of pre-fire conditions and assess the stability of the affected area during this restoration period.

The activity is divided into three lines: 1) identification of areas recently affected by fire by means of remote sensing techniques and assessment of the relative magnitude, possibly also through integration with existing forest fires static risk mapping; 2) experimental analyses in the laboratory to study - by means of controlled fire tests - the variation of hydrogeological parameters in the terrain; 3) use of literature models to verify the stability of slopes in burnt areas. The overall objective is to develop a dynamic hydrogeological model that allows the thresholds for the triggering of landslide phenomena in burnt areas to be defined, considering the variation of the hydrogeological characteristics of the site during the period of restoration of initial conditions. On the basis of this model, new EWSs will also be defined that take into account the legacy of the forest fire.

3.3.c.2.2 Literature and remote sensing analysis of area recently affected by wildfires

Among the different types of landslides, shallow landslides and debris flows are the most influenced by climate changes, as their triggering is related to a rainfall regime and a particular predisposing factor expected to increase with the global temperature rise is the wildfire occurrence. Several scientific studies demonstrate the variation of slope stability after wildfires, highlighting also how this problem could increase in the future because of the climate change. For instance, Huang et al. (2015) showed that the occurrence of wildfires is highly sensitive to fire meteorology (such as temperature, precipitation, and relative humidity), vegetation type and coverage, as well as anthropogenic ignition sources. In specific, the authors investigate the potential impacts of climate change on wildfire frequencies over the period of 2000–2050 and demonstrate that the fire frequencies under the 2050 conditions would be projected to increase by approximately 27% globally relative to the 2000 levels. Significant increases in fire occurrence will be calculated over the Amazon area, Australia and Central Russia, while Southeast Africa will show a large decreasing trend due to significant increases in land use and population. In a different location, in a Mediterranean locality of NE Spain, Pinol et al, 1998 calculated two wildfire hazard indices based on daily meteorological data for a period from 1941 to 1994 and both increased as a consequence of increasing mean daily maximum temperature and decreasing minimum daily relative humidity. Cannon et al., 2009 showed that the increasing urbanization of the western USA (in specific southern California and the intermountain west of the USA), combined with the increased wildfire magnitude and frequency, provoke an increase of debris-flow occurrence. Parise et al., 2012 identified two primary processes for the initiation of fire-related debris flows: the first was the runoff-dominated erosion by surface overland flow and the second infiltration-triggered failure and mobilization of a discrete landslide mass. They studied a Mediterranean area in Western USA and stated that surficial landslide failures in burned areas most frequently occur in response to prolonged periods of storm rainfall, or prolonged rainfall in combination with rapid snowmelt or rain-on-snow events. Doerr et al. (2006) studied the effects of different fire severities on soil water repellency in eucalypt forest catchments in the Sandstone Tablelands near Sydney, burnt in 2001 and 2003. Their results demonstrate that existing fire severity classifications are not well suited to predict fire impacts on soil hydrological responses and highlight the need for a new fire severity evaluation scheme. A scheme encompassing not only foliage and ground cover status, but also changes to surface and subsurface soil hydrological properties, would provide a better prediction of the immediate hydrological effects of wildfires on catchments such as flash flooding and erosion. Giannaros et al. (2023) highlighted that fire weather is one prominent driver of fire activity and the relationship between fire weather extremes and burned area in Europe revealed that the number of extreme fire weather days per year correlates positively with the annual burned area over most of the study domain. Their analysis revealed that, at the regional scale, significant change-points occurred around the late 1990s and mid-2000s in the Mediterranean, marking an abrupt rise in the median of extreme fire weather days per year.

As for the case studies discussed above, the relevance of the wildfire research for mountainous environments in temperate climatic areas, such as the Alpine region, is clear. Abbate et al. (2019) used a hydrological model to assess wildfire impacts on slope stability, comparing results with existing stability thresholds. Case studies in Italy (Ardenno, Province of Sondrio) and Switzerland (Ronco sopra Ascona, Locarno district) showed that post-fire conditions drastically reduce soil water absorption, making slopes more vulnerable to even light rainfall events. The results quantitatively indicated how the post-fire circumstances strongly modify the ability of the terrain to absorb rainfall water; this resulted in a persistently drier terrain until a corner point is reached, after which the stability of the slope could be undermined by a rainfall event of negligible intensity. Conedera et al. (2003) simulated with a good degree of reliability the debris flow of 28 August 1997 which occurred in the Riale Buffaga, a torrent channel in the territory of the village of Ronco s./Ascona (Ticino, Switzerland) and early quantifies the possible consequences of a forest fire in terms of territorial safety. Hyde et al. (2016) provided a summary of the present knowledge of the processes involved in this postfire debris flow hazard cascade and identified uncertainties in terms of knowledge gaps, contradictions in current process understanding, stochastic system variables, and limits to data to support hazard prediction.

The urgency of an in-depth analysis of landslide triggering after 28 wildfires arises in relation to the different characteristics of newly affected regions in terms 29 of vegetation, soil composition and climatic regimes. Wildfires have been widely recognised as a preliminary stage of a ripple effect that starts from the reduction

of vegetation coverage and often leads to a higher chance of slope instabilities (Cannon et al., 2009; Parise et al., 2012). The relationship between rainfall and soil hydrological response grows more intricate as the water balance alters with burning. The disruption of canopy interception influences a significant reduction of evapotranspiration, with a heightened solar radiation at ground level (Greppi, 2005), and a higher net rainfall amount that reaches the soil enhancing erosive processes (Doerr et al.,2006; Abbate et al., 2019; Rosso et al., 2007). The cumulative effect results in increased runoff, coupled with an accelerated velocity, due to the factors and the loss of terrain surface roughness. Additionally, infiltration capacity experiences a modification due to the pore clogging caused by ash deposition (Hyde et al., 2016) and the alteration of natural soil water repellency, as observed by many authors (Doerr et al.,2006; Larson-Nash et al., 2018). Depending on severity and duration of the fire, a shift of some centimetres down of this hydrophobic layer may occur (Doerr et al.,2006). As a result, the superficial burnt layer becomes wettable, and the layer below becomes impermeable. This leads to the potential for rapid saturation in the topsoil, which may evolve into a shallow landslide (Parise et al., 2012; Rengers et al., 2020). Considering the dynamic nature of the post-fire environment, the assessment of possible slope instabilities should account for different recovery timings of vegetation species and possible interactions among phenomena (Stoof et al., 2012; Shakesby, 2011). In the case of burned slopes, the absence of vegetation and the burning of the soil represent two novel elements compared to the classical slope stability problem.

3.3.c.2.3 Field case description

The study focuses on an Alpine wildfire case to derive the impact on the hydrological conditions of the slope at different scales, and to evaluate the recovery time of soils to pre-fire conditions. Soil burning conditions and their evolutions were monitored after the wildfire over the span of three years by field surveys and by remote sensing analyses. The study area is located in Sorico municipality (province of Como), northern Italy, in Central Alps (Figure 12). Here, a wildfire event took place from the 30th December 2018 to the 17th January 2019, burning an approximative area of 1 km^2. The burnt area is on a watershed exposed to south at an elevation around 1000 m asl. The area presents coniferous woods in the less steep part of the slope, and grasslands and shrubs where the slope is steeper (> 25°). Considering the geological setting, the area is covered by glacial deposits from the Last Glacial Maximum and by recent colluvial deposits. The regolith has a heterogeneous granulometry and has an average thickness of one meter. The outcrops consist of gneiss from the zone of Bellinzona-Dascio (BD), a high-grade metamorphic unit, composed by different types of gneisses, minor marble lenses, amphibolites and ophiolitic rocks.

Several analyses with different working scales (from large to small) were carried out in this area: starting from remote sensing analysis to field and laboratory tests on different sample of soil collected in-situ. Sentinel-2 images from the European Copernicus mission were implied for remote monitoring of the study area. Remote sensing allows burnt areas to be identified at larger scales throughout indices based on vegetation reflectance. Also, it enables to estimate fire severity, which is often difficult to derive because the temperatures reached are normally unknown and to investigate large areas, with a high temporal resolution and low cost, is not easy. Field test related to falling-head infiltration tests were performed to investigate also the soil hydrological properties of the three areas over time. At the same time, the collection of some sample of the un-burned and burned soil allowed to carry out different laboratory test by means of landslide and fire simulators.

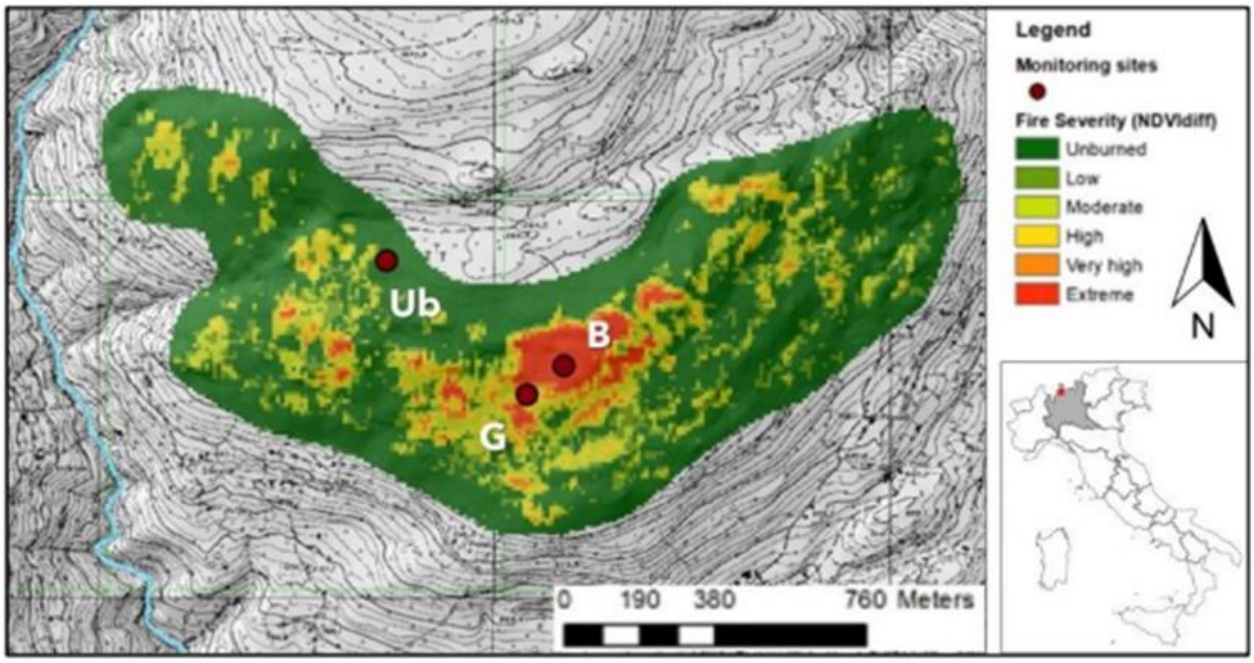

Figure 12. Location of the study area and of the three sub-areas identified for monitoring (B is burnt woods, G is burnt grassland, Ub is unburned woods). Fire severity is also displayed as the difference of NDVI before and after the wildfire, according to Chafer et al. (Chafer et al., 2004).

3.3.c.2.4 Remote sensing analysis

The area monitored in Sorico was distributed over two different vegetation sub-areas inside the former wildfire perimeter, one characterized by burnt conifer woods and the other by grassland; the third monitored sub-area was in a conifer woods, located outside the burnt area. The remote sensing analysis was performed through different remote sensing indices, computed from Copernicus Sentinel-2 raw bands (complete list in Table 4). These indices mainly consider spectral bands that refer to living vegetation characteristics (e.g. chlorophyll absorption peaks, the integrity of leaf cell structure, or the decrease of leaves water content related to the burning of vegetation). Specific indicators of fire occurrence were also considered, as the Normalized Burn Ratio (NBR) and as the Burned Area Index (BAI), which is related to charcoal presence on the ground. Fire severity and its change over time was also estimated, considering the difference of NDVI and NBR indices before and after fire, following Chafer et al. (2004) classification. Initial fire severity is shown in Figure 12. Sentinel-2 images were selected considering favourable meteorological conditions, with a maximum cloud coverage of 30%, and without snow cover, in order to avoid alterations in the moisture evaluations.

Table 4. Remote sensing indices taken into account for the burnt recovery analysis, referred to Sentinel-2 spectral bands (B3 is Green, B4 is Red, B8 is Near InfraRed, B8A is Narrow NIR, B11 and B12 are Short-Wave InfraRed).

Index	Equation
False Color	$[B8 \mid B4 \mid B3]$
Normalized Difference Vegetation Index (NDVI)	$\frac{B8 - B4}{B8 + B4}$
Moisture Index (MI)	$\frac{B8A - B11}{B8A + B11}$
Moisture Index (MSI)	$\frac{B11}{B8}$
Normalized Difference Moisture Index (NDMI)	$\frac{B8 - B11}{B8 + B11}$
Normalized Difference Water Index (NDWI)	$\frac{B3 - B8}{B3 + B8}$
Normalized Burn Ratio (NBR)	$\frac{B8 - B12}{B8 + B12}$
Burned Area Index (BAI)	$\frac{1}{(0.1 - B4)^2 + (0.06 - B8)^2}$

3.3.c.2.5 Experimental analysis: field test execution

Falling-head infiltration tests were performed to assess post-fire infiltration capacity of soils in the three sub-areas, and their potential change over time. The tests were carried out using a single ring infiltrometer and a double-ring infiltrometer (Figure 13). The single ring infiltrometer was a plastic tube with a diameter of 12 cm and a height of 100 cm. The double-ring apparatus was composed by two stainless steel cylinders with a height of 15 cm and diameters of 30 and 60 cm. The main advantage of this kind of test is the low cost, particularly for the plastic single-ring infiltrometer. Falling-head method was preferred to the constant-head method because of the lack of water supply in the nearby of the study area, given that falling-head tests require less water. The test procedure consisted in pouring water into the infiltrometer, and then measuring the variation of the hydraulic head over time. The obtained infiltration rate was corrected to exclude lateral flow divergence component by single-ring tests results, measuring the distance of lateral wetting as in (Bouwer, 1999). The resulting data of infiltration velocity versus test time are infiltration curves that follow the exponential model from Horton (Horton, 1941).

$$f = f_c + (f_0 - f_C) \cdot e^{-K_f t} \quad (3.3.14)$$

where f_c is the field capacity, the asymptotic value of infiltration rate that is related to saturated hydraulic conductivity, f_0 is the initial infiltration rate, which is inversely proportional to the initial soil moisture, and K is a decay constant.

The obtained field infiltration rates were fitted to the following simpler exponential equation, where a is the difference between f_0 and f_c, and b corresponds to the decay constant K of Horton's model:

$$V_{inf} = a \cdot e^{-bt} \quad (3.3.15)$$

These fitting coefficients, a and b, and an approximated f_c value, considered as the infiltration rate value at 4000 s, were evaluated for the three zones over time.

Figure 13. Single (a) and double (b) ring infiltrometers used to perform falling head infiltration tests in Sorico.

Hydraulic conductivity was also estimated as in the Lefranc infiltration test procedure (Norme Français, 2000). Moreover, during the first survey (October 2019), burnt and unburnt soil samples were collected to evaluate their saturated hydraulic conductivity in laboratory, using a falling-head permeameter (Olson et al., 1981). Relations between all the parameters measured on the field over time (a, b, f_c, k) and some meteorological variables (cumulative rainfall of the ten and twenty days prior the survey, solar radiation, temperature and relative humidity) were also investigated by factor analysis (principal components analysis method) (Bro et al., 2014).

3.3.c.2.6 Experimental analysis: laboratory test execution

Focusing on a more detailed working scale, different laboratory tests were carried out on soil sample collected in Sorico study area. In specific, downscaled landslide simulators that are used in a controlled laboratory environment allow to mimic real-world slope conditions and simulate various landslide scenarios by applying different conditions (Wang et al., 2001, Wu et al., 2015). These experiments represent a good strategy to analyse better the influence of the different triggering and predisposing factors to land sliding, such as precipitation intensity and slope. A series of downscaled rainfall-induced landslide simulations were performed with a custom-built simulator where the reclinable surface hosting the material for tests has a size of 2 x 0.8 meters and can be inclined up to 45° (Figure 14). A geogrid positioned at the base of the flume serves to enhance traction between the inclined surface and the material susceptible to landslides. The structure incorporates a system of four sprinklers designed to emulate rainfall at diverse intensities, with each nozzle capable of delivering up to 20.6 mm/h. These sprinklers are arranged in two parallel rows on the structure's top, positioned at a height of 0.6 meters. The distribution of rainfall spray is regulated to be uniform. A pressure reduction valve governs the discharge from the sprinklers and the rainfall intensity can be determined by referencing the pressure-discharge characteristic curve supplied by the manufacturer. This experimental setup provides a controlled environment to investigate the influence of varying rainfall intensities on slope stability, with the geogrid and inclined surface interacting with landslide-prone material. The precise adjustment of simulated rainfall is facilitated by the pressure-discharge characteristic curve, ensuring accurate measurement and control of the experimental conditions (more details of landslide simulator are provided in Ivanov et al. (2020) and Longoni et al. (2022) studies). The simulator was outfitted with a range of monitoring instruments to provide real-time and comprehensive information on parameters such as water content, infiltration, pore water pressure, and degree of saturation. The analysis of these parameters enables a detailed assessment of the progression of infiltration, filtration, and fracture formation processes leading up to collapse. During the tests, the following monitoring tools were employed:

- Time – Domain Reflectometer (TDR)Sensor: Installed for continuous calculation of volumetric water content.

- Tensiometers: up to three devices were utilized to calculate pore water pressure.

In addition to these techniques, geophysical and photogrammetric approaches were employed to cross-compare the information gathered from the sensors. The downscaled landslide body was reconstructed by loading material onto the simulator in three 5-cm-thick layers, compacted to approximately 15 cm thick (with variations depending on the material type), and adopting a trapezoidal shape as illustrated in the Figure 4.

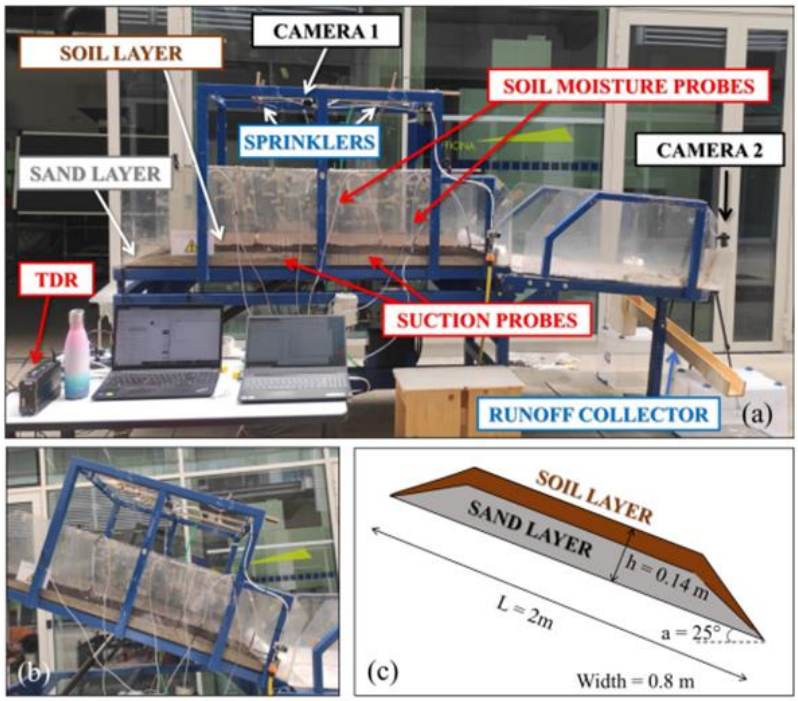

Figure 14. Landslide simulator setup.

The experiments involved different types of the previous collected materials, in fact, tests with un-burnt and burnt soil were compared with tests carried out with homogeneous sand. This comprehensive monitoring and testing approach provides valuable insights into the dynamic processes leading to landslide collapse. Other typology of tests carried out in laboratory deals with fire-controlled test on soil samples. In specific samples of soil are included in a steel cylinder with diameter lower than 50 cm and height of approximately 50 cm, with a vertical lateral opening. Thermocouples are installed every 10 centimeters. The time duration of test is approximately 20 minutes and different target temperatures can be settled into the little hoven (i.e. 150°C, 300°C, 400°C). Similar tests can be carried out into the shock tube (Colombo et al., 2021), that is a rolled steel sheet with a lateral opening of 5 centimeters to look at the developing phases of ground during fire conditions and to carry out test on water repellency.

3.3.d Enhanced methodology for deriving drought effects on the water supply system

3.3.d.1 Drought water service interruptions - Water supply management (reservoir management and integration of different sources) under drought conditions, including analysis of future scenarios of water availability and user demand

3.3.d.1.1 Introduction

An effective and integrated management of drinking-water resources requires the assessment of the impacts of water scarcity, related to periods of hydrological drought, on the use of the available sources. Mediterranean regions are facing more and more frequent water scarcity conditions and are destined to see a further intensification of the gap between water supply and demand in the coming years, due to a combination of climatic and anthropogenic factors. In a context of growing concern about the impacts of climate change and drought events on water availability, sustainable management of different drinking water sources is crucial to ensure the resilience of water supply systems.

Under these circumstances, the implementation of numerical models of the water systems aimed to the optimal management of water supply reservoirs is of fundamental importance. During the last decades, significant scientific advances have been made, as reported in the most recent review papers (e.g. Beiranvand and Ashofteh, 2023; Dobson et al., 2019; Giuliani et al., 2021). Within the different categories of approaches for the optimal reservoir operation, the so-called "parameterization-simulation-optimization" (PSO, Koutsoyiannis and Economou, 2003) is one of the most common optimisation strategies (e.g. Giuliani et al., 2021; Zhang et al., 2017). Moreover, planning adaptation strategies for water supply systems in response to potential climate change impacts is essential (Felisa et al., 2022). In particular, it is important to evaluate the effectiveness of reservoir management rules, typically optimized based on historical hydro-climatic variability, for meeting demand under future climatic stress conditions. To this end, several experts have tested the resilience of operational reservoir rules by forcing the system with an ensemble of regional climate scenarios (e.g. Mereu et al., 2016), while others have compared the results of optimizations conducted on historical or future hydro-climatic series (e.g. Beça et al., 2023; Zhang et al., 2017).

A comprehensive planning process should not only consider expected changes in water availability due to climate change, but also potential variations in water demand, which are influenced by both climate and socioeconomic factors (and, of course, depend on the type of water use). Therefore, water demand analysis and modelling are also required, especially in areas characterised by strong seasonal consumptions (Toth et al., 2018, Cominola et al., 2023).

A methodology for the optimal management of water supply reservoirs in a context of changing climate is here proposed. The approach is developed for water supply systems served by different water sources, i.e. water supply reservoir, rivers and groundwater. The aim is to understand how their exploitation varies as a function of both water demand (current and modelled for future scenarios) and water availability related to droughts conditions and optimise the withdrawal from the reservoir in order to be socially, economically and environmentally sustainable. Once applied, the framework can help to understand the link between hydrological droughts and the exploitation of the different surface and groundwater sources, providing the water managers with insights for short- and long-term planning.

Even if the proposed methodological framework can be applied anywhere, here it is presented in reference to a test-case study. In particular, the approach is applied for the sustainable management of the water resources for drinking water supply in the Romagna region, through the optimisation of the withdrawal rule curves from the Ridracoli reservoir.

The possibility to replicate the approach in other national and international water systems is supported by additional companion researches and by the tools developed within the framework of other Spokes (see Section 3.3.d.1.4).

3.3.d.1.2 Methodology

The proposed methodological framework is represented in Figure 15. The essential data required as inputs (for more details see Section 3.3.d.1.3) are highlighted in grey drums, and include i) meteorological forcings, ii) historical water consumption and iii) historical water supply volumes, along with information on the reservoir (i.e. on spillways, outlets, level/volume/surface relationships, technical and legal constraints on the reservoir operation, etc.), and information on the water availability for the possible alternative sources in the water supply system.

The first step of the approach consists in the set up of the simulation framework (yellow block in the figure), which is composed by two macro modules: i) the rainfall-runoff modelling of the basins feeding the reservoir(s) and ii) the model for the management of the entire system. The rainfall-runoff model, which simulates the hydrological processes leading to the transformation of precipitation into river runoff, is needed to estimate the inflows to the reservoir(s) and the discharges in correspondence of the river intakes (if any) where streamgauges (or reliable flow rating curves) are not available. Furthermore, its use is required to simulate the future streamflow, obtained when providing in input future climatic scenarios. Here, we propose the use of a lumped and parsimonious model structure which can be easily applied everywhere, since it requires minimum amount of input data (meteorological forcings exclusively). On the other hand, the reservoir-system model is necessarily case specific and requires the definition of reservoir operations: intake and release controls, as well as flood protection and maintenance protocols. Its level of detail and temporal resolution may depend on the available historical data and on the complexity of the system itself, and can be adapted to the specific case study. In general, while operational manoeuvres concerning intakes and releases depends on technical regulations and on the current state of the system (e.g. reservoir level), withdrawals are mainly driven by the water demand from the downstream water supply network and are treated separately, being the focus of the approach.

In fact, one of the main goals of the methodology is the formulation of optimal withdrawal rule curves, as function of the system state variables, as for instance the reservoir level. Such process starts with the definition of the domain of the withdrawal rule curves, which primarily depends on the admissible maximum and minimum withdrawal volumes along the year (e.g. daily or monthly). While the maximum is typically related to the technical constraints of pipes and treatment plants, the minimum withdrawal volume represents such portion of demand which cannot be provided by alternative sources. Therefore, it depends both on the water demand from the customers served by the water supply network and on the potential of the alternative sources themselves.

The green block of the diagram in the figure highlights the portion of the methodological framework which can be used for assessing the minimum withdrawal volumes from the reservoir. Historical data of water consumption are first analysed in order to define “critical” demand scenarios in the present scenario. In addition, historical data can be used to set up a water demand model forced climatic and possibly also socio-economic variables and project the demand into the future, to simulate expected changes in the water consumption and future critical demand scenarios.

At the same time, the potential (in terms of daily/monthly volumes) of the less sustainable and more energy demanding alternative water sources (such as wellfields and treatment of poor quality river water) serving the network have to be assessed. Depending on data availability and/or on the depth of system’s knowledge (e.g. expert judgment), such information can be extracted either from historical water supply time series, from numerical models or as function of solely technical constraints. Once critical water demand scenarios and the potential of the alternative sources are assessed, minimum withdrawal volumes can be derived taking into account the architecture and the technical constrains of the water supply network.

Once upper and lower limits of withdrawal have been set, a functional form of the withdrawal rule curves as function of system state variables (e.g. function of the reservoir level) and their corresponding admissible domain are defined. Such domain and the form of the defined functional forms should of course take into account technical limits of pipes, channels, network and treatment plants (e.g. rapid changes in flow rate should usually be avoided). Such withdrawal rule curves are assumed to be defined by one or more parameters which can vary along the year (e.g. weekly, monthly or seasonally) and have to be optimised.

The last step of the approach is the multi-objective optimisation of the parameters of the withdrawal rule curves, with the aim of i) maximizing the withdrawal volumes over the entire simulation period and, at the

same time, ii) minimizing "water deficit volumes", defined as the volumes of resource that, although requested by the downstream network (in particular by such customers who are not served by alternative water sources), it is not possible to withdraw and deliver to the users due to lack of availability in the reservoir.

The optimisation process may be performed multiple times for testing different scenarios by combining i) different meteorological forcings, provided as input to the simulation framework, and ii) different boundary conditions on water demand and on the potential of the alternative sources which influences minimum requests from the reservoir(s). In particular, withdrawal rule curves are optimised by forcing the model either with historical meteorological time series or with climatic future projections (GMC-RCM modelling chains), in order to take into account expected future climatic changes. On the other hand, different water demand scenarios may be used, as well as different boundary conditions on the potential of the less sustainable water sources, due for instance either to a decreasing water availability or to changes in water policies.

The relative changes between the obtained optimal withdrawal rule curves for the different climate or demand scenarios can help to evaluate their impact on the reservoir management, while the historical and future pattern of withdrawal and deficit volumes that are provided as output of the modelling chain can help to improve water resource planning and to estimate future water stress on the different sources. In fact, if sufficient information on the past use of the alternative sources is available, the analysis allows to understand also how the exploitation of the different sources (i.e. reservoir, rivers and groundwater) varies as a function of both urban water demand (current and modelled for future scenarios) and water availability related to droughts conditions (see Toth et al., 2018).

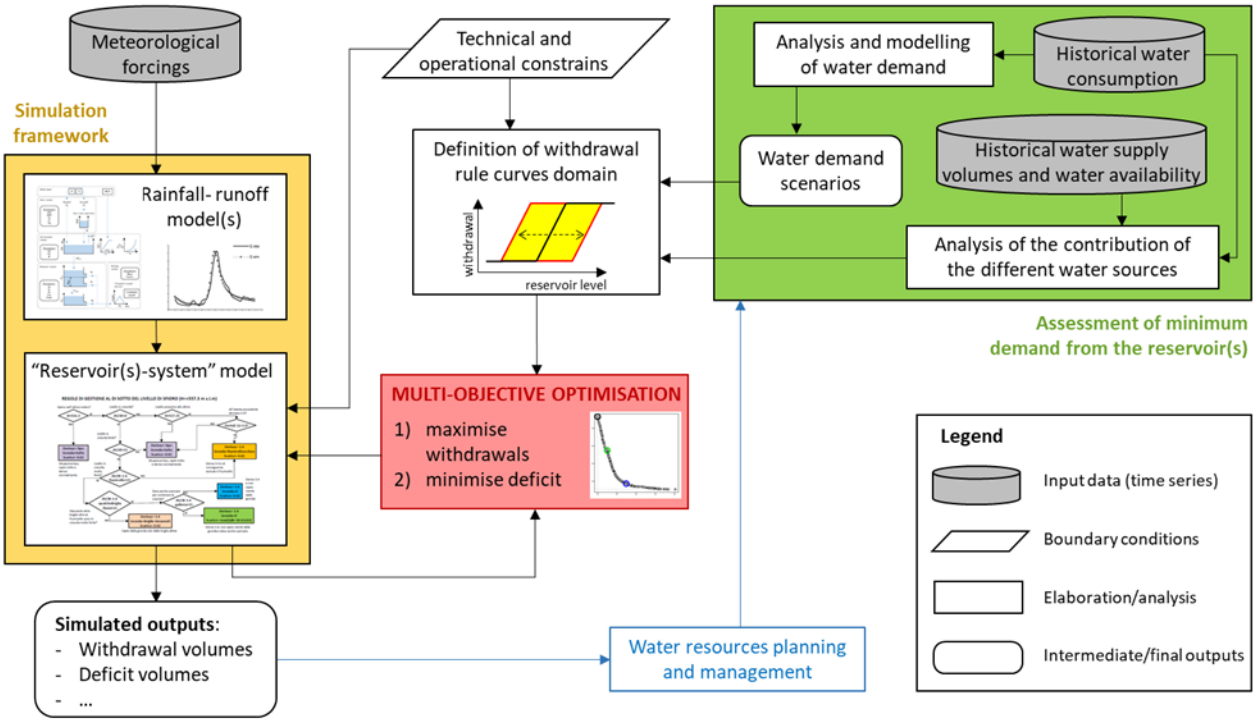

Figure 15. Methodological framework for the sustainable management of a water resource system, through the optimisation of the withdrawal rule curves from the reservoir(s).

3.3.d.1.3 Required data

As already mentioned, the level of detail of the modelling framework and of the boundary conditions is strictly related to data availability. Since in case of missing data assumptions have to be made, the collection of all possible data and useful information represents an essential preliminary phase of the approach. In the following, a list of all useful data and information is reported.

Reservoir geometrical and hydraulic relationships

- level-volume curves (and their updates over time);
- level-lake surface curves (and their updates over time);
- flow rating curves of every outlet and spillway.

Documents and information about the reservoir-system functioning

Information about existing reservoir management rules, operative constraints on intakes, releases, outlet flows, environmental flows and their changes over time, allowed withdrawals. Additional information which helps the reservoir-system model set up can be also used, if available (e.g. operating and maintenance protocols, sediment management protocol and its evolution over time, flood control protocols, agreements with water utilities and/or irrigation consortia about seasonal withdrawal volumes, information on the work schedule, testing, sediment removal, etc. that could explain any anomalies in the data, information about past water shortages).

Documents and information about the other water sources

Information about source management rules, operative and technical constraints, environmental constraints, maximum allowed withdrawal volumes and their changes over time.

Time series (at the finest possible time scale and for the longest possible observation period)

Reservoir:

- reservoir level;
- discharges (volumes) from outlets and spillways;
- withdrawal flows (volumes);
- meteorological data (temperature, precipitation, wind, humidity, etc.);
- "direct" basin (headwater basin closed at the dam) flows calculated through internal water balances;
- other possible inflows (volumes) apart from the direct basin.

Water demand: volumes provided to the users at all the delivery points across the drinking and/or irrigation water supply network. Information on the past and expected climatic (temperatures, rainy days, etc) and socio-economic (such as population, tariff, tourist fluxes) drivers for the water demand modelling.

Additional water sources: withdrawals flows/volumes.

3.3.d.1.4 Companion studies to enhance the replicability of the approach and connections with other Spokes

Choice of the reference meteorological forcing datasets and regionalisation approaches for modelling the streamflow

The rainfall-runoff transformation is one of the two macro modules of the simulation framework and it is needed to simulate the inflows into the reservoir(s) and the discharges in correspondence of the river intakes (if any) in any stream section that is either ungauged or poorly-gauged (since historical flow observations are unfortunately available only for a few stream sections). In many operational cases the rainfall-runoff modelling is thus the only way to obtain information on either past or future water availability in the water system.

A crucial step in the rainfall-runoff modelling approach is the selection of the historical meteorological dataset both to be used i) as input to the rainfall-runoff models in the simulation framework and ii) as reference to validate climatic scenarios during the control period. In order to allow the proposed methodology to be replicated in multiple case studies over the country, the use of gridded meteorological products is convenient to enhance the replicability of the approach. However, the accuracy of such products varies considerably in space and time, and rigorous validation of these products is essential before their application. For this reason, a companion study was conducted (in cooperation with Spoke DS) for the large-scale evaluation of five national and international meteorological products, assessing their ability to

reproduce streamflow when used to force a hydrological model in a large set of basins in Northern Italy. For additional details, please refer to Sarigil et al. (2024).

A second key issue is the application of rainfall-runoff models in totally ungauged basins, where no streamgauges (or reliable flow rating curves) are available. In such cases, rainfall-runoff modelling involves the regionalisation of the model parameters (e.g. He et al., 2011; Neri et al., 2020; Oudin et al., 2008), which cannot be calibrated and are transferred from one or more gauged basins, assumed to be hydrologically similar to the target (ungauged) catchments. Within the framework of the project, a regionalisation approach was implemented to assess water resource availability in small basins to support the planning an management of reservoirs for agricultural use (Neri et al., 2024).

Use of VS1/DS national drought indicators to analyse the impact of water scarcity conditions on the water supply systems.

For each considered climatic or demand scenario, the proposed methodology identifies "water deficit events", i.e. water scarcity periods in which the reservoir(s) availability is not able to meet entirely the water demand. The timing and magnitude of such deficit events can be compared to different drought indicators in order to better understand how drought dynamics impact water availability and the exploitation of the different kind of sources. Within the scope of Spoke VS1 and Spoke DS, a national drought indicators database is being developed and made available on a dedicated web platform (WASDI). This will facilitate the identification of the past drought events all over the country, for a successive analysis of their impact on the water supply systems, since it may help to understand the link between hydrological droughts and the exploitation of the different surface and groundwater sources, providing the water managers with insights for short- and long-term planning.

3.3.d.2 Water supply service interruptions: reservoir management under drought conditions

3.3.d.2.1 Introduction

Reservoirs are a crucial component of water resource systems, ensuring a reliable and secure water supply for domestic, industrial, and agricultural uses (Huang et al., 2024). However, extreme weather events, such as prolonged droughts and floods, are becoming increasingly challenging for their management, threatening not only storage capacity but also the availability of safe water, which is essential for public health, economic development and wellbeing (Khazaei et al., 2024; Lebu et al., 2024; Mujtaba et al., 2024; Rong et al., 2024). The increased variability of watercourses and the increasing consumption of water determine increased understanding on the role of design and operational choices in balancing short-term regulation and long-term compliance. Multi-purpose reservoir storage helps control hydrological variability, increasing reliability and productivity of water supply. Particularly, reservoirs can provide a buffer as climate change or upstream variations increase streamflow variability or reduce average streamflow.

Reservoir management during droughts becomes particularly complex due to the interplay of various factors that affect both the availability and the use of water. On one hand, population growth and the expansion of agricultural and industrial activities increase the demand for drinking and irrigation water, making it essential to ensure an adequate supply to meet these needs (Ahmadalipour et al., 2019; Brown et al., 2019; Schilstra et al., 2024). On the other hand, reservoirs should meet strategic needs, such as supporting agricultural irrigation to ensure food security and producing hydroelectric energy, which is a primary source of renewable energy in many regions (Hurford and Harou, 2014; Turner et al., 2022).

One of the main challenges in managing reservoirs during extreme weather events is the need to accurately forecast inflows and water availability. In this context, predictive models, such as those based on Artificial Neural Networks (ANNs), have proven effective in improving water resource management, especially in arid and semi-arid regions (Rezaeianzadeh et al., 2016). Furthermore, the use of deep learning techniques, such as Long Short-Term Memory (LSTM) networks, has shown promising results (Kratzert et al., 2018). Specifically, Herbert et al. (2021) demonstrated that LSTM algorithms outperform traditional statistical techniques, significantly improving the accuracy of long-term forecasts and, consequently, the reliability of water resource management, especially during critical months.

Another crucial aspect of reservoir management is the optimization of resources for multiple objectives, such as irrigation, hydroelectric energy production, and the availability of drinking water. Reservoirs are often designed to meet various needs, which requires balancing these different goals through robust policies that can adapt to uncertain scenarios and ensure resource sustainability (Amaranto et al., 2022), particularly during periods of drought (Yang et al., 2015).

An additional key aspect of reservoir management is the integration of design and operational decisions. Design decisions influence the reservoir's resilience, while operational choices determine its efficiency in responding to water stress. The optimization of operational rules can improve the ability to respond to water shortages, fostering more timely adaptive actions, Garcia et al. (2020). Large storage volumes may lead to delayed responses to water stress, but the adoption of appropriate operational policies, such as reducing demand in advance, increases the salience of the issue and promotes a faster adaptive response. Moreover, water resource management must account for social dynamics and attitudes toward risk, as these factors can significantly influence the ability to adopt effective adaptation measures. Moreover, different social attitudes in facing and responding to risk, influence water resource management with different outcomes in terms of water shortage risk Mazzoleni et al. (2024). The results highlighted that more homogeneous and integrated risk management tends to reduce losses caused by droughts and floods.

Reservoir performance is determined by the characteristics of the physical infrastructure itself and by the operating rules that balance multiple objectives, maximizing present benefits and minimizing future risks. However, the optimal control of reservoirs is characterized by uncertainties, due to the hydrological inputs, the different purposes of design and the non-linearity of the system. The objective of the analysis is the definition of a methodology to determine the optimal management strategy to cope with changes in boundary conditions, e.g. variability of streamflow and growing water consumption which intensify the risk of water stress and shortage.

3.3.d.2.2 Inflow prediction and management optimization

We propose a two-step methodology for reservoir management. First, a method is presented for forecasting inflows into the reservoirs, which is crucial for accurate planning and decision-making. Subsequently, an optimization approach is introduced to determine the optimal operating policies for the reservoirs. This approach aims to optimize concurrent uses of the impounded water resources, such as hydropower production, irrigation supply and urban water demands, while accounting for the uncertainties and complexities inherent in reservoir operations.

3.3.d.2.2.1 Streamflow forecasting

This study focuses on streamflow forecasting at multiple lead times, employing a data-driven approach based on Long Short-Term Memory (LSTM) neural networks. Long Short-Term Memory (LSTM) networks are a specialized type of Recurrent Neural Network (RNN) designed to address challenges in capturing long-term dependencies, particularly those arising from the vanishing gradient problem that traditional RNNs face (Hochreiter and Schmidhuber, 1997). The defining feature of LSTM networks lies in their ability to selectively retain or discard information over time, making them well-suited for processing sequential data (Hochreiter and Schmidhuber, 1997).

Each LSTM cell contains three gates (forget gate, input gate and output gate) that collectively regulate the flow of information. The forget gate determines what information should be removed from the cell state, while the input gate manages the integration of new data. The output gate controls which information from the cell state is transmitted to the next layer (Hochreiter and Schmidhuber, 1997). This mechanism allows LSTMs to effectively model complex temporal relationships and adapt to varying patterns in time series data (Hochreiter and Schmidhuber, 1997).

Due to their versatility in handling temporal dependencies and capturing non-linear dynamics, LSTM models have been extensively applied in hydrology, including rainfall-runoff modeling and streamflow forecasting, both at local and regional scales. These models have demonstrated their effectiveness in recognizing seasonal patterns and improving prediction accuracy (e.g., Kratzert et al., 2018).

In this study, a two-layer LSTM architecture was employed, comprising layers with 32 and 40 units, followed by a dense layer to produce the final prediction of cumulative inflow for a given lead time. This configuration was selected based on its ability to extract sophisticated data representations and enhance predictive skill, especially for capturing seasonal and non-linear behaviors (Hua et al., 2019; Kong et al., 2024). The architecture was consistent across all targets, with individual models developed for each lead time. Training utilized the Adam optimizer with Mean Squared Error (MSE) as the loss function, and early stopping was applied to minimize overfitting based on validation set performance.

3.3.d.2.2.2 Experimental Framework

Two experimental setups were employed to evaluate the LSTM model's performance:

1. Baseline Observational Experiments:

The first set of experiments uses observed data as input, combining historical precipitation, temperature and inflow records to train LSTM models. Separate models were developed for each lead time, exploring the ability of the LSTM to predict inflows based solely on past observed variables.

2. Forecast Integration Experiments:

To explore potential improvements in predictability, the second set of experiments integrates extended-range forecasts for precipitation and temperature. These forecasts, available for sub-seasonal scales, were combined with observational data to provide a richer set of input features for the LSTM.

3.3.d.2.2.3 Model Architecture

The LSTM model architecture includes two sequential LSTM layers with 32 and 40 units, respectively, followed by a dense output layer. This configuration was selected through trial and error to balance computational efficiency and model performance. Each LSTM model was trained separately for the specific lead time it aimed to predict, using the Adam optimizer and mean squared error as the loss function. Early stopping was employed to prevent overfitting.

Additionally, the LSTM model's results were compared with those from a physically-based hydrological model to benchmark its performance against existing state-of-the-art forecasting approaches. The European HYdrological Predictions for the Environment (E-HYPE), developed by the Swedish Meteorological and Hydrological Institute (SMHI), simulates river flows at a pan-European scale using observed and forecasted meteorological variables (Lindström et al., 2010). For this study, we used inflow forecasts produced by E-HYPE, forced with the HydroGFD 2.0 dataset, a bias-corrected version of the ECMWF-ER forecasts (Berg et al., 2018; Yang et al., 2010). These predictions, available at daily timesteps and updated weekly, include 11 ensemble members (E-HYPE, 2024), with the ensemble mean used for analysis. Specifically, the forecasts represent the inflow into the Barrios de Luna reservoir, derived from upstream catchments. By comparing the LSTM model's performance with E-HYPE, we aim to assess the potential of data-driven methods in enhancing hydrological prediction capabilities relative to a widely used, physically-based forecasting tool.

3.3.d.2.2.4 Optimal operating policies

The optimal operating policies for the reservoir are defined by a sequence of release and diversion decisions that optimize objectives related to the management of the impounded water, such as hydropower production, irrigation usage and urban water supply demands. The utility functions that model the objectives of the different stakeholders are as follows (Amaranto et al., 2022): i) upstream irrigation deficit, minimized as the squared difference between demand and supply of water; ii) downstream irrigation deficit, minimized with a similar formulation, whereby the quadratic water supply deficit, a traditional formulation in reservoir operations since Hashimoto et al. (1982), penalizes larger irrigation deficits, which are more detrimental to crop growth compared to smaller, more frequent shortages, Amaranto et al. (2022) ; iii) urban deficit, to be minimized as the difference between demand and availability of water for urban use; iv) hydropower production, to be maximized.

The optimal operating policies are calculated using a multi-objective optimization approach based on evolution, known as Evolutionary Multi-Objective Direct Policy Search (EMODPS) (Giuliani et al., 2016). This method combines direct policy search, nonlinear approximating networks, and multi-objective evolutionary algorithms to overcome the limitations of traditional stochastic dynamic programming methods. The EMODPS method consists of three main modules: direct policy search (DPS), nonlinear approximating networks and multi-objective evolutionary algorithms (MOEAs) (Amaranto et al., 2022; Giuliani et al., 2016).

The optimal policy parameter π_θ^* is found through the minimization of a cost function composed of the objectives described above (Amaranto et al., 2022):

$$\pi_\theta^* = arg\, \min_\theta(J_\theta) \tag{3.3.16}$$

where the cost function J_θ is defined as a weighted combination of the irrigation, urban supply, and hydropower objectives (Amaranto et al., 2022):

$$J_\theta = \{J_{IU}, J_{ID}, J_{UD}, -J_{HP}\} \tag{3.3.17}$$

3.3.d.2.3 Assessing the Impact of Climate Change on Hydropower Production

Modeling the impact of climate change on water systems has become a central focus in scientific research, with numerous studies exploring various approaches to evaluate adaptation and resilience (Zhao et al., 2021).

Hydropower, as a renewable energy source reliant on consistent water availability, is particularly vulnerable to climatic shifts, making it fundamental to assess its potential under future scenarios. The following section outlines the procedure adopted.

Historical precipitation data and daily records of inflow, elevation, and hydropower production were collected for the case study under consideration. We analyze hydropower production data for the analyzed power plant, focusing on fluctuations at various time scales: daily, weekly, monthly and annually. This preliminary step identifies any artificial modifications or notable trends in production patterns over time. For subsequent analyses, we adjust hydropower series to exclude these events. Moreover, usually dam operations are subject to restrictions on minimum and maximum daily flows, daily maximum ramp rates, and the maximum rate of decline. The climate model outputs are sourced from the Coupled Model Intercomparison Project Phase 6 (CMIP6), spanning spatial resolutions from 25 km to 200 km. Historical simulations cover the period from 1981 to 2014, while precipitation projections for four shared socioeconomic pathway scenarios (i.e. SSP1-2.6, SSP2-4.5, SSP3-7.0, SSP5-8.5) are provided up to the year 2100 (Haarsma et al 2016).

To understand the underlying physical processes influencing hydropower production, we explore the relationships between paired variables within the system: precipitation and inflow, inflow and elevation, and elevation and hydropower production. Hydropower production is a function of both reservoir elevation (head) and streamflow volume (Christensen et al., 2004). Using data from the common period, we calculate the Spearman correlation coefficient (ρ) on a monthly scale, with aggregation windows at the weekly scale, to assess how these variables interact over time. We examine the temporal aggregation scale that maximizes the Spearman correlation coefficient (ρ) between monthly hydropower production and antecedent basin-averaged precipitation. The aggregation periods range from a minimum of 4 weeks to a maximum of 156 weeks (3 years). Beyond this timeframe, correlation coefficients tend to stabilize, indicating a limit to the correlation's sensitivity to longer aggregation windows. Next, we model the relationship between spatially and temporally averaged precipitation across the basin and monthly hydropower production using the Generalized Additive Model in Location, Scale, and Shape (GAMLSS) (Rigby and Stasinopoulos, 2005). We test multiple distributions for the response variable, including the one-parameter (i.e., μ) exponential distribution, the two-parameter (i.e., μ, σ) gamma, inverse gamma, inverse Gaussian, and lognormal distributions, as well as the three-parameter (i.e., μ, σ, ν) generalized gamma distribution. After evaluating multiple candidate distributions, we select the most suitable one and configure its parameters, choosing between constant and precipitation dependent parameterizations. The general parameter equations where X_1 represents precipitation are:

$$\log(\mu) = \mu_0 + \mu_1 \times X_1 \quad (3.3.18)$$

$$\log(\sigma) = \sigma_0 + \sigma_1 \times X_1 \quad (3.3.19)$$

$$\nu = \nu_0 \quad (3.3.20)$$

Distribution and parameter configuration selection is guided by the Schwarz Bayesian Criterion (SBC) (Schwarz, 1978). To evaluate and compare monthly models between precipitation (X_1) and hydropower (Y) in four configurations $X_1 - Y, \log(X_1) - Y, X_1 - \log(Y), \log(X_1) - \log(Y)$, a skill score is estimated based on the Standardized Mean Squared Error (SS_{MSE}), which serves as a metric for model performance (Hashino et al., 2007; Murphy and Winkler, 1992). The SS_{MSE} is calculated as follows:

$$\boldsymbol{SS_{MSE}} = \boldsymbol{\rho_{FX}^2} - \left[\frac{\mu_F - \mu_X}{\sigma_X}\right]^2 - \left[\boldsymbol{\rho_{FX}} - \left(\frac{\sigma_F}{\sigma_X}\right)\right]^2 (21) \quad (3.3.21)$$

where:

$\boldsymbol{\rho_{FX}}$ is the correlation between the reference data and the model output;

$\boldsymbol{\sigma_F}$ and $\boldsymbol{\sigma_X}$ are the standard deviations of the reference data and the model output, respectively;

μ_F and μ_X are the means of the reference data and the model output.

The SS_{MSE} ranges from -∞ to 1, with values closer to 1 indicating a stronger agreement between the reference data and model output. This score comprises three components: the coefficient of determination reflects the model's potential skill in explaining variance; the unconditional bias represents a standardized mean error, capturing shifts from the one-to-one line; and the conditional bias assesses the reliability of the model's slope relative to the one-to-one line (Bradley, et al., 2019; Kim et al., 2024).

In parallel, we compute basin-averaged daily precipitation outputs from various climate models in CMIP6. We apply bias correction and downscaling using the Empirical Quantile Mapping (EQM) method (Amengual et al., 2012; Cannon et al., 2015). We utilize the bias-corrected basin-averaged precipitation projections as input of the identified statistical models to assess potential changes in hydropower production under the four CMIP6 future scenarios (SSP1-2.6, SSP2-4.5, SSP3-7.0, SSP5-8.5) over the 2015-2100 period. We perform a screening of the GCMs. It is based on trend analysis for the SSP2-4.5 scenario during the 2005-2022 period, comparing observed and simulated hydropower production. We apply Kendall's tau correlation coefficient, using the Mann-Kendall test (Mann, 1945), on both observed and modeled hydropower series. We evaluate trend consistency by selecting models with coherent monthly trends, defined as either both significant or both not significant across all months within the common period. We calculate the ensemble mean across all selected models for each SSP scenario. Subsequently, we evaluate long-term trends in hydropower production by calculating Kendall's tau across temporal windows of variable length (a minimum of 10 years) from 2005 to 2100, using a significance level of $\alpha = 0.05$. Additionally, for each time window, we estimate the number of models indicating a significant positive or negative trend, providing insights into the evolution of trends over different timescales throughout the 21st century. Using the bias-corrected, basin-averaged precipitation projections as input for the identified statistical models, we evaluate potential changes in hydropower production under four future scenarios. For each SSP scenario, we calculate the ensemble mean and envelope across all selected models, resulting in a range of hydropower production projections for each scenario extending through 2100.

3.3.d.3 Water shortage hazard on urban water distribution users, under current and future climate scenarios

3.3.d.3.1 Introduction

When unexpected water shortage events have to be faced, water managers have few options that can be adopted with short forewarning and with almost no need for structural measures. Pressure reduction, intermittent supply and public uses containment are usually adopted as common practices in urban areas. Considering their detrimental impact on the users and on the pipe assets, such practices are usually limited to short periods but they create inequalities among users with some of them being geographically, topographically or structurally advantaged and receiving more water resources and the others suffering more severe water

supply cuts. The proposed activity is aimed to water shortage hazard inside urban areas by defining and computing water supply equality indices and users vulnerability to shortage based on structural, topographical or topological aspects. The activity will be based on the integration of water shortage scenarios coming from the analysis of water sources and water supply pipes (UNIBO) and water distribution network advanced modelling (either in continuous or intermittent supply).

Urban water shortage situations are commonly solved by discontinuous water distribution and rationing the available water resources. This approach is widely adopted in developing countries (Vairavamoorthy et al., 2001) and developed ones for solving short-term scarcity conditions, which can be caused by drought periods (Cubillo Gonzales et al., 2003; McIntosh et al., 1997; Hardoy et al. 2001; Totsuka et al., 2004).

Droughts can significantly impact urban water supply systems in various ways, affecting both water availability and socio-economic aspects of cities. Drought events reduce freshwater resources, severely threatening urban water supply systems and limiting sustainable urban development (Szalińska et al., 2018). This water shortage can affect multiple socio-economic sectors and urban ecosystems. In water-stressed regions, droughts force water providers to invest in additional supplies or implement expensive emergency measures, often increasing water fees and household taxes (Rachunok and Fletcher, 2023). This can disproportionately affect low-income households, altering their water consumption patterns and exacerbating water affordability issues. Interestingly, the impact of droughts on urban water supply can vary significantly even between geographically close regions due to differences in adaptive capacities and water resource management strategies (Chuah et al., 2018). For instance, despite their proximity, Singapore and Johor, Malaysia show distinct variations in drought impacts and responses.

The impacts extend beyond just water scarcity, affecting aquatic ecology, energy production, waterborne transportation, tourism, and recreation (Stahl et al., 2023). To mitigate these impacts, cities need to develop comprehensive drought resilience strategies that consider both short-term and long-term measures, integrating physical, socio-economic, and political aspects in their implementation (Dewi and Prihestiwi, 2022; Li et al., 2022).

Intermittent Water Supply (IWS) is also quite frequent in Mediterranean countries. In this area, the lack of natural resources management and network maintenance plans, explicitly considering the possibility of scarcity scenarios, produces unexpected water shortage situations that can be handled only by means of emergency interventions. Intermittent water distribution has the advantage of requiring small financial efforts, but it leads to network operating conditions that are very far from the usual design. The network is subjected to cyclical filling and emptying periods, and users need to collect water during distribution periods to cover their needs when supply service is not available. IWS is characterised by regular flow restarting and pipe draining, significantly impacting water quality and service reliability (Kumpel and Nelson, 2016). In IWS systems, water utilities typically supply water to different zones or neighbourhoods on a rotational basis, with varying supply schedules. In intermittent distribution, the users try to compensate water service intermittency by searching new local resources, when available (as an example by perforating private wells), or, more commonly, by building private reservoirs, used for collecting water during serviced periods and distributing it when public water service is not available. During intermittent distribution periods, the public network is greatly influenced by the presence of such reservoirs that are usually filled in a very short period after the reactivation of water service, leading to very high peak flows and, consequently, inequity in water resources allocation among population. Moreover, those local reservoirs are often over-designed in order to take into account higher water consumption and possible leakages. In these cases, the intermittent distribution is useful to limit water losses due to pressurization more than to limit water consumption by users. Intermittency generates inequitable water distribution due to pressure dependent flow conditions, with obvious disadvantages for consumers located far away from the supplying nodes or at higher elevation in the network. In distribution systems designed for continuous water supply, the consumers exposed to intermittent supply conditions are likely to collect as much water as possible in their reservoirs whenever the service resumes. In this condition, consumer reservoirs are filled once the supply has been restored and this contemporary use of water service generates larger peak flows than predicted in the network design process, increasing the pressure losses in the network. Consequently, disadvantaged consumers will always collect less water than those nearer to the source. Intermittent distribution can also have a large impact on water quality, allowing for the introduction of soil in the pipes when they are empty (Yepes et al., 2003).

For these reasons, it is essential to design and manage water distribution systems according to their operational conditions to improve system performances and to deliver equitably the available water resource. Intermittent distribution networks, therefore, have to be designed in a particular way, absolutely different to those applied to systems delivering water 24-hours per day (Batish, 2003).

To efficiently analyse urban distribution networks in scarcity conditions, it can be helpful to evaluate how water scarcity and intermittent service affect water consumption. This present proposes a methodology for identifying those users that are more disadvantaged by the intermittent distribution condition providing a useful tool to be used when managing a network in such a delicate operational condition. The identification of disadvantaged users is carried out by the mean of network performance indicators specifically defined for intermittent distribution and described in the next paragraph. In the study, a real distribution network has been analysed, proposing some indexes for assessing the equity of water service in intermittent distribution conditions.

3.3.d.3.2 Estimating the impact of water shortage on urban population

The primary objective of a water distribution system is to provide water at a sufficient pressure and quantity to all its users. In traditional demand-driven analysis, the network solution is achieved by assigning the assumed demands for all nodes and computing the nodal pressure heads. Link flows from the equations of mass balance and pipe friction headloss. For networks operating under intermittent conditions, a demand-driven analysis can yield nodal pressures lower than the minimum required service level or even become negative. In real networks, the design demands would not be met. Although this is a well-known problem that has been tackled by many researchers, it is still sometimes ignored. Since the 1980s, researchers have proposed various methods to compute the actual water consumption, node pressures and flows of networks operating in conditions different from design ones (such as intermittent systems). Most proposed methods assume the relationship between pressure and outflow at the demand nodes. These methods are generally termed head-driven analyses.

Bhave (1981) was the first who acknowledged demand driven analysis does not behave well when node heads are lower than required service standard ones. The cited study proposed the following pressure-consumption relationship:

$$\text{If } H_j^{avl} < H_j^{\min}, \quad q_j^{avl} = 0 \tag{3.3.22a}$$

$$\text{If } H_j^{avl} \geq H_j^{\min}, \quad q_j^{avl} = q_j^{req} \tag{3.3.22b}$$

where q_j^{avl} is the actual outflow at node j, q_j^{req} is the required outflow at that node (water demand), H_j^{avl} is the available head and $H_j^{\min}$ is the minimum head required to have outflow at the node.

Germanopoulos (1985) suggested the use of an empirical pressure-consumption relationship to predict the outflows at various nodal head:

$$\text{If } H_j^{avl} \leq H_j^{\min}, \quad q_j^{avl} = 0 \tag{3.3.23a}$$

$$\text{If } H_j^{avl} > H_j^{\min}, \quad q_j^{avl} = q_j^{req}\left\{1-10^{-c_j\left[\left(H_j^{avl}-H_j^{\min}\right)/\left(H_j^{des}-H_j^{\min}\right)\right]}\right\} \tag{3.3.23b}$$

where H_j^{des} is the head required to satisfy the water demand, q_j^{req}, at the node *j* and c_j is a calibration parameter ranging from 1 to 5.

Then, Wagner et al. (1988) proposed the use of a parabolic curve to represent the pressure-consumption relationship at a demand node for head between $H_j^{\min}$ and H_j^{des} :

If $H_j^{avl} \le H_j^{\min}$, $q_j^{avl} = 0$ (3.3.24a)

If $H_j^{\min} < H_j^{avl} < H_j^{des}$, $q_j^{avl} = q_j^{req}\left(\frac{H_j^{avl} - H_j^{\min}}{H_j^{des} - H_j^{\min}}\right)^{\frac{1}{n}}$ (3.3.24b)

If $H_j^{avl} \ge H_j^{des}$, $q_j^{avl} = q_j^{req}$ (3.3.24c)

where *n* is a calibration parameter ranging from 2 to 1.

Reddy and Elango (1989) introduced a method completely different from the others previously referred to. The authors suggested a pressure-consumption function without above boundary as the following equations show:

If $H_j \le H_j^{\min}$, $q_j^{avl} = 0$ (3.3.25a)

If $H_j \ge H_j^{\min}$, $q_j^{avl} = S_j\left(H_j - H_j^{\min}\right)^p$ (3.3.25b)

taking the value of the coefficient S_j from the following condition:

If $H_j = H_j^{des}$, $q_j^{avl} = q_j^{req}$ (3.3.26)

and being *p* a coefficient ranging from 0.5 to 1.

This method has been introduced to evaluate the node consumptions in water distribution networks operating in intermittent conditions. In this case, all the users are endowed with private reservoirs and the node outflow is the maximum taken by the network, only related to the available nodal head. The outflow stops when the reservoir is just completely full.

Where water distribution is periodically provided on intermittent basis, the users often provide private reservoirs with pumps to collect as much water as possible even if nodal pressure is lower than minimum required to have outflow at the node. In such situations, the method proposed by Reddy and Elango (1989) has to be modified to take into account the pressure-consumption relationship in the range of node head lower than the minimum value. In order to do this, Eq. 3.3.27 has been defined setting $H_j^{\min}$ equal to zero in Eq. 3.3.25b:

$$q_j^{avl} = k \cdot H_j{}^p \quad (3.3.27)$$

where *k* and *p* are calibration coefficients.

This algorithm has been readily implemented into an existing hydraulic network solver, EPANET 2. Furthermore, a private reservoir under the roof and a pump have been associated with each node (Fig. 16) thus providing a complete model for analysing intermittent distribution networks.

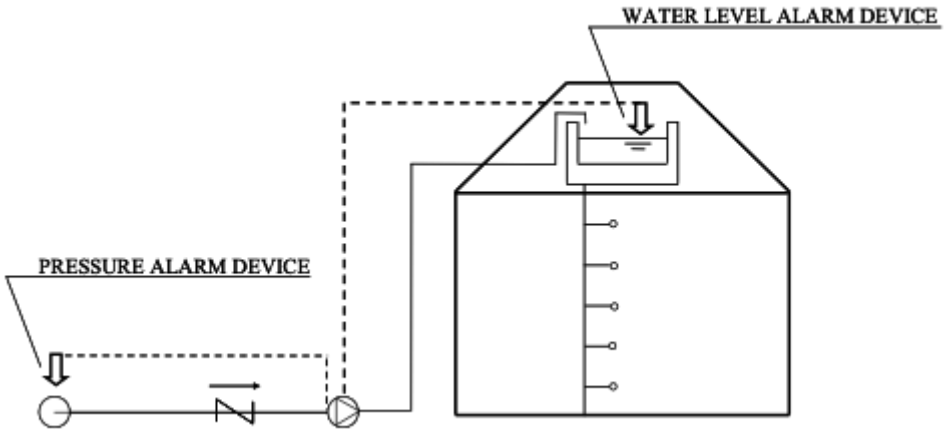

Figure 16. Distribution node numerical scheme.

The reservoir has been designed according to nodal daily water demand and a pump has been chosen being able to fill the reservoir in 4 or 5 hours. The pump is turned on if the reservoir is empty and turned off if the reservoir is full or the pressure on the network is negative.

In order to evaluate the equity in the distribution during intermittent operational conditions, two performance indexes have been proposed in the present study:

- the ratio between the water volume supplied to the users in a service cycle (if the service is intermittent on daily basis, the service cycle is correspondent to two days) and the user demand:

$$EQ1 = \frac{V_{int}}{D} \tag{3.3.28a}$$

where V_{int} is the water volume supplied to the users in a service cycle and D is the user water demand in the same period.

- the ratio between the water flow discharged to the user during a service day in intermittent and continuous distribution conditions:

$$EQ2 = \frac{Q_{int,i}}{Q_{cont,i}} \tag{3.3.28b}$$

where $Q_{int,i}$ is the water volume supplied to the users in a service cycle and $Q_{cont,i}$ is the user water demand in the same period.

The index EQ1 represents the ratio between supplied and demanded water volumes in intermittent distribution and it is able to identify the users that will obtain less water than their needs and advantaged users that have available volumes even higher than their needs. But even if globally in a service cycle water volumes distributed at the users do not greatly differs among the users, wide differences may be possible during the distribution period because advantaged users can fill their reservoirs much faster than disadvantaged ones. This aspect can create difficulties in the water supply of disadvantaged users, and it can modify the user's perception of the water service reliability. For this reason, the index EQ2 can be useful for analysing the behaviour of the network in different operational periods (at the start or at the end of the distribution service after a 24-hour stop).

6. References

Abbate, A., Longoni, L., Ivanov, V. I., & Papini, M. (2019). Wildfire impacts on slope stability triggering in mountain areas. Geosciences, 9, 417. https://doi.org/https://doi.org/10.3390/geosciences9100417

Adinolfi, M., Raffa, M., Reder, A., & Mercogliano, P. (2023). Investigation on potential and limitations of ERA5 reanalysis downscaled on Italy by a convection-permitting model. Clim. Dyn. 61, 4319–4342. http://dx.doi.org/10.1007/s00382-023-06803-w

Ahmadalipour, A., Moradkhani, H., Castelletti, A., & Magliocca, N. (2019). Future drought risk in Africa: Integrating vulnerability, climate change, and population growth. Science of the Total Environment, 662, 672-686.

Alasia, A., Bollman, R. D., Parkins, J. R., & Reimer, B. (2017). Measuring remoteness and accessibility: a set of indices for Canadian communities. Canadian Journal of Regional Science, 40(1), 1-15.

Alexander L.V., Zhang X., Peterson T.C., Caesar J., Gleason B., Klein Tank A.M.G. et al. (2006). Global observed changes in daily climate extremes of temperature and precipitation. J. Geophys. Res., 111, D05109. https://doi.org/10.1029/2005JD006290

Amaranto, A., Juizo, D., & Castelletti, A. (2022). Disentangling sources of future uncertainties for water management in sub-Saharan river basins. Hydrology and Earth System Sciences, 26(2), 245-263.

Amengual, A., Homar, V., Romero, R., Alonso, S., & Ramis, C. (2012). A statistical adjustment of regional climate model outputs to local scales: application to Platja de Palma, Spain. Journal of Climate, 25(3), 939-957.

Arnone, E., Pumo, D., Viola, F., Noto, L.V., & La Loggia, G. (2013). Rainfall statistics changes in Sicily. Hydrol. Earth Syst. Sci., 17, 2449–2458.

AS/NZS 1170.2:2021 (2021). Australian / New Zeland Standard - Structural Design Actions, Part 2: Wind Actions. Standard, Standards New Zealand, Auckland, New Zeland.

Avino A., Cimorelli L., Furcolo P., Noto L.V., Pelosi A., Pianese D., Villani P., & Manfreda S. (2024). Are rainfall extremes increasing in southern Italy? Journal of Hydrology, 631, 130684. https://doi.org/10.1016/j.jhydrol.2024.130684

Avino, A., Manfreda, S., Cimorelli, L., & Pianese, D. (2021). Trend of annual maximum rainfall in Campania region (Southern Italy). Hydrological Processes, 35(12), e14447. https://doi.org/10.1002/hyp.14447

Balistrocchi, M., Metulini, R., Carpita, M., & Ranzi, R. (2020). Dynamic maps of human exposure to floods based on mobile phone data. Natural Hazards and Earth System Sciences, 20(12), 3485–3500. https://doi.org/10.5194/nhess-20-3485-2020

Ballio, G., Battisti, L., & Tognaccini, R. (1999). Il vento in Italia: analisi statistica per il dimensionamento strutturale. Atti del Congresso Nazionale di Ingegneria del Vento, 3, 12-26.

Ballio, G., Lagomarsino, S., Piccardo, G., Solari, G. (1991a). A first step towards the map of Italian extreme winds. Part 1: General principles and analysis methodology. Costruzioni Metall. 3, 147–172.

Ballio, G., Lagomarsino, S., Piccardo, G., Solari, G. (1991b). A first step towards the map of Italian extreme winds. Part 2: Results, repercussion on standards, design implications. Costruzioni Metall. 4, 209–242.

Bárdossy, A., Seidel, J., & El Hachem, A. (2020). The use of personal weather station observation for improving precipitation estimation and interpolation. Hydrology and Earth System Sciences Discussions, 2020, 1-23.

Bartholomé, E., & Belward, A. (2005). GLC2000: a new approach to global land cover mapping from earth observation data. Int. J. Remote Sens. 26, 1959–1977. http://dx.doi.org/10.1080/01431160412331291297

Batish, R., (2003). A New Approach to the Design of Intermittent Water Supply Networks. Proceedings of World Water and Environmental Resources Congress 2003, eds. Paul Bizier & Paul DeBarry: Philadelphia, Pennsylvania, USA.

Beça, P., Rodrigues, A.C., Nunes, J.P., Diogo, P., & Mujtaba, B., (2023). Optimizing Reservoir Water Management in a Changing Climate. Water Resour. Manag. 37, 3423–3437. https://doi.org/10.1007/s11269-023-03508-x

Becciu, G., & Paoletti, A. (2010). Fondamenti di costruzioni idrauliche. Wolters Kluwer Italia.

Beiranvand, B., & Ashofteh, P.-S. (2023). A Systematic Review of Optimization of Dams Reservoir Operation Using the Meta-heuristic Algorithms. Water Resour. Manag. 37, 3457–3526. https://doi.org/10.1007/s11269-023-03510-3

Berg, P., Donnelly, C., & Gustafsson, D. (2018). Near-real-time adjusted reanalysis forcing data for hydrology. Hydrology and Earth System Sciences, 22(2), 989-1000.

Bertola M., Viglione A., Vorogushyn S., Lun D., Merz B., & Blöschl G. (2021). Do small and large floods have the same drivers of change? A regional attribution analysis in Europe. Hydrol. Earth Syst. Sci., 25, 1347–1364. https://doi.org/10.5194/hess-25-1347-2021

Bhave, P.R. (1981). Node Flow Analysis of Water Distribution Systems. Transportation Engineering Journal, 117(4), pp. 457–467.

Blöschl, G., Hall, J., Viglione, A. et al. (2019). Changing climate both increases and decreases European river floods. Nature 573, 108–111. https://doi.org/10.1038/s41586-019-1495-6

Bonaccorso, B., Cancelliere, A., & Rossi, G. (2005). Detecting trends of extreme rainfall series in Sicily. Adv. Geosci., 2, 7–11.

Bouwer, H., Back, J. T., & Oliver, J. M. (1999). Predicting infiltration and ground-water mounds for artificial recharge. Journal of Hydrologic Engineering, 4, 4, 350– 357.

Bozzo, E., & Franceschet, M. (2013). Resistance distance, closeness, and betweenness. Social Networks, 35(3), 460-469. https://doi.org/10.1016/j.socnet.2013.05.003

Bradley, A. A., Demargne, J., & Franz, K. J. (2019). Attributes of forecast quality. In Handbook of hydrometeorological ensemble forecasting (pp. 849-892). Springer Berlin Heidelberg.

Brandimarte, L., & Di Baldassarre, G. (2012). Uncertainty in design flood profiles derived by hydraulic modelling. Hydrology Research, 43(6), 753-761. https://doi.org/10.2166/nh.2011.086

Bro, R., & Smilde, A. K. (2014). Principal component analysis. Analytical methods, 6(9), 2812-2831.

Brown, T. C., Mahat, V., & Ramirez, J. A. (2019). Adaptation to future water shortages in the United States caused by population growth and climate change. Earth's Future, 7(3), 219-234.

Brunner, G. (2016). HEC-RAS River Analysis System Hydraulic Reference Manual. www.hec.usace.army.mil

Bruno, L., Coste, N., Mannini, C., Mariotti, A., Patruno, L., Schito, P., & Vairo, G. (2023). Codes and standards on computational wind engineering for structural design: state of art and recent trends. Wind Struct. 37, 133–151. http://dx.doi.org/10.12989/was.2023.37.2.133

Cannon, A. J., Sobie, S. R., & Murdock, T. Q. (2015). Bias correction of GCM precipitation by quantile mapping: how well do methods preserve changes in quantiles and extremes? Journal of Climate, 28(17), 6938-6959.

Cannon, S. H., & DeGraff, J. (2009). The increasing wildfire and post-fire debris-flow threat in western USA, and implications for consequences of climate change. Landslides–disaster risk reduction 2009, pp. 177–190. https://doi.org/https://doi.org/10.1007/97 199 8-3-540-69970-5_9

Caporali, E., Lompi, M., Pacetti, T., Chiarello, V., & Fatichi, S. (2021). A review of studies on observed precipitation trends in Italy. Int J Climatol., 41 (Suppl. 1): E1–E25. https://doi.org/10.1002/joc.6741

Cavanaugh, N. R., Gershunov, A., Panorska, A. K., & Kozubowski, T. J. (2015). The probability distribution of intense daily precipitation. Geophysical Research Letters, 42(5), 1560-1567.

Chafer, C. J., Noonan, M., & Macnaught, E. (2004). The post-fire measurement of fire severity and intensity in the Christmas 2001 Sydney wildfires, International Journal of Wildland Fire, 13(2), 227–240.

Chen, A., Yang, C., Kongsomsaksakul, S., & Lee, M. (2015). Network-based accessibility measures for vulnerability analysis of degradable transportation networks. Networks and Spatial Economics, 7(3), 241–256.

Chen, A. B., Behl, M., & Goodall, J. L. (2021). Assessing the trustworthiness of crowdsourced rainfall networks: A reputation system approach. Water Resources Research, 57(12), e2021WR029721.

Chow, V. Te, Maidment, D. R., & Mays, L. W. (1988). Applied hydrology. McGraw-Hill.

Christensen, N. S., Wood, A. W., Voisin, N., Lettenmaier, D. P., & Palmer, R. N. (2004). The effects of climate change on the hydrology and water resources of the Colorado River basin. Climatic change, 62, 337-363.

Chuah, C. J., Ho, B. H., & Chow, W. T. L. (2018). Trans-boundary variations of urban drought vulnerability and its impact on water resource management in Singapore and Johor, Malaysia. Environmental Research Letters, 13(7), 074011.

Cian, F., Giupponi, C., & Marconcini, M. (2021). Integration of earth observation and census data for mapping a multi-temporal flood vulnerability index: a case study on Northeast Italy. Natural Hazards, 106, 3, 2163–2184. https://doi.org/10.1007/s11069-021-04535-w

CIMA Research Foundation, Global Earthquake Model (GEM), British Geological Survey (BGS) & Malawi University of Business and Applied Sciences (MUBAS) (2023). Hazard Scenarios for the Comprehensive Multi-Hazard Risk Assessment of Malawi.

CIMA Research Foundation & Internal Displacement Monitoring Centre (2024). Floods and drought displacement risk in Ethiopia, Somalia, and Sudan (HABITABLE research paper). Geneva: IDMC.

CNR-DT 207 R1/2018 (2018). Istruzioni per la valutazione delle azioni e degli effetti del vento sulle costruzioni. Consiglio Nazionale delle Ricerche.

Colombo, M., Martinelli, P., Arano, A., Øverli, J. A., Hendriks, M. A., Kanstad, T., & di Prisco, M. (2021). Experimental investigation on the structural response of RC slabs subjected to combined fire and blast. In Structures (Vol. 31, pp. 1017-1030). Elsevier.

Cominola, A., Preiss, L., Thyer, M., Maier, H.R., Prevos, P., Stewart, R.A., & Castelletti, A. (2023). The determinants of household water consumption: a review and assessment framework for research and practice. Npj Clean Water 6, 11. https://doi.org/10.1038/s41545-022-00208-8

Conedera, M., Peter, L., Marxer, P., Forster, F., Rickenmann, D., & Re, L. (2003). Consequences of forest fires on the hydrogeological response of mountain catchments: a case study of the Riale Buffaga, Ticino, Switzerland. Earth Surf. Process. Landf. 2003, 28, 117–129.

Copernicus Urban Atlas Land Cover dataset (2018). https://land.copernicus.eu/en/products/urban-atlas/urban-atlas-2018

Crisci, A., Gozzini, B., Meneguzzo, F., Pagliara, S., & Maracchi, G. (2002). Extreme rainfall in a changing climate: regional analysis and hydrological implications in Tuscany. Hydrol. Process., 16, 1261–1274.

Cubillo Gonzales, F. L. & Ibanez Carranza, J. C. (2003). Manual de abastecimento del Canal de Isabel II, Graficas Fanny: Madrid, 2003.

Davenport, A. G. (1960). Rationale for determining design wind velocities. Journal of the Structural Division, ASCE, 86(2), 39-68.

Davenport, A. G. (1961). The application of statistical concepts to the wind loading of structures. Proceedings of the Institution of Civil Engineers, 19(4), 449–472.

De Vos, L. W., Leijnse, H., Overeem, A., & Uijlenhoet, R. (2019). Quality control for crowdsourced personal weather stations to enable operational rainfall monitoring. Geophysical Research Letters, 46(15), 8820-8829.

De Vos, L., Leijnse, H., Overeem, A., & Uijlenhoet, R. (2017). The potential of urban rainfall monitoring with crowdsourced automatic weather stations in Amsterdam. Hydrology and Earth System Sciences, 21(2), 765-777.

Deville, P., Linard, C., Martin, S., Gilbert, M., Stevens, F. R., Gaughan, A. E., ... & Tatem, A. J. (2014).

Deville, P., Linard, C., Martin, S., Gilbert, M., Stevens, F. R., Gaughan, A. E., Blondel, V. D., & Tatem, A. J. (2014). Dynamic population mapping using mobile phone data. Proceedings of the National Academy of Sciences of the United States of America, 111(45), 15888–15893. https://doi.org/10.1073/pnas.1408439111

Dewan, A. M. (2013). Hazards, Risk, and Vulnerability (pp. 35–74). https://doi.org/10.1007/978-94-007-5875-9_2

Dewi, S. P., & Prihestiwi, R. C. (2022). Urban Design Initiatives in Drought-prone Areas dealing increasing Water Demand as Pandemic Covid-19 Impact. International Journal of Built Environment and Sustainability, 9(2–2), 75–86.

Di Salvo, C., Ciotoli, G., Pennica, F., & Cavinato, G. P. (2017). Pluvial flood hazard in the city of Rome (Italy). Journal of Maps, 13(2), 545–553. https://doi.org/10.1080/17445647.2017.1333968

Dijkstra, E. W. (1959). A note on two problems in connexion with graphs. Numerische Mathematik, 1, 269–271.

DM 17-01-2018 (2018). Norme tecniche per le costruzioni. Gazzetta Ufficiale della Repubblica Italiana.

Dobson, B., Wagener, T., & Pianosi, F. (2019). An argument-driven classification and comparison of reservoir operation optimization methods. Adv. Water Resour. 128, 74–86. https://doi.org/10.1016/j.advwatres.2019.04.012

Doddy Clarke, E., Griffin, S., McDermott, F., Monteiro Correia, J.a., & Sweeney, C. (2021). Which reanalysis dataset should we use for renewable energy analysis in Ireland? Atmosphere, 12. http://dx.doi.org/10.3390/atmos12050624

Doerr, S., Shakesby, R., Blake, W., Chafer, C., Humphreys, G., & Wallbrink, P. (2006). Effects of differing wildfire severities on soil wettability and implications for hydrological response. Journal of Hydrology, 319, 295–311. https://doi.org/https://doi.org/10.1016/j.jhydrol.2005.06.038

Doms, G., Forstner, J., Heise, E., Herzog, H., Mironov, D., Raschendorfer, M., Reinhardt, T., Ritter, B., Schrodin, R., Schulz, J., & Vogel, G. (2013). A Description of the Nonhydrostatic Regional COSMO-Model. Part II: Physical Parametrizations. Technical Report, http://dx.doi.org/10.5676/DWD_pub/nwv/cosmo-doc_5. 00_II, Consortium for Small-Scale Modelling.

Dunn, R.J.H., Willett, K.M., & Parker, D.E. (2019). Changes in statistical distributions of sub-daily surface temperatures and wind speed. Earth Syst. Dyn. 10, 765–788. http://dx.doi.org/10.5194/esd-10-765-2019

Dunn, R.J.H., Willett, K.M., Parker, D.E., & Mitchell, L. (2016). Expanding HadISD: quality-controlled, sub-daily station data from 1931. Geosci. Instrum. Methods Data Syst., 5, 473–491. http://dx.doi.org/10.5194/gi-5-473-2016

Dyrbye, C., & Hansen, S. (1996). Wind Loads on Structures. Wiley.

E-HYPE (2024). Standard data package, 1-10 Day Forecast, Europe-HYPE - HypeWeb. URL https://hypeweb.smhi.se/water-services/data-delivery-services/standard-1-10-day-e-hype/.

El Adlouni, S., Bobée, B., & Ouarda, T. B. (2008). On the tails of extreme event distributions in hydrology. Journal of hydrology, 355(1-4), 16-33.

El Hachem, A., Seidel, J., O'hara, T., Villalobos Herrera, R., Overeem, A., Uijlenhoet, R., ... & De Vos, L. (2024). A guide to using three open-source quality control algorithms for rainfall data from personal weather stations. Hydrology and Earth System Sciences, 28(20), 4715-4731.

EN 1991-1-4:2005 (2005). Eurocode 1 – Actions on Structures – Part 1-4: General Actions – Wind Actions. Standard, European Committee for Standardization (CEN), Brussels, Belgium.

Felisa, G., Panini, G., Pedrazzoli, P., & Di Federico, V. (2022). Combined Management of Groundwater Resources and Water Supply Systems at Basin Scale Under Climate Change. Water Resour. Manag. 36, 915–930. https://doi.org/10.1007/s11269-022-03059-7

Fiorucci, P., Pernice, U., Meschi, G., Trucchia, A., & Ponte, E. (2024). Technical Guidelines for Forest Fire Risk Assessment: an output of the programme "EU support to flood prevention and forest fires risk management in the Western Balkans and Turkey – IPA Floods and Fires".

Forestieri, A., Lo Conti, F., Blenkinsop, S., Cannarozzo, M., Fowler, H. J., & Noto, L. V. (2018). Regional frequency analysis of extreme rainfall in Sicily (Italy). International Journal of Climatology, 38, e698-e716.

Fowler, H. J., Lenderink, G., Prein, A. F., Westra, S., Allan, R. P., Ban, N. et al. (2021a). Anthropogenic intensification of short-duration rainfall extremes. Nat Rev Earth Environ 2, 107–122. https://doi.org/10.1038/s43017-020-00128-6

Freeman, L. C. (1977). A set of measures of centrality based on betweenness. Sociometry, 40(1), 35-41.

Fujita, T.T. (1986). Mesoscale Classifications: Their History and their Application to Forecasting. American Meteorological Society, Boston, MA, pp. 18–35. http://dx.doi.org/10.1007/978-1-935704-20-1_2

Garcia, M., Ridolfi, E., & Di Baldassarre, G. (2020). The interplay between reservoir storage and operating rules under evolving conditions. Journal of Hydrology, 590, 125270.

Germanopoulos, G. (1985). A technical note on the inclusion of pressure dependent demand and leakage terms in water supply network models. Civil Engineering and Environmental Systems, 2(3), 171-179. http://dx.doi.org/10.1080/02630258508970401

Giannaros, T. M., & Papavasileiou, G. (2023). Changes in European fire weather extremes and related atmospheric drivers. Agricultural and Forest Meteorology, 342, 1–11. https://doi.org/https://doi.org/10.1016/j.agrformet.2023.109749

Gibson, J., Kållberg, P., Uppala, S., Hernandez, A., Nomura, A., & Serrano, E. (1997). ERA Description. Shinfield Park, Reading.

Giuliani, M., Castelletti, A., Pianosi, F., Mason, E., & Reed, P. M. (2016). Curses, tradeoffs, and scalable management: Advancing evolutionary multiobjective direct policy search to improve water reservoir operations. Journal of Water Resources Planning and Management, 142(2), 04015050.

Giuliani, M., Lamontagne, J.R., Reed, P.M., & Castelletti, A. (2021). A State-of-the-Art Review of Optimal Reservoir Control for Managing Conflicting Demands in a Changing World. Water Resour. Res. 57, e2021WR029927. https://doi.org/10.1029/2021WR029927

Giupponi, C., Giove, S., & Giannini, V. (2013). A dynamic assessment tool for exploring and communicating vulnerability to floods and climate change. Environmental Modelling and Software, 44, 136–147. https://doi.org/10.1016/j.envsoft.2012.05.004

Greppi, M. (2005). Idrologia; Hoepli: Milan, Italy, pp. 1–222.

Gualtieri, G. (2021). Reliability of ERA5 reanalysis data for wind resource assessment: a comparison against tall towers. Energies, 14. http://dx.doi.org/10.3390/en14144169

Gualtieri, G. (2022). Analysing the uncertainties of reanalysis data used for wind resource assessment: a critical review. Renew. Sustain. Energy Rev., 167. http://dx.doi.org/10.1016/j.rser.2022.112741

Guerreiro S. B., Fowler H. J., Barbero R., Westra S., Lenderink G., Blenkinsop S. et al. (2018). Detection of continental-scale intensification of hourly rainfall extremes. Nature Clim Change, 8, 803–807. https://doi.org/10.1038/s41558-018-0245-3

Gumuscu, I., Islek, F., Yuksel, Y., & Sahin, C. (2023). Spatiotemporal long-term wind and storm characteristics over the eastern mediterranean sea. Reg. Stud. Mar. Sci., 63, 102996. http://dx.doi.org/10.1016/j.rsma.2023.102996

Gupta, N., & Chavan, S. R. (2022). Characterizing the tail behaviour of daily precipitation probability distributions over India using the obesity index. International Journal of Climatology, 42(4), 2543-2565.

Haarsma, R. J., Roberts, M. J., Vidale, P. L., Senior, C. A., Bellucci, A., Bao, Q., ... & von Storch, J. S. (2016). High resolution model intercomparison project (HighResMIP v1. 0) for CMIP6. Geoscientific Model Development, 9(11), 4185-4208.

Hammond, M. J., Chen, A. S., Djordjević, S., Butler, D., & Mark, O. (2013). Urban flood impact assessment: A state-of-the-art review. Urban Water Journal, 12(1), 14–29. https://doi.org/10.1080/1573062X.2013.857421

Hardoy, J. E., Mitlin, D. & Satterthwaite, D. (2001). Environmental Problems in a Urbanizing World: Finding Solutions for Cities in Africa, Asia and Latin America, Earthscan: London.

Hartmann, S., Pedoth, L., Dalla Torre, C., & Schneiderbauer, S. (2021). Beyond the expected - residual risk and cases of overload in the context of managing alpine natural hazards. International Journal of Disaster Risk Science, 12(2), 205-219.

Hashimoto, T., Stedinger, J. R., & Loucks, D. P. (1982). Reliability, resiliency, and vulnerability criteria for water resource system performance evaluation. Water resources research, 18(1), 14-20.

Hashino, T., Bradley, A. A., & Schwartz, S. S. (2007). Evaluation of bias-correction methods for ensemble streamflow volume forecasts. Hydrology and Earth System Sciences, 11(2), 939-950.

Hastings, D., Dumbar, P., Elphingstone, G., Bootz, M., Murakami, H., Maruyama, H., Masaharu, H., Holland, P., Payne, J., Bryant, N., Logan, T., Murre, J., Schreier, G., & MacDonald, J. (1999). The Global Land One-Kilometer Base Elevation (GLOBE) Digital Elevation Model. National Oceanic and Atmospheric Administration, National Geophysical Data Center, 325 Broadway, Boulder, Colorado 80305-3328, U.S.A, Version 1.0. URL: http://www.ngdc.noaa.gov/mgg/topo/globe.html

He, Y., Bárdossy, A., & Zehe, E. (2011). A review of regionalisation for continuous streamflow simulation. Hydrol. Earth Syst. Sci. 15, 3539–3553. https://doi.org/10.5194/hess-15-3539-2011

Herbert, Z. C., Asghar, Z., & Oroza, C. A. (2021). Long-term reservoir inflow forecasts: Enhanced water supply and inflow volume accuracy using deep learning. Journal of Hydrology, 601, 126676.

Hersbach, H., Bell, B., Berrisford, P., Hirahara, S., Horányi, A., Muñoz Sabater, J., Nicolas, J., Peubey, C., Radu, R., Schepers, D., Simmons, A., Soci, C., Abdalla, S., Abellan, X., Balsamo, G., Bechtold, P., Biavati, G., Bidlot, J., Bonavita, M., De Chiara, G., Dahlgren, P., Dee, D., Diamantakis, M., Dragani, R., Flemming, J., Forbes, R., Fuentes, M., Geer, A., Haimberger, L., Healy, S., Hogan, R.J., Hólm, E., Janisková, M., Keeley, S., Laloyaux, P., Lopez, P., Lupu, C., Radnoti, G., de Rosnay, P., Rozum, I., Vamborg, F., Villaume, S., & Thépaut, J.N. (2020). The ERA5 global reanalysis. Q. J. R. Meteorol. Soc., 146, 1999–2049. http://dx.doi.org/10.1002/qj.3803

Hyde, K. D., Riley, K., & Stoof, C. (2016). Uncertainties in predicting debris flow hazards following wildfire. Natural Hazard Uncertainty Assessment: Modeling and Decision Support, pp. 287–299. https://doi.org/https://doi.org/10.1002/9781119028116.ch19

Hochreiter, S., & Schmidhuber, J., (1997). Long Short-Term Memory. Neural Computation. 9, 1735–1780.

Hong, H. P., & Ye, W. (2014). Extreme wind speed evaluation for Canada. Journal of Wind Engineering and Industrial Aerodynamics, 129, 33-40.

Horton, R. E. (1941). An approach toward a physical interpretation of infiltration-capacity. Soil Science Society of America Journal, 5(C), 399–417.

Hua, Y., Zhao, Z., Li, R., Chen, X., Liu, Z., & Zhang, H. (2019). Deep learning with long short-term memory for time series prediction. IEEE Communications Magazine, 57(6), 114-119.

Huang, J., Wu, W., Maier, H. R., Wang, Q. J., & Hughes, J. (2024). A multi-objective optimization-based framework for extending reservoir service life in a changing world. Journal of Hydrology, 131409.

Huang, Y., Wu, S., & Kaplan, J.O. (2015). Sensitivity of global wildfire occurrences to various factors in the context of global change. Atmospheric Environment, 121, 86–92. https://doi.org/https://doi.org/10.1016/j.atmosenv.2015.06.002

Hurford, A. P., & Harou, J. J. (2014). Balancing ecosystem services with energy and food security–Assessing trade-offs from reservoir operation and irrigation investments in Kenya's Tana Basin. Hydrology and Earth System Sciences, 18(8), 3259-3277.

Islam, M. T., & Meng, Q. (2024). Spatial dynamic analysis and thematic mapping of vulnerable communities to urban floods. Cities, 145. https://doi.org/10.1016/j.cities.2023.104735

Ivanov, V., Arosio, D., Tresoldi, G., Hojat, A., Zanzi, L., Papini, M., & Longoni, L. (2020). Investigation on the role of water for the stability of shallow landslides—Insights from experimental tests. Water, 12, 1203. https://doi.org/https://doi.org/10.3390/w12041203

Khazaei, M. R., Heidari, M., Shahid, S., & Hasirchian, M. (2024). Consideration of climate change impacts on a hydropower scheme in Iran. Theoretical and Applied Climatology, 155(4), 3119-3132.

Kim, T., Villarini, G., Done, J. M., Johnson, D. R., Prein, A. F., & Wang, C. (2024). Dominant sources of uncertainty for downscaled climate: A military installation perspective. Journal of Geophysical Research: Atmospheres, 129(12), e2024JD040935.

Kong, Y., Wang, Z., Nie, Y., Zhou, T., Zohren, S., Liang, Y., ... & Wen, Q. (2024). Unlocking the power of lstm for long term time series forecasting. arXiv preprint arXiv:2408.10006.

Koutsoyiannis, D. (2022). Stochastics of Hydroclimatic Extremes - A cool Look at Risk, 2nd ed., Kallipos Open Academic Editions.

Koutsoyiannis, D., & Economou, A. (2003). Evaluation of the parameterization-simulation-optimization approach for the control of reservoir systems. Water Resour. Res. 39, 2003WR002148. https://doi.org/10.1029/2003WR002148

Kratzert, F., Klotz, D., Brenner, C., Schulz, K., & Herrnegger, M. (2018). Rainfall–runoff modelling using long short-term memory (LSTM) networks. Hydrology and Earth System Sciences, 22(11), 6005-6022.

Kreibich, H., Schröter, K., Di Baldassarre, G., Van Loon, A., Mazzoleni, M., Abeshu, G. W., ... & Ward, P. J. (2023). Panta Rhei benchmark dataset: socio-hydrological data of paired events of floods and droughts. Earth System Science Data Discussions, 2023, 1-27.

Kumpel, E., & Nelson, K. L. (2016). Intermittent Water Supply: Prevalence, Practice, and Microbial Water Quality. Environmental Science & Technology, 50(2), 542–553.

Kundzewicz, Z. W., & Pińskwar, I. (2022). Are pluvial and fluvial floods on the rise? Water, 14(17), 2612. https://doi.org/10.3390/w14172612

Larson-Nash, S. S., Robichaud, P. R., Pierson, F. B., Moffet, C. A., Williams, C. J., Spaeth, K. E., Brown, R. E., & Lewis, S. A. (2018). Recovery of small-scale infiltration and erosion after wildfires. Journal of Hydrology and Hydromechanics 2018, 66, 261–270. https://doi.org/https://doi.org/10.1515/johh-2017-0056

Lebu, S., Lee, A., Salzberg, A., & Bauza, V. (2024). Adaptive strategies to enhance water security and resilience in low-and middle-income countries: A critical review. Science of the Total Environment, 171520.

Legambiente, 2025. Mappa del rischio climatico nelle città italiane. Osservatorio Nazionale Città Clima. Retrieved March 17, 2025, from https://cittaclima.it/mappa/.

Li, H., Sun, J., Zhang, H., Zhang, J., Jung, K., Kim, J., ... & Li, F. (2018). What large sample size is sufficient for hydrologic frequency analysis? A rational argument for a 30-year hydrologic sample size in water resources management. Water, 10(4), 430.

Li, Q., Liang, Q., & Xia, X. (2020). A novel 1D-2D coupled model for hydrodynamic simulation of flows in drainage networks. Advances in Water Resources, 137, 103519. https://doi.org/10.1016/j.advwatres.2020.103519

Li, Z., Zhang, J., Liu, J., Shao, Z., & Zhao, H. (2022). Evaluation and promotion strategy of resilience of urban water supply system under flood and drought disasters. Scientific Reports, 12(1).

Libertino, A., Ganora, D., & Claps, P. (2018). Technical note: Space–time analysis of rainfall extremes in Italy: Clues from a reconciled dataset. Hydrol. Earth Syst. Sci. 2018, 22, 2705–2715

Libertino, A., Ganora, D., & Claps, P. (2019). Evidence for increasing rainfall extremes remains elusive at large spatial scales: the case of Italy. Geophys. Res. Lett., 46, 7437–7446. https://doi.org/10.1029/2019GL083371

Lindström, G., Pers, C., Rosberg, J., Strömqvist, J., & Arheimer, B. (2010). Development and testing of the HYPE (Hydrological Predictions for the Environment) water quality model for different spatial scales. Hydrology research, 41(3-4), 295-319.

Longoni, L., Ivanov, V., Ferrario, M., Brunero, M., Papini, M., & Arosio, D. (2022). Laboratory tests with interferometric optical fibre sensors to monitor shallow landslides triggered by rainfalls. Landslides, 19, 761–772. https://doi.org/10.1007/s10346-021-01803-5.2

Mann, H. B. (1945). Nonparametric tests against trend. Econometrica: Journal of the econometric society, 245-259.

Mazzoglio P., Butera I., & Claps P. (2020). I^2-RED: a massive update and quality control of the Italian annual extreme rainfall dataset. Water, 12, 3308.

Mazzoglio, P., Ganora, D., & Claps, P. (2022). Long-term spatial and temporal rainfall trends over Italy. Environ. Sci. Proc., 21, 28. https://doi.org/10.3390/environsciproc2022021028

Mazzoleni, M., Mondino, E., Matanó, A., Van Loon, A. F., & Barendrecht, M. H. (2024). Modelling the role of multiple risk attitudes in implementing adaptation measures to reduce drought and flood losses. Journal of Hydrology, 636, 131305.

McCabe, M. F., Rodell, M., Alsdorf, D. E., Miralles, D. G., Uijlenhoet, R., Wagner, W., ... & Wood, E. F. (2017). The future of Earth observation in hydrology. Hydrology and Earth System Sciences, 21(7), 3879-3914.

McIntosh, A. C. & Yñiguez, C. E. (1997). Second Water Utilities Data Book: Asia and Pacific Region, Asian Development Bank: Manila, 1997

Mereu, S., Sušnik, J., Trabucco, A., Daccache, A., Vamvakeridou-Lyroudia, L., Renoldi, S., Virdis, A., Savić, D., & Assimacopoulos, D. (2016). Operational resilience of reservoirs to climate change, agricultural demand, and tourism: A case study from Sardinia. Sci. Total Environ. 543, 1028–1038. https://doi.org/10.1016/j.scitotenv.2015.04.066

Miller, C. (2003). A once in 50-year wind speed map for Europe derived from mean sea level pressure measurements. J. Wind Eng. Ind. Aerodyn. 91, 1813–1826. http://dx.doi.org/10.1016/j.jweia.2003.09.024

Mo, K., Keislar, R. E., & Stevens, T. (2015). Long-term wind monitoring and extreme wind analyses in China. Energy, 89, 845-854.

Moccia, B., Mineo, C., Ridolfi, E., Russo, F., & Napolitano, F. (2021a). Probability distributions of daily rainfall extremes in Lazio and Sicily, Italy, and design rainfall inferences. Journal of Hydrology: Regional Studies, 33, 100771.

Moccia, B., Papalexiou, S. M., Russo, F., & Napolitano, F. (2021b). Spatial variability of precipitation extremes over Italy using a fine-resolution gridded product. Journal of Hydrology: Regional Studies, 37, 100906.

Moccia, B., Ridolfi, E., Mineo, C., Russo, F., & Napolitano, F. (2024). On the Occurrence of Extreme Rainfall Events Across Italy: Should We Update the Probability of Failure of Existing Hydraulic Works? Water Resources Management, 1-14.

Molina, M.O., Gutiérrez, C., & Sánchez, E. (2021). Comparison of ERA5 surface wind speed climatologies over Europe with observations from the HadISD dataset. Int. J. Climatol. 41, 4864–4878. http://dx.doi.org/10.1002/joc.7103

Mujtaba, G., Shah, M. U. H., Hai, A., Daud, M., & Hayat, M. (2024). A holistic approach to embracing the United Nation's Sustainable Development Goal (SDG-6) towards water security in Pakistan. Journal of Water Process Engineering, 57, 104691.

Muñoz Sabater, J., Dutra, E., Agustí-Panareda, A., Albergel, C., Arduini, G., Balsamo, G., Boussetta, S., Choulga, M., Harrigan, S., Hersbach, H., Martens, B., Miralles, D.G., Piles, M., Rodríguez-Fernández, N.J., Zsoter, E., Buontempo, C., & Thépaut, J. N. (2021). ERA5-land: a state of-the-art global reanalysis dataset for land applications. Earth Syst. Sci. Data 13, 4349–4383. http://dx.doi.org/10.5194/essd-13-4349-2021

Murphy, A. H., & Winkler, R. L. (1992). Diagnostic verification of probability forecasts. International Journal of Forecasting, 7(4), 435-455.

Nasiri, H., Mohd Yusof, M.J., & Mohammad Ali, T.A. 2016. An Overview to Flood Vulnerability Assessment Methods. Sustainable Water Resources Management, 2(3), 331–336. https://doi.org/10.1007/s40899-016-0051-x

Nerantzaki, S. D., & Papalexiou, S. M. (2022). Assessing extremes in hydroclimatology: A review on probabilistic methods. Journal of Hydrology, 605, 127302.

Neri, M., Montanari, A., & Toth, E. (2024). Pianificazione e gestione dei serbatoi ad uso irriguo: stima dei volumi di risorsa disponibili tramite la modellazione afflussi-deflussi di bacini non strumentati. Atti del XXXIX Convegno Nazionale di Idraulica e Costruzioni Idrauliche, Parma, 15-18 settembre 2024.

Neri, M., Parajka, J., & Toth, E. (2020). Importance of the informative content in the study area when regionalising rainfall-runoff model parameters: the role of nested catchments and gauging station density. Hydrol. Earth Syst. Sci. 24, 5149–5171. https://doi.org/10.5194/hess-24-5149-2020

Newman, M. E. J. (2010). Networks: An introduction. Oxford University Press.

Nielsen, J. M., van de Beek, C. Z. R., Thorndahl, S., Olsson, J., Andersen, C. B., Andersson, J. C. M., ... & Nielsen, J. E. (2024). Merging weather radar data and opportunistic rainfall sensor data to enhance rainfall estimates. Atmospheric Research, 300, 107228.

Norme Français (2000). Association Française de Normalisation (AFNOR), Reconnaissance et essais, Essai d'eau LEFRANC [Recognition and tests, LEFRANC water test], Norme Française NF P 94-132 Sols.

Olson, R. E., & Daniel, D. E. (1981). Measurement of the Hydraulic Conductivity of FineGrained Soils, ASTM Special Technical Publication, pp 18–64.

Orlanski, I. (1975). A rational subdivision of scales for atmospheric processes. Bull. Am.

Oudin, L., Andréassian, V., Perrin, C., Michel, C., & Le Moine, N. (2008). Spatial proximity, physical similarity, regression and ungaged catchments: A comparison of regionalization approaches based on 913 French catchments. Water Resour. Res. 44, 48–54. https://doi.org/10.1029/2007WR006240

Overeem, A., Leijnse, H., van der Schrier, G., van den Besselaar, E., Garcia-Marti, I., & de Vos, L. W. (2024). Merging with crowdsourced rain gauge data improves pan-European radar precipitation estimates. Hydrology and Earth System Sciences, 28(3), 649-668.

Papalexiou, S. M., & Montanari, A. (2019). Global and regional increase of precipitation extremes under global warming. Water Resources Research, 55, 4901–4914. https://doi.org/10.1029/2018WR024067

Papalexiou, S. M., Koutsoyiannis, D., & Makropoulos, C. (2013). How extreme is extreme? An assessment of daily rainfall distribution tails. Hydrology and Earth System Sciences, 17(2), 851-862.

Papilloud, T., Röthlisberger, V., Loreti, S., & Keiler, M. (2020). Flood exposure analysis of road infrastructure – Comparison of different methods at national level. International Journal of Disaster Risk Reduction, 47, 101548. https://doi.org/10.1016/j.ijdrr.2020.101548

Papilloud, T., Sahin, O., & Stewart, R. A. (2021). A comprehensive review of accessibility measures in transport resilience studies. Transport Reviews, 41(5), 618–639.

Parise, M., & Cannon, S. H. (2012). Wildfire impacts on the processes that generate debris flows in burned watersheds. Natural hazards, 61, 217–227. https://doi.org/https://doi.org/10.1007/s11069-011-9769-9

Peng, S. C., Zhou, Y. M., Cao, L. H., Yu, S., Niu, J. W., & Jia, W. J. (2018). Influence analysis in social networks: A survey. Journal of Network and Computer Applications, 106, 17-32.

Persiano S., Ferri E., Antolini G., Domeneghetti A., Pavan V., & Castellarin A. (2020). Changes in seasonality and magnitude of sub-daily rainfall extremes in Emilia-Romagna (Italy) and potential influence on regional rainfall frequency estimation. J. Hydrol. Reg. Stud., 32, 100751.

Pescaroli, G., & Kelman, I. (2017). How Critical Infrastructure Orients International Relief in Cascading Disasters. Journal of Contingencies and Crisis Management, 25(2), 56–67. https://doi.org/10.1111/1468-5973.12118

Picozzi, V., Akbaba, A., Avossa, A., & Ricciardelli, F. (2022). Correction of historical records to improve the reliability of design wind speeds. Eng. Struct., 265. http://dx.doi.org/10.1016/j.engstruct.2022.114473

Poschlod, B., & Ludwig, R. (2021). Internal variability and temperature scaling of future sub-daily rainfall return levels over Europe. Environ. Res. Lett., 16, 064097. 10.1088/1748-9326/ac0849

Rachunok, B., & Fletcher, S. (2023). Socio-hydrological drought impacts on urban water affordability. Nature Water, 1(1), 83–94.

Raffa, M., Reder, A., Marras, G.F., Mancini, M., Scipione, G., Santini, M., & Mercogliano, P. (2021). VHR-REA_IT dataset: Very high resolution dynamical downscaling of ERA5 reanalysis over Italy by COSMO-CLM. Scientific Data 6. http://dx.doi.org/10.3390/data6080088

Read, L. K., & Vogel, R. M. (2015). Reliability, return periods, and risk under nonstationarity. Water Resources Research, 51(8), 6381-6398.

Reddy, L. S. & Elango, K. (1989). Analysis of water distribution networks with head dependent outlets. Civ. Eng. Syst., 6(3), 102–110.

Rengers, F. K., McGuire, L. A., Oakley, N. S., Kean, J. W., Staley, D. M., & Tang, H. (2020). Landslides after wildfire: Initiation, magnitude, and mobility. Landslides, 17, 2631–2641. https://doi.org/https://doi.org/10.1007/s10346-020-01506-3

Rezaeianzadeh, M., Stein, A., & Cox, J. P. (2016). Drought forecasting using Markov chain model and artificial neural networks. Water Resources Management, 30, 2245-2259.

Rigby, R. A., & Stasinopoulos, D. M. (2005). Generalized additive models for location, scale and shape. Journal of the Royal Statistical Society Series C: Applied Statistics, 54(3), 507-554.

Rong, Q., Zhu, S., Yue, W., Su, M., & Cai, Y. (2024). Predictive simulation and optimal allocation of surface water resources in reservoir basins under climate change. International Soil and Water Conservation Research, 12(2), 467-480.

Rosenzweig, B., Ruddell, B. L., McPhillips, L., Hobbins, R., McPhearson, T., Cheng, Z., Chang, H., & Kim, Y. (2019). Developing knowledge systems for urban resilience to cloudburst rain events. Environmental Science & Policy, 99, 150–159. https://doi.org/10.1016/j.envsci.2019.05.020

Roseto, R., Dellino, P., Schena, P., & Capolongo, D. (2023). Spatial distribution and trend analysis of extreme rainfall time series in Apulia region (Italy). Geografia Fisica e Dinamica Quaternaria, 46(1), 163-177

Rosso, R., Rulli, M. C., & Bocchiola, D. (2007). Transient catchment hydrology after wildfires in a Mediterranean basin: runoff, sediment and woody debris. Hydrology and Earth System Sciences, 11, 125–140. https://doi.org/https://doi.org/10.5194/hess-11-125-2007. 2

Rudari, R., Abbashar, A., Conijn, S., de Moel, H., Denis-Loupot, A., Luca Ferraris, L., Ghizzoni, T., Gignac-Eddy, A., Gomes, I., Mosquera Calle, D., Mouakkid Soltesova, K., Massabò, M., Njoroge Kabubi, J., Rossi, L., Rossi, L., Schiano Lomoriello, R., Trasforini, E., & Wens, M. (2019). UR Tanzania disaster risk profile. Nairobi: UNDRR and CIMA Research Foundation.

Sacré, C. (1993). Carte des vents extrêmes en France. Revue Française de Génie Civil, 15(2), 127-135.

Safaei Pirooz, A., Sadeghi, A., & Bazargan, M. (2021). Extreme wind maps for New Zealand: Development and validation. Journal of Wind Engineering and Industrial Aerodynamics, 214, 104644.

Sarigil, G., Neri, M., & Toth, E. (2024). Evaluation of national and international gridded meteorological products for rainfall-runoff modelling in Northern Italy. J. Hydrol. Reg. Stud. 56, 102031. https://doi.org/10.1016/j.ejrh.2024.102031

Schilstra, M., Wang, W., van Oel, P. R., Wang, J., & Cheng, H. (2024). The effects of reservoir storage and water use on the upstream–downstream drought propagation. Journal of Hydrology, 631, 130668.

Schwarz, G. (1978). Estimating the dimension of a model. The annals of statistics, 461-464.

Sfetsos, A., Giroud, F., Clemencau, A., Varela, V., Freissinet, C., LeCroart, J., Vlachogiannis, D., Politi, N., Karozis S., Gkotsis, I., Eftychidis, G., Hedel, R. & Hahmann, S. (2021). Assessing the effects of forest fires on interconnected critical infrastructures under climate change. Evidence from South France. Infrastructures, 6(2), 16. https://doi.org/10.3390/infrastructures6020016

Shakesby, R.A. (2011). Post-wildfire soil erosion in the Mediterranean: review and future research directions. Earth-Science Reviews, 105, 71–100. https://doi.org/https://doi.org/10.1016/j.earscirev.2011.01.001

Simões, N. E., Ochoa-Rodríguez, S., Wang, L. P., Pina, R. D., Marques, A. S., Onof, C., & Leitão, J. P. (2015). Stochastic urban pluvial flood hazard maps based upon a spatial-temporal rainfall generator. Water, 7(7), 3396–3406. https://doi.org/10.3390/w7073396

Singh, H., Nielsen, M., & Greatrex, H. (2023). Causes, impacts, and mitigation strategies of urban pluvial floods in India: A systematic review. International journal of disaster risk reduction, 93, 103751.

Smith, A., Martin, D., & Cockings, S. (2016). Spatio-Temporal Population Modelling for Enhanced Assessment of Urban Exposure to Flood Risk. Applied Spatial Analysis and Policy, 9(2), 145–163. https://doi.org/10.1007/s12061-014-9110-6

Solari, G., Ballio, G., & Pagnini, L. (1991a). Gust wind speed statistics in Italy. Journal of Wind Engineering and Industrial Aerodynamics, 38(3), 209-218.

Solari, G., Ballio, G., & Pagnini, L. (1991b). Extreme wind speed estimation by the generalized extreme value distribution. Journal of Wind Engineering and Industrial Aerodynamics, 39(1-3), 283-293.

Spassiani, D., & Mason, M. S. (2021). Extreme wind risk assessment for Australia. Journal of Wind Engineering and Industrial Aerodynamics, 210, 104457.

Stahl, K., Blauhut, V., Barker, L. J., & Stagge, J. H. (2023). Chapter 12 - Drought impacts. In Hydrological Drought (pp. 563–594).

Stoof, C. R., Vervoort, R., Iwema, J., Van Den Elsen, E., Ferreira, A., & Ritsema, C. (2012). Hydrological response of a small catchment burned by experimental fire. Hydrology and Earth System Sciences, 16, 267–285. https://doi.org/https://doi.org/10.5194/hess-16-267-2012

Szalińska, W., Tokarczyk, T., & Otop, I. (2018). Urban drought. E3S Web of Conferences, 45, 00095.

Taramelli, A., Righini, M., Valentini, E., Alfieri, L., Gatti, I., & Gabellani, S. (2022). Building-scale flood loss estimation through vulnerability pattern characterization: application to an urban flood in Milan, Italy. Natural Hazards and Earth System Sciences, 22(11), 3543-3569. https://nhess.copernicus.org/articles/22/3543/2022/

Taylor, M. A. P., & Susilawati. (2012). Remoteness and accessibility in the vulnerability analysis of regional road networks. Transportation Research Part A: Policy and Practice, 46(5), 761-771. https://doi.org/10.1016/j.tra.2012.02.008

Thépaut, J.N., Dee, D., Engelen, R., & Pinty, B. (2018). The Copernicus programme and its climate change service. In: IGARSS 2018-2018 IEEE International Geoscience and Remote Sensing Symposium. pp. 1591–1593. http://dx.doi.org/10.1109/IGARSS. 2018.8518067

Thrysøe, C., Balstrøm, T., Borup, M., Löwe, R., Jamali, B., & Arnbjerg-Nielsen, K. (2021). FloodStroem: a fast dynamic GIS-based urban flood and damage model. Journal of Hydrology, 600. https://doi.org/10.1016/j.jhydrol.2021.126521

Tingsanchali, T. (2012). Urban flood disaster management. Procedia Engineering, 32, 25–37. https://doi.org/10.1016/j.proeng.2012.01.1233

Toth, E., Bragalli, C., & Neri, M. (2018). Assessing the significance of tourism and climate on residential water demand: Panel-data analysis and non-linear modelling of monthly water consumptions. Environ. Model. Softw. 103, 52–61. https://doi.org/10.1016/j.envsoft.2018.01.011

Totsuka, N., Trifunovic, N. & Vairavamoorthy, K. (2004). Intermittent urban water supply under water starving situations. Proceedings of 30th WEDC International Conference, Vientiane, Lao PDR, 2004.

Trasforini, E., Campo, L., Ghizzoni, T., Libertino, A., Ottonelli, D., Ponserre, S., Rossi, L., & Rudari, R. (2024). Regional probabilistic flood displacement risk assessment: the Horn of Africa case study. EGU General Assembly 2024. https://doi.org/10.5194/egusphere-egu24-16971.

Treppiedi D., Cipolla G., Francipane A., & Noto L.V. (2021). Detecting precipitation trend using a multiscale approach based on quantile regression over a Mediterranean area. Int. J. Clim., 41, 5938–5955. https://doi.org/10.1002/joc.7161

Treppiedi, D., Cipolla, G., Francipane, A., Cannarozzo, M., & Noto, L. V. (2023). Investigating the reliability of stationary design rainfall in a mediterranean region under a changing climate. Water, 15(12), 2245.

Turner, S. W., Voisin, N., Nelson, K. D., & Tidwell, V. C. (2022). Drought impacts on hydroelectric power generation in the western United States (No. PNNL-33212). Pacific Northwest National Lab. (PNNL), Richland, WA (United States).

U.S. Army Corps of Engineers (2024). HEC-RAS User's Manual, version 6.4. Hydrologic Engineering Center, Davis.

U.S. Army Corps of Engineers (USACE). (2024). HEC-RAS (River Analysis System). Hydrologic Engineering Center. Retrieved from https://www.hec.usace.army.mil/software/hec-ras/

Vairavamoorthy, K., Akinpelu, E., Lin, Z.& Ali, M. (2001). Design of sustainable system in developing countries. Proceedings of the World Water and Environmental Resources Challenges, Environmental and Water Resources Institute of ASCE, Orlando, Florida, 20-24 May, 2001.

Villarini, G. (2012). Analyses of annual and seasonal maximum daily rainfall accumulations for Ukraine, Moldova, and Romania. International Journal of Climatology, 32(14).

Volpi, E. (2019). On return period and probability of failure in hydrology. Wiley Interdisciplinary Reviews: Water, 6(3), e1340.

Volpi, E., & Fiori, A. (2014). Hydraulic structures subject to bivariate hydrological loads: Return period, design, and risk assessment. Water Resources Research, 50(2), 885-897.

Wachs, M., & Kumagai, T. G. (1973). Physical accessibility as a social indicator. Socio-Economic Planning Sciences, 7(5), 437–456.

Wagner, J. M., Shamir, U. & Marks, D. H., (1988). Water distribution reliability: Analytical methods. Journal of Water Resources Planning and Management, 114(3), 253–275.

Wang, G., & Sassa, K. (2001). Factors affecting rainfall-induced flowslides in laboratory flume tests. Geotechnique, 51, 587–599. https://doi.org/https://doi.org/10.1680/geot.2001.51.7.587

Wang, T., Wang, H., Wang, Z., & Huang, J. (2023). Dynamic risk assessment of urban flood disasters based on functional area division—A case study in Shenzhen, China. Journal of environmental management, 345, 118787. https://doi.org/10.1016/j.jenvman.2023.118787

Westra S., Fowler H.J., Evans J.P., Alexander L.V., Berg P., Johnson F., Kendon E.J., Lenderink G., & Roberts N.M. (2014). Future changes to the intensity and frequency of short-duration extreme rainfall. Rev. Geophys., 52, 522–555. https://doi.org/10.1002/2014RG000464

World Meteorogical Organization (1998). Analyzing Long Time Series of Hydrological Data With Respect To Climate Variability. WMO Publication.

World Meteorogical Organization (2021). WMO - No. 8/2021. Guide To Meteorological Instruments and Methods of Observation, Standard, eighth ed. World Meteorological Organization (WMO), Geneva, Switzerland.

Wu, L., Huang, R., Xu, Q., Zhang, L., & Li, H. (2015). Analysis of physical testing of rainfall-induced soil slope failures. Environmental earth sciences, 73, 8519–8531. https://doi.org/10.1007/s12665-014-4009-8

Yang, T., Gao, X., Sellars, S. L., & Sorooshian, S. (2015). Improving the multi-objective evolutionary optimization algorithm for hydropower reservoir operations in the California Oroville–Thermalito complex. Environmental Modelling & Software, 69, 262-279.

Yang, W., Andréasson, J., Phil Graham, L., Olsson, J., Rosberg, J., & Wetterhall, F. (2010). Distribution-based scaling to improve usability of regional climate model projections for hydrological climate change impacts studies. Hydrology Research, 41(3-4), 211-229.

Yepes, G., Ringskog, K., & Sarkar, S. (2001). The High Cost of Intermittent Water Supplies. Journal of Indian Water Works Association, 33(2).

Yu, J., Stathopoulos, T., & Li, M. (2023). Exposure factors and their specifications in current wind codes and standards. J. Build. Eng. 76, 107207. http://dx.doi.org/10.1016/j.jobe.2023.107207

Zhang, W., Liu, P., Wang, H., Chen, J., Lei, X., & Feng, M. (2017). Reservoir adaptive operating rules based on both of historical streamflow and future projections. J. Hydrol. 553, 691–707. https://doi.org/10.1016/j.jhydrol.2017.08.031

Zhao, Y., Dong, N., Li, Z., Zhang, W., Yang, M., & Wang, H. (2021). Future precipitation, hydrology and hydropower generation in the Yalong River Basin: Projections and analysis. Journal of Hydrology, 602, 126738.

Zimmermann, E., Bracalenti, L., Piacentini, R., & Inostroza, L. (2016). Urban Flood Risk Reduction by Increasing Green Areas for Adaptation to Climate Change. Procedia Engineering, 161, 2241–2246. https://doi.org/10.1016/j.proeng.2016.08.822